DISS. ETH NO. 19945

Composite laminates with integrated vibration damping treatments

A dissertation submitted to

ETH Zurich

for the degree of

Doctor of Sciences

presented by

Grégoire Lepoittevin

MSc in Engineering, Chalmers University of Technology

born on September 5, 1983

citizen of France

accepted on the recommendation of

Prof. Dr. P. Ermanni, examiner
Prof. Dr. D. Saravanos, co-examiner

2012

Acknowledgements

"Perfection is achieved, not when there is nothing more to add, but when there is nothing left to take away."
Antoine de Saint-Exupéry
Wind, Sand and Stars

Abstract

This thesis deals with the design of composite laminates with integrated damping layers. The damping capability of structural elements is an important design aspect. It enables to reduce the amplitude of vibrations which increases the long-term reliability and fatigue life. In transportation systems, it also improves the acoustical comfort of the passengers. A typical solution is to bond a viscoelastic material layer on the surface of the load-carrying structure. When the damping treatment is constrained by a stiff layer, high damping rates can be obtained. With the use of fiber-reinforced composite materials, it is possible to have one of the layers made of a soft damping layer. In that case, the damping treatment is constrained by composite laminates that have also to fulfill mechanical requirements. The goal of this PhD thesis is to propose design guidelines for composite laminates with integrated damping treatments. The objective is to obtain a structural component having simultaneously high mechanical and vibration damping properties at the lowest possible weight. The first part of the work deals with the design and the optimization of segments of constrained layer damping treatment. It is shown that free edges of the damping layer have to be placed where the bending curvature of the load-carrying structure is the highest. The results also demonstrate that there is a number of segments of constrained layer damping treatments for each bending modes that maximizes their modal loss factor. An optimization technique has been developed with the goal to maximize the damping rate by adjusting the segments' position. This enables to further increase the damping rates. In the second part, a numerical model of a composite beam with a soft core layer is validated using an analytical solution. The presence of the damping layer tends to decouple the sublaminates: they behave as two separate bodies experiencing the same bending cur-

vature. This effect vanishes by increasing the length-to-thickness ratio of the structure. In the third part, the influence of the different damping layer design variables on the laminate's deflection, maximal flexural force, stability and in-plane stiffnesses is studied. Different integration solutions are considered: a damping layer integrated with open edges (like a sandwich configuration), a damping layer integrated with closed edges along its width and a damping layer integrated with closed edges both along its length and width. The results show that two distinctive design rules have to be followed depending on whether the goal is to achieve high mechanical properties or high damping rates. The damping layer should be integrated with open edges, should be placed in the middle of the laminate lay-up, should be significantly long and should have a low shear modulus to obtain high damping rates. The damping layer should be integrated with closed edges, should be placed as far away as possible from the plate's mid-plane, should be short and should have a high shear modulus to obtain high mechanical performances. The most promising solution is for a damping layer integrated with all edges closed. This enables to reduce the decoupling effect. As a consequence, the structural bending stiffness and strength and stability properties are significantly improved. Nonetheless, the damping material has to have special properties. It must have simultaneously high shear modulus to ensure high mechanical properties and high loss factor to ensure a high damping rate. Additionally, such damping treatment has to have much larger dimensions than a classical constrained layer damping treatment. Therefore, the latter is the most suitable solution as it ensures to have high mechanical properties, high damping rate at the lowest weight.

Zusammenfassung

Diese Dissertation behandelt die Auslegung von Faserverbundlaminaten mit integrierten Dämpfungsschichten. Das Dämpfungsvermögen von Strukturelementen ist eine bedeutende Auslegungsgrösse, welche es erlaubt, Schwingungsamplituden zu reduzieren und damit Langzeitzuverlässigkeit und Lebensdauer zu vergrössern. In Verkehrssystemen führt eine Schwingungsdämpfung überdies zu verbessertem akustischem Komfort für die Passagiere. Das Aufbringen einer viskoelastischen Materialschicht auf die Oberfläche einer lasttragenden Struktur stellt eine typische Lösung hierfür dar. Wenn das Dämpfungselement durch eine steife Deckschicht begrenzt wird (sog. "Constrained-layer damping"), lässt sich eine grosse Dämpfung erzielen. Werden Faserverbundwerkstoffe verwendet, so kann eine der Lagen des Schichtverbundes als weiche Dämpfungslage ausgeführt werden. In diesem Fall ist das Dämpfungselement durch ein Faserlaminat begrenzt, welches zudem mechanische Anforderungen erfüllen muss. Das Ziel dieser Doktorarbeit besteht darin, Richtlinien für die Auslegung von Faserverbundlaminaten mit integrierten Dämpfungselementen zu entwickeln. Auf diese Weise sollen Strukturbauteile realisiert werden, die bei geringstmöglichem Gewicht sowohl gute mechanische als auch schwingungsdämpfende Eigenschaften aufweisen. Der erste Teil der Arbeit beschäftigt sich mit der Auslegung und Optimierung segmentierter "Constrained-layer damping"-Elemente. Es wird gezeigt, dass die freien Ränder eines Dämpfungselements dort platziert werden müssen, wo die Krümmung infolge Biegung der lasttragenden Struktur am grössten ist. Die Ergebnisse demonstrieren zudem, dass für jede Biegeeigenform eine Anzahl von Segmenten existiert, welche den modalen Verlustfaktor maximiert. Mit dem Ziel, die Dämpfung durch Anpassung der Segmentlängen zu maximieren, wurde ein Optimierungsverfahren entwickelt, welches er-

laubt, das Dämpfungsvermögen leicht zu erhöhen. Im zweiten Teil wird das numerische Modell eines Faserverbundbalkens mit einer weichen Kernschicht mithilfe einer analytischen Lösung validiert. Es zeigt sich, dass das Vorhandensein der Dämpfungsschicht zu einer Entkopplung der Unterlaminate des Faserverbundes führt. Diese verhalten sich wie zwei getrennte Elemente, welche die gleiche Biegung erfahren. Dieser Effekt verschwindet bei Strukturen mit grösserem Schlankheitsgrad. Im dritten Teil wird der Einfluss der verschiedenen Variablen für die Auslegung der Dämpfungsschichten auf die Durchbiegung der Laminate sowie auf deren maximale Biegespannung, deren Stabilität und deren Steifigkeit in der Ebene untersucht. Hinsichtlich der Integration werden mehrere Lösungsvarianten betrachtet: eine integrierte Dämpfungsschicht mit offenen Rändern (wie bei einer Sandwichkonfiguration), eine Schicht mit geschlossenen Querrändern sowie eine mit geschlossenen Längs- und Querrändern. Die Ergebnisse zeigen, dass zwei unterschiedliche Auslegungsregeln befolgt werden müssen, abhängig davon, ob gute mechanische Eigenschaften oder eine grosse Schwigungsdämpfung angestrebt werden. Die Dämpfungsschicht sollte mit offenen Rändern integriert werden, in der Mitte des Laminats positioniert werden und einen niedrigen Schubmodul aufweisen, um ein grosses Dämpfungsvermögen zu erreichen. Falls gute mechanische Eigenschaften erzielt werden sollen, sind geschlossene Ränder, eine Platzierung mit grösstmöglichem Abstand von der Plattenmittelebene sowie ein hoher Schubmodul vorzusehen. Die meistversprechende Lösung besteht in einer integrierten Dämpfungsschicht mit allseitig geschlossenen Rändern. Es ist möglich, den Effekt der Entkopplung zu verringern, was zu einer signifikanten Verbesserung der Biegesteifigkeit, -festigkeit und Stabilität führt. Gleichwohl muss das Dämpfungsmaterial spezielle Eigenschaften aufweisen: sowohl einen hohen Schubmodul, um gute mechanische Eigenschaften zu gewährleisten, als auch einen hohen Verlustfaktor, um eine grosse Dämpfung zu erreichen. Darüber hinaus sind Dämpfungselemente mit viel grösseren Abmessungen als im Fall des klassischen "Constrained-layer damping" erforderlich. Somit handelt es sich bei der letztgenannten Variante, welche gute mechanische Eigenschaften und grosses Dämpfungsvermögen bei geringem Gewicht verspricht, um die geeignetste Lösung.

Contents

List of symbols

$[A]$	In-plane stiffness matrix
$[B]$	Coupling stiffness matrix
$[C]$	Damping matrix
$[D]$	Bending stiffness matrix
$[K]$	Stiffness matrix
$[M]$	Mass matrix
$\{F\}$	External forces vector
$\{u\}$	Displacement vector
B	Bending stiffness
E	Young's modulus
$E^{'}$	Storage Young's modulus
$E^{''}$	Loss Young's modulus
F_c	Coulomb damping force
F_d	Viscous damping force
G	Shear modulus
$G^{'}$	Storage shear modulus
$G^{''}$	Loss shear modulus
H	Thickness
I	Moment of inertia
M	Bending moment
N	In-plane force
P	Normal force
T	Temperature
T_g	Transition temperature
U_d	Dissipated energy
U_k	Kinetic energy
U_p	Potential energy

U_{rad}	Radiated energy
U_{rev}	Reversible energy
U_s	Strain energy
k	Stiffness coefficient
c	Coefficient of viscosity
g	Shear parameter
h	Thickness
p	Wavelength
t	Time
u	Displacement in x-direction
v	Displacement in y-direction
v_f	Fiber volume content
v_m	Matrix volume content
w	Displacement in z-direction
ϵ	Extensional strain
η	Loss factor
γ	Shear strain
κ	Curvature
μ	Coefficient of friction
ν	Poisson's ratio
ω	Circular frequency (radian per second)
ψ	Phase lag
ρ	Density
σ	Extensional stress
τ	Shear stress

Chapter 1

Introduction

This dissertation deals with the design of structural composite laminates with integrated vibration damping treatments. Conventional design requirements for structural elements can be summarized as follows: high stiffness, high strength and low weight. The main limitation is that the dynamic response is not taken into account. Nowadays, a structure has also to fulfill other design criteria such as low noise, long life and increased reliability. In order to reach these objectives, the solution is to add to the structure a mechanism of energy dissipation.

Damping is defined as a mechanism that dissipates vibratory energy in another form of energy (e.g. heat in the case of viscoelastic damping). In the transportation industry, vibration damping solutions are used to reduce the vibration level of the different panels. This gives an improvement of the long term reliability of the different parts and an increase of the acoustical comfort of the passengers. Figure 1.1 shows typical areas on a car body where damping treatments are applied [1].

Vibration damping solutions are also widely used for commercial aircraft applications. Local vibration damping treatments are added to the fuselage to reduce the overall vibrations which leads to a noise reduction in the cabin. Figure 1.2 shows the typical locations for damping treatments on an aircraft fuselage section.
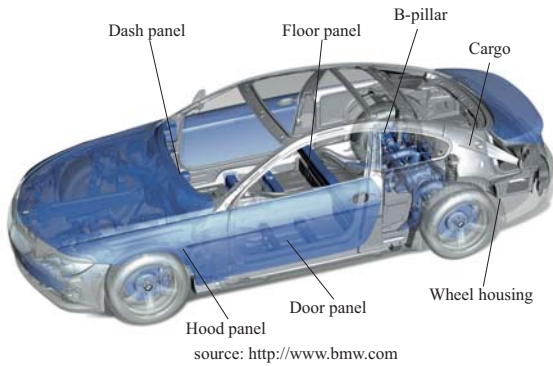
Figure 1.1: Damping treatment locations on an automotive body structure
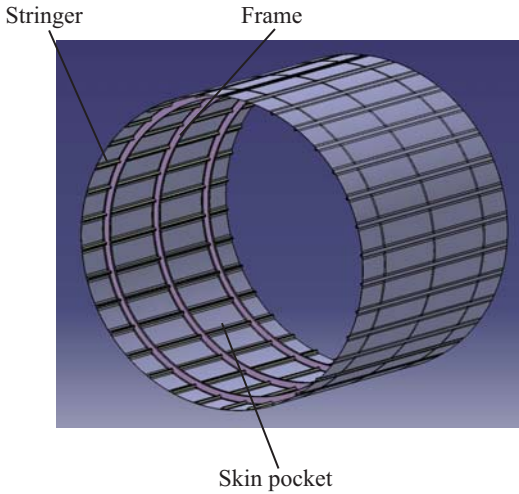
Figure 1.2: Damping treatment locations on an aircraft fuselage structure

Since decades, the use of fiber-reinforced composites has significantly increased in domains such as aerospace, aircraft and automotive industries. Their main advantages are the high specific stiffness, strength and tailorable properties. Although fiber-reinforced composites exhibit better viscoelastic properties than conventional metal alloys, it is not enough to reach a significant level of damping. A solution is to add within the stacking sequence a viscoelastic material layer to further increase the structural damping. Therefore, the amplitude of the vibrations is reduced, which improves the fatigue endurance and the impact resistance of the laminate. In the later case, viscoelastic materials can actually limit the damaged area and the damage propagation, because they have the capacity to absorb energy. However, the presence of a soft layer in the lay-up leads to a decoupling of the laminate in two sublaminates. This changes the overall mechanical properties of the composite structure and increases its weight.

This thesis aims at understanding and quantifying the effect of an integrated damping material layer on the mechanical properties of a fiber-reinforced composite laminate, and at evaluating if a trade-off between weight, mechanical and vibration damping design criteria is possible.

1.1 State-of-the-art

In this section, the available literature on the damping of composites and viscoelastic damping treatments is presented. First, the different damping mechanisms of composite materials are detailed. A review of the laminate theories is also done. Then, the different possibilities to apply viscoelastic materials to structural elements are discussed. The state-of-the-art of composite laminates with embedded damping layers is presented. Finally, previous works on the damping optimization of laminated structures are detailed.

1.1.1 Damping of composites

The damping mechanisms of composite materials are completely different of those ones of conventional materials. The sources of energy dissipation in fiber-reinforced composites are [2]:

1. Viscoelastic properties of matrix and fiber. Because of their viscous

properties, composite materials have a time-dependent behaviour which enable them to dissipate energy. Schlutz and Tsai [3, 4] were among the first to perform experimental work on the damping of composites. They showed that the damping rate of a glass fiber beam is almost five times larger than the one of an aluminium beam. Bert and coworkers [5] correlated experimental and analytical results to determine the damping capacity of E-glass epoxy. Gibson [6] also performed experimental and analytical analysis on composite laminates to estimate their damping properties under flexural vibrations. Hashin [7] proposed analytical expressions for the on-axis ply-damping. Adams and coworkers [8, 9] showed that the damping ratio decreases as the fiber volume content increases. Adams also correlated experimental results with theoretical investigations. It was shown that the shear deformation is an important parameter that gives high damping, that the transverse stress gives sometimes high energy dissipation and the longitudinal stress is negligible. Saravanos and Chamis [10] developed an integrated theory for the modeling of composite damping. The proposed equations based on hysteretic damping show the effect of temperature, moisture and interply hysteretic damping. They also presented a unified micromechanics theory for the damping capacity of composites for all damping coefficients of a composite ply associated with the longitudinal stress, transverse stress, through the thickness normal stress, in-plane shear stress, through the thickness shear stress [11]. The theory includes the damping capacities based on elastic and dissipative properties, interface properties, ply temperature and moisture, off-axis loading and temperature rise due to continuous vibration.

2. Damping due to interphase. The interphase is the region adjacent to the fiber surface along the fiber length. Energy dissipation is due to the high shear strain in the interphase region. Ziegel and Ramanov [12] defined parameters to cover the range of interfacial imperfection: from weak to ideal. Ideal interface means there is a perfect bonding and therefore no damping occurs. Chinquin et al. [13] and Murayama [14] observed a direct relation between the damping at the interface of fiber/matrix and the interfacial shear strength. Hwang and Gibson [15] presented a strain energy approach for the micromechanical modeling of both damping and stiffness in composite including the fiber/matrix interface.

3. Damping due to damage: frictional damping in the unbonded regions between fiber and matrix interface or delamination. Damping occurs because of energy dissipation in the area of matrix cracks. Hence, the damping capacity can be used to measure damages in composites [16, 17]. Saravanos and Hopkins [18] developed a laminate theory for stiffness, damping and inertia terms to handle delaminated composite laminates. They correlated analytical and experimental results for graphite-epoxy delaminated beams.

4. Viscoplastic damping. There is a limited number of papers on this aspect. Jenny and Marchetti [19] developed a micromechanical model including the plastic behaviour of the matrix in order to study the nonlinear behaviour of composite laminates. They showed that there is a correlation between the plastic deformation and the increase of damping at high stresses.

5. Thermoelastic damping. It is described as the coupling between the elastic deformation in the matrix and the temperature field. In any vibrating structures, the strain field causes a change in the internal energy such that compressed regions become hotter and extended regions become colder. Energy is dissipated because of the lack of thermal equilibrium. Thermoelastic damping is preponderant for metal composites.

1.1.2 Laminate theories and models

The classical laminate theory (CLT) is usually used to analyze laminates and to determine their stiffness properties. As the CLT does not consider the effect of the out-of-plane strains, more accurate theories, like first order deformation and higher order theories, have been used for thick laminates. The works of Pagano [20, 21], Reddy [22], Srinivas [23] and Di Sciuva [24] have been used as a reference for the development and validation of several improved laminate theories and related finite elements to analyze the damping of composite laminates. Saravanos [25] presented a layerwise damping plate theory for sandwich composite plates including a semi-analytical solution for predicting the modal damping and natural frequencies. Alam and Asmani [26] used the variational principles to derive governing equations of motion for laminated plate. Hwang and coworkers [27, 28] developed a three-dimensional finite element and used the strain

energy to characterize the damping of angle-ply composites. Koo and Lee
[29] applied the finite element method based on the transverse incompressibility and layerwise linear distribution of in-plane displacement to
determine the modal loss factor and resonance frequency of anisotropic
plates. They showed that the resonance frequency and loss factor are
strongly influenced by the fiber orientation and the length-to-thickness
ratio.

1.1.3   Structural elements with viscoelastic damping treatments

Viscoelastic damping treatments can be applied in two ways as presented
in Figure 1.3.
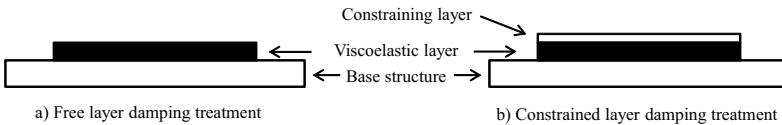
Figure 1.3: Surface damping treatments

For the free layer damping treatment (FLD treatment), a viscoelastic
layer is bonded on the surface on the load-carrying structure. The energy
dissipation is due to the extensional strain occuring in the damping layer.
Oberst [30] proposed an equation to calculate the effective flexural rigidity
and the loss factor of the damped membre.

For the constrained layer damping treatment (CLD treatment), a thin
metallic sheet is applied on top of the viscoelastic layer. During bending vibrations, the damping material is mainly deformed in shear which
leads to energy dissipation. It is important to note that the top layer is
not used to improve the overall mechanical properties of the structure.
Kerwin [31] was one of the first to observe that a stiff constraining layer,
placed on top of the viscoelastic layer, can increase the structural damping rate. Di Taranto [32] developed an analytical model to determine
the damping rate of freely vibrating beams having any possible boundary
conditions. Mead and Markus [33] derived a mathematical expression for

the transverse displacement of a three-layered sandwich beam with a viscoelastic core. They assumed different boundary conditions at one end of the beam such as no transverse displacement, no rotation, no bending moment, or no shear force. Rao [34] also presented a formula for the frequency and loss factor of a sandwich beam under the following boundary conditions: clamped-free, clamped-simply supported, clamped-clamped, simply supported-simply supported and free-free. Ohayon et al. [35, 36] presented a finite element formulation using fractional derivative operators for the transient dynamic analysis of sandwich structures with constrained layer damping treatment. Grootenhuis et al. [37, 38, 39, 40] studied the flexural vibrations of symmetrical multi-layer beams with viscoelastic damping, and compared numerical and experimental results.

With the use of fiber-reinforced composite laminates, it is possible to integrate in the laminate lay-up a viscoelastic layer. The stiff laminates constrain the damping material that is deformed in shear during bending vibrations, like for a CLD treatment. The major difference is that both of the stiff parts are also designed according to mechanical criteria. Moser and Lumassegger [41] were actually among the first to show that the damping of laminated fiber-reinforced composite structures can be increased by means of a soft shear-deformable ply. Biggerstaff and Kosmatka [42] performed experimental and analytical studies of cocurred graphite/epoxy composite laminates with embedded damping materials. Cao et al. [43] realized an experimental parametric study of alternately laminated damped structures. They investigated the influence of the fiber orientation angle and layer thicknesses. Rao and coauthors [34] presented an analysis of the dynamic properties of fiber-reinforced composite laminates with embedded damping layers by means of finite elements based on a modal strain energy approach. Saravanos and Pereira [44] developed a discrete damping layer mechanics by using a semi-analytical method for predicting the modal damping of simply-supported composite plates. They also proposed a finite element to predict the damping of thick composite plates with interlaminar damping layers [45]. Plagianakos and Saravanos [46, 47] presented a high-order discrete-layer theory and the corresponding finite element for the prediction of the damping of laminated composite sandwich beams and plates.

1.1.4   Damping optimization

The damping of composite depends strongly on the plies elastic properties
and fiber volume content. By selecting an appropriate design, one can ob-
tain an improvement of the dynamic properties. On the other hand, the in-
crease of damping of composite structures leads to a decrease of structural
stiffness and strength properties. Hence, the optimal design is based on a
trade-off between damping and mechanical performances. Saravanos and
Chamis [48] presented a multi-objective optimal design methodology for
lightweight, low-cost composite structures with improved dynamic perfor-
mances. They included the effect of composite damping on the dynamics
of composite structures. Kam and Chang [49] performed an optimization
of a composite plate with the goal to minimize the weight considering as
constraints the first natural frequency, the damping of the first vibration
modes and the deflection. The design variables were the layer thickness
and fiber orientation. They did two case studies on simply-supported
and cantilever composite plates to demonstrate the feasibility of their ap-
proach. Park et al. [50] presented a multi-constrained optimization for
the design of composite plates manufactured with resin transfer molding
method. The objective was to minimize the weight by minimizing the
layer thickness and considering the strength as structural constraint and
the maximum allowable mold filling time as process requirement. They
compared the strength and the filling time for different number of layers.
Araujo et al. [51] performed a multiple objective optimization of com-
posite laminates with a viscoelastic layer. They used a gradient based
approach to maximize the loss factor of the first bending mode consider-
ing a maximum allowable mass and displacement. The design variables
were the thickness and fiber orientation of each ply. They showed the
validity of their approach for simply supported beams and plates. Hao
and Rao [52] presented a procedure for the maximization of damping and
the minimization of the weight of a simply-supported beam covered with
a constrained layer damping treatment. The design variables were the
thicknesses of the different layers. Marcelin and coworkers [53] also per-
formed a damping optimization of constrained layer damping treatment
considering treatment position and location as design variables. Zheng et
al. [54] did a similar study but they also considered the shear modulus
of the viscoelastic layer as design variable. Trindade [55] performed a ge-
ometrical optimization of composite beams with shear deformable layers
with the goal to minimize the transverse velocities and to maximize the

loss factors of the first five eigenmodes. The design variables were the number of composite layers, their thickness and orientation.

1.2   Research needs

From the literature research presented in the previous section, most of the studies on composite structures with integrated damping layers were focused only on their performances regarding damping [41, 44, 46, 47]. To the author's knowledge, few studies looked at the static properties of such laminated composite [49]. There is no work where the mechanical properties of laminates with interlaminar shear deformable layers considering tension, compression and shear load-cases are reported. In the field of the optimization of multi-layered structures with viscoelasic materials, the design variables are typically the thickness and orientation of the fibrous layers [51, 55]. Only Zheng [54] included the material properties of the damping layer in the list of design variables but the optimization objectives were only on the dynamic properties of the vibrating beam. There is actually no research work where the optimization of damping of composites with integrated damping treatments is considered together with weight and static requirements.

However, structures are designed according to multiple objectives. They have to fulfill conventional mechanical criteria but also to perform other functions, like vibration damping. It is demanded to dissipate the largest amount of energy over the largest frequency range. For structural elements with embedded shear deformable layers, it would be required to obtain a design solution that provides: high stiffness, high strength, high vibration damping capacities and low weight. Such design requirements raise the following questions:

- Is it possible to use a viscoelastic layer not only for vibration damping purposes but also to improve the mechanical properties of the load-carrying structure?

- Is it possible to design a composite laminate with an integrated damping layer that is lighter than a composite laminate with a classical CLD treatment?

1.3   Goals and approach

The goals of this thesis work can be divided as following:

1. To develop complete knowledge on modeling and optimization of constrained viscoelastic materials.

2. To have a clear understanding on the effect of a soft core layer on the overall mechanical properties of a composite laminate.

3. To propose design rules for structural composite components with integrated damping treatments considering mechanical and vibration damping criteria with the goal to minimize the weight.

In order to answer the questions and to reach the goals above presented, the present work is divided in three parts.

First, an analysis of the state-of-art on the vibration damping of structural elements is done. The main analytical and numerical methods and theories for structures with damping layer treatments are reviewed. A numerical model of a plate with a constrained damping layer treatment is validated. The performances of segmented constrained layer damping treatment on two- amd three-dimensional structures are investigated.

With the second part of this thesis starts the integration of damping materials in composite laminates. A finite element model of a composite beam with a soft core layer in cylindrical bending is built up and validated using Pagano's exact solution [20]. The numerical model is used to gain a first understanding of the effect of the damping layer on the bending properties of the laminated beam.

In the third part, a parametric study on a composite plate with an embedded damping material layer is realised. The influence of each design variable of the damping layer on the mechanical properties of the laminate is investigated. An optimization method is used to obtain a structural element with the minimum weight and simultaneously high mechanical and vibration damping properties. Finally, design rules for composite laminates with integrated damping layers are proposed.

1.4 Thesis outline

In chapter 2, the available analytical and numerical models and theories for the analysis of the dynamic response of lightweight structures are reviewed. Chapter 3 studies the possibility to increase the damping rates of constrained layer damping treatments by means of segmentation. The validation of the numerical model of a composite beam with a soft core layer is shown in chapter 4. Chapter 5 is focused on the parametric study of a composite plate with an integrated damping layer considering mechanical and vibration damping criteria. Design recommendations are extracted. Chapter 6 deals with the optimization of a composite plate with an integrated damping layer. For different mechanical situations, a trade-off between weight, damping and mechanical requirements is estimated. Chapter 7 summarizes the results. Final conclusions are presented and suggestions for future works are proposed.

Chapter 2

Vibration damping of lightweight structures

This chapter presents theoretical, analytical and numerical approaches to analyze the dynamic response of lightweight structures with viscoelastic damping treatments. At first, basics of structural dynamic are recalled to introduce the concept of damping. The different mechanisms of energy dissipation are presented using the nonmaterial and material damping classification. Then, a deeper study on the damping properties of viscoelastic materials is performed as they are used in this thesis. Typical design solutions using such damping treatments are presented as well as related analytical and numerical methods. Finally, theories for the anaylsis of the dynamic response of composite laminates without and with viscoelastic damping layers are presented.

2.1 Basics of structural dynamics

The dynamic behaviour of structural systems can be described with the folllowing equation

$$[M]\{\ddot{u}\} + [C]\{\dot{u}\} + [K]\{u\} = \{F\} \tag{2.1}$$

$[M]$ is the mass matrix. It is a generalization of the concept of mass to generalize coordinates. The damping matrix $[C]$ is used to describe the energy dissipation mechanism, also called damping mechanism, of the considered system. Damping refers to the ability of a structure to dissipate vibration energy into an other form of energy, like heat for example [56]. $[K]$ is the stiffness matrix used to describe the stiffness between all the degrees of freedom of the system. $\{u\}$ is the displacement vector and $\{F\}$ is the vector of external forces applied to the system.

2.2　Classification of damping

According to Sun and Lu [56], damping can be classified in two categories: nonmaterial damping and material damping.

2.2.1　Nonmaterial damping

2.2.1.1　Viscous damping

Viscous damping is due to a non-conservative force that is directly proportional to the velocity of vibration. In schematics of vibrating systems, it is usually represented as a dashpot. A force is created by the fluid resistance during oscillation and the mechanical behaviour is described by the equation

$$F_d = c\frac{dx}{dt} \tag{2.2}$$

where c is the coefficient of viscosity. It is a measure of the resistance of the fluid which is being deformed. dx/dt is the velocity of the particle relative to the fluid. The dissipated energy U_d is equal to

$$U_d = \oint F_d dx \tag{2.3}$$

U_d depends on the frequency, amplitude and temperature. A measure of damping can be defined with the loss factor η. It is the ratio between

the energy dissipated per radian and the peak of potential energy and is defined by

$$\eta = \frac{U_d}{2\pi U_p} \tag{2.4}$$

where U_p is the peak of potential energy.

2.2.1.2 Coulomb damping

The Coulomb damping, also named dry damping, comes from the friction of two dry surfaces. The Coulomb damping force is described with the following equation

$$F_c = \mu N \tag{2.5}$$

where N is the normal force between the two surfaces and μ the coefficient of friction. F_c is assumed to be independent of the relative velocity of motion between the surfaces. The sign of the damping force is always opposite to that of the motion.

2.2.1.3 Radiation

Structures are usually considered in vacuum when discussing their dynamic behaviour. In reality, the surrounding medium (e.g. air or water) interacts with the structure changing its vibrational behaviour. Additionally, the structure radiates energy into the medium. The loss factor due to radiation is defined as

$$\eta = \frac{U_{rad}}{2\pi U_{rev}} \tag{2.6}$$

where U_{rad} is the radiated energy and U_{rev} is the reversible energy.

2.2.1.4   Gas pumping

Gas pumping or linear air pumping comes from entrapped air between two plates. The air is alternately compressed and rarified during vibration. The energy is dissipated because of the viscous friction of the gas between the surfaces of the plates. For thin plates, this damping mechanism can be dominant.

2.2.2   Material damping

Materials dissipate energy during cyclic deformation. For conventional structural materials (e.g. steel or aluminium), the energy dissipation is much smaller than for high damping alloys, polymer matrix composites and rubberlike materials.

2.2.2.1   High damping alloys

High damping alloys have lower stiffness, strength, corrosion resistance and thermal properties than structural materials. Their damping properties are highly nonlinear with respect to the mode of vibration, strain amplitude and temperature.

2.2.2.2   Composite laminates

The author refers to section 1.1.1 for a detailed description of the damping mechanisms in composite materials. Damping properties, like stiffness properties, are highly dependent of the fiber orientation. The loss factor along the fibers is different from the one of the transverse direction of the fiber. Section 2.5 details damping properties of laminated composites in terms of constituent material properties, fiber volume fraction, fiber orientation and stacking sequence.

2.2.2.3   Viscoelastic materials

The properties of viscoelastic materials are detailed in section 2.3.

2.3 Damping properties of viscoelastic materials

Viscoelastic materials are also called materials with memory: their behaviour depends of the loading history. The vibrational energy is dissipated into heat because of the relaxation process occuring in the long-chain molecules during vibration. They have frequency- and temperature-dependent properties.

2.3.1 Viscoelastic models

Viscoelasticity is the subject of materials with both elastic and viscous properties. The elastic element can be modeled by a linear spring with a stiffness coefficient k and the viscous element by a dashpot with a coefficient of viscosity c. Hence, viscoelastic models are combinations of linear springs and dashpots. The four classic viscoelastic models are here discussed [56].

2.3.1.1 The Maxwell model

It can be represented by a purely viscous damper and a purely elastic spring in series, as shown in Figure 2.1. The total strain is given by

$$\epsilon_{total} = \epsilon_{spring} + \epsilon_{dashpot} \tag{2.7}$$

with $\sigma_{spring} = k\epsilon_{spring}$ and $\sigma_{dashpot} = c\frac{d\epsilon_{dashpot}}{dt}$. The Maxwell model can be represented by the following equation

$$\frac{d\epsilon_{total}}{dt} = \frac{d\epsilon_{spring}}{dt} + \frac{d\epsilon_{dashpot}}{dt} \tag{2.8}$$

If the material is put under a constant strain, the stresses decrease gradually. If the material is put under a constant stress, the strain has two components: an elastic component corresponding to the applied stress and a viscous component that grows with time as long as the stress is

applied. One limitation of the model is that it does not predict creep
accurately.

Figure 2.1: Maxwell model

2.3.1.2   The Kelvin-Voigt model

This model, also known as the Voigt model, consists of a spring and a
dashpot in parallel as shown in Figure 2.2. It is used to explain the creep
behaviour of polymers. The constitutive relation is a linear first-order
differential equation

$$\sigma(t) = k\epsilon(t) + c\frac{d\epsilon(t)}{dt} \tag{2.9}$$

If a constant stress is applied, the material deforms at a decreasing rate,
asymptotically approaching the steady-state strain. When the stress is
released, the material relaxes gradually to its undeformed state. This
model is very good to model creep in materials but is much less accurate
to model relaxation.
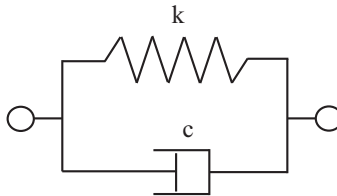
Figure 2.2: Kelvin-Voigt model

2.3.1.3 Standard linear model

The standard linear model is shown in Figure 2.3: it is a combination of the Maxwell model and a linear spring in-parallel. The governing constitutive equation is

$$\frac{d\epsilon}{dt} = \frac{k_2}{c_2\,(k_1 + k_2)} \left(\frac{c_2}{k_2}\frac{d\sigma}{dt} + \sigma - k_1 + \epsilon \right) \tag{2.10}$$

Under a constant stress, the modeled material will instantaneously deform to some strain, which is the elastic portion of the strain, and after that it will continue to deform and asymptotically approach a steady-state strain. This last portion is the viscous part of the strain.
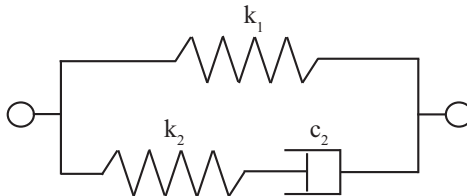
Figure 2.3: Standard linear model

2.3.1.4 Generalized Maxwell model

The generalized Maxwell model, also called the Maxwell-Weichert model, is the most general form of the models above described. It takes into account that the relaxation does not occur at a single time, but at a distribution of times (see Figure 2.4). This is realized by having as many Maxwell elements as necessary to accurately represent the distribution.
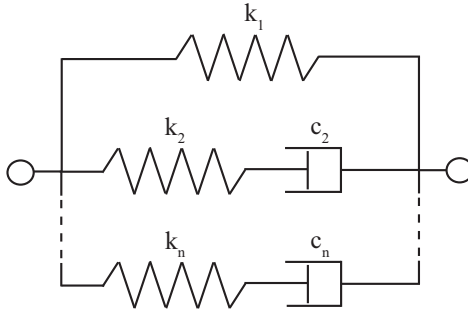
Figure 2.4: Generalized Maxwell model

2.3.2 Frequency domain behaviour

In the section, the behaviour of viscoelastic materials in the frequency domain is explained.

2.3.2.1 Viscoelastic behaviour

For most purposes, it is convenient to study the vibrational behaviour of viscoelastic materials in the frequency domain. Figure 2.5 presents the strain- and stress-time history for a viscoelastic material. The phase lag means that there is a velocity-dependent term in the stress-strain relationship, which, for $\tau(t) = \tau_0 sin(\omega t)$ and $\gamma = \gamma_0 sin(\omega t - \psi)$ is

$$
\begin{aligned}
\tau(t) &= \tau_0 sin(\omega t) \\
&= \tau_0 sin\left[(\omega t - \psi) + \psi\right] \\
&= \tau_0 sin(\omega t - \psi) cos(\psi) + \tau_0 cos(\omega t - \psi) sin(\psi) \\
&= \frac{\tau_0}{\gamma_0} cos(\psi \gamma(t)) + \frac{\tau_0}{\gamma_0 |\omega|} sin(\psi) \frac{d\gamma(t)}{dt}
\end{aligned}
$$

By writing that $G = (\tau_0/\gamma_0) cos(\psi)$ and $\eta = tan(\psi)$, it follows

$$\tau = G\gamma + \frac{G\eta}{|\omega|}\frac{d\gamma}{dt} \tag{2.11}$$

One obtains a similar equation for extensional deformation

$$\sigma = E\epsilon + \frac{E\eta}{|\omega|}\frac{d\epsilon}{dt} \tag{2.12}$$

where E is the Young's modulus for extensional deformation, G is the shear modulus and η is the loss factor. The second terms of Equation 2.11 and 2.12 represent the energy dissipation characteristics of the material under harmonic excitation.
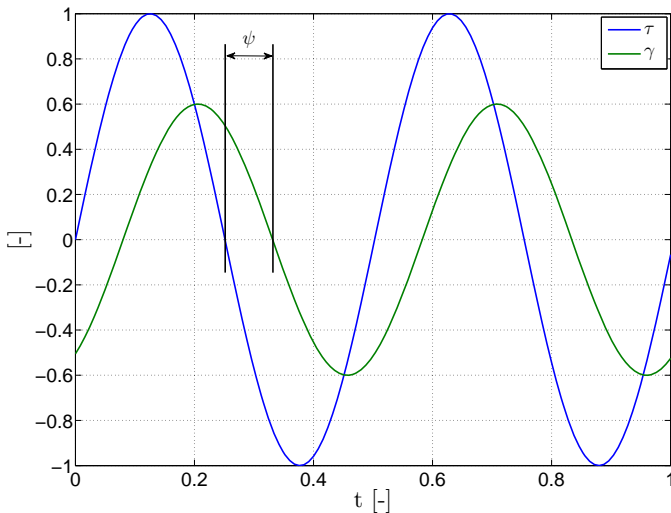
Figure 2.5: Harmonic excitation and response for a viscoelastic solid

2.3.2.2   Complex modulus model

It is difficult to use the approach described in the previous section to address most problems. A representation in terms of complex numbers is prefered. The strain is represented by $\gamma = \gamma_0 exp\,(i\omega t)$ and the strain rate by $\frac{d\gamma}{dt} = i\omega\gamma$. Equations 2.11 and 2.12 become

$$\tau = G\gamma + \frac{G\eta}{|w|}i\omega\gamma = G\left(1 + i\eta\frac{\omega}{|\omega|}\right)\gamma \qquad (2.13)$$

$$\sigma = E\epsilon + \frac{E\eta}{|w|}i\omega\epsilon = E\left(1 + i\eta\frac{\omega}{|\omega|}\right)\epsilon \qquad (2.14)$$

Assuming that ω is always positive, this reduces to

$$\tau = G\,(1 + i\eta)\,\gamma \qquad (2.15)$$

$$\sigma = E\,(1 + i\eta)\,\epsilon \qquad (2.16)$$

From Equations 2.15 and 2.16, one can define the complex moduli

$$G^* = G^{'} + G^{''} = G\,(1 + i\eta) \qquad (2.17)$$

$$E^* = E^{'} + E^{''} = E\,(1 + i\eta) \qquad (2.18)$$

where $G^{'}$ and $E^{'}$, the storage moduli, are a measure of the stiffness of the material, and $G^{''}$ and $E^{''}$, the loss moduli, are a measure of the capacity of the material to dissipate energy. The loss factor can also be expressed in terms of potential energies. The energy dissipated per cycle of vibration is calculated from

$$
\begin{aligned}
U_d &= \oint \tau d\gamma \\
&= \int_0^{2\pi/\omega} \tau \left(\frac{d\gamma}{dt} \right) \\
&= \int_0^{2\pi/\omega} \left[G' \gamma_0 sin\left(\omega t\right) + G'' \gamma_0 cos\left(\omega t\right) \right] \omega \gamma_0 cos\left(\omega t\right) dt \\
&= G'' \omega \gamma_0^2 \int_0^{2\pi/\omega} cos\left(\omega t\right)^2 dt \\
&= \pi G'' \epsilon_0^2
\end{aligned}
$$

The energy dissipated per cycle of vibration is proportional to the square of the strain amplitude but is independent of the frequency of excitation ω. The potential energy U_p can be evaluated in terms of the strain amplitude γ_0

$$
U_p = \frac{1}{2} G' \gamma_0^2 \tag{2.19}
$$

Finally, the loss factor can be defined as

$$
\eta = \frac{G''}{G'} = \frac{U_d}{2\pi U_p} \tag{2.20}
$$

A similar equation may be derived for the extensional strain. The loss factors for extension and shear are generally not equal. However, the differences are very small and unmeasurable in most cases.

2.3.3 Hysteresis behaviour

The stress-strain relation for a linear viscoelastic material under a repeated cyclic loading is an ellipse. The deformation occuring in the viscoelastic material follows a different path when a force is applied than when a force is released. Figure 2.6 presents the measured stress as a
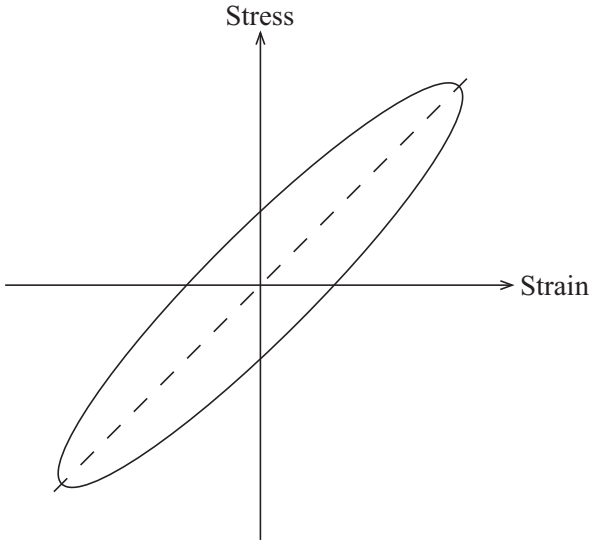
Figure 2.6: Ideal elliptical hysteresis loop

function of the measured strain. The slope of the major axis of the ellipse is a measure of stiffness and the aspect ratio (the ratio of the minor axis to the major axis is a measure of damping). The equation of the elliptical loop has the following form in the case of shear deformation

$$\tau(t) = G\gamma(t) \pm G\eta\sqrt{\gamma_0^2 - \gamma(t)^2} \tag{2.21}$$

where $\tau(t)$ is the shear stress at time t, $\gamma(t)$ is the shear strain at time t, γ_0 is the maximal strain amplitude at each cycle of the hysteresis loop, G is the shear modulus and η is the material loss factor. The positive and negative signs refer, respectively, to the upper and to the lower path of the loop. If the strain varies harmonically, one can write $\gamma(t) = \gamma_0 sin(\omega t)$ with ω being the frequency in radians. Equation 2.21 becomes

$$\begin{aligned}
\tau(t) &= G\gamma(t) \pm G\eta\gamma_0\sqrt{1-sin(\omega t)^2} \\
&= G\gamma(t) \pm G\eta\gamma_0 |cos(\omega t)| \\
&= G\gamma(t) \pm \frac{G\eta}{|\omega|}\frac{d\gamma(t)}{dt}
\end{aligned} \qquad (2.22)$$

A similar equation can be derived for extensional strain. The shape of the ellipse does not change with the strain amplitude but it changes with the loss factor.

2.3.4 Effects of environmental factors

The performances of viscoelastic materials are affected by temperature, frequency of vibration, amplitude of strain and static preload. This section presents the effects of these factors on the storage modulus and loss factor as they are the most important quantitites to describe such materials.

2.3.4.1 Effects of temperature

Temperature is considered as the most important environmental factor affecting the properties of damping materials. A typical plot of the storage modulus E' and η of rubberlike materials is presented in Figure 2.7. Temperature-affected material states can be divided into four regions: the glassy region, the transition region, the rubberlike region and the flow region. The glassy region occurs at room temperature: the storage modulus changes slowly in the glassy region while the loss factor increases sharply as the temperature increases. The second region is characterized by having a modulus that decreases rapidly with increasing temperature, while the loss factor reaches a maximum value at the transition temperature T_g. In the rubberlike region, E' and η remain nearly constant. In the fourth region, the material continues to soften with increasing temperature as it melts. The loss factor takes on a very high value. In engineering applications, most structures will not be used beyond T_g. The storage modulus could be as high as 10^5 GPa in the glassy region and as low as 10^{-2} GPa in the rubberlike region. The width of the transition region can go from 20°C to 200°C [57]. The loss factor in the glassy region is usually below

10^{-2} or 10^{-3}. It can reach values up to 1 or 2 in the transition region. In the rubberlike region, η varies between 0.1 and 0.3.
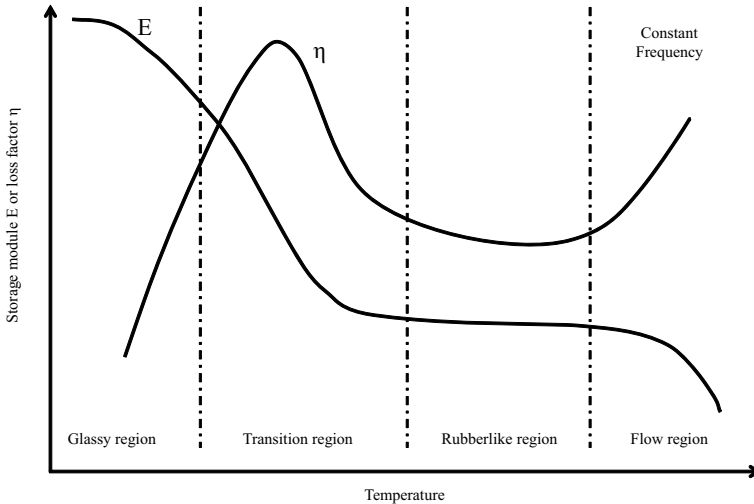
Figure 2.7: Effects of temperature on the storage modulus and loss factor from [57]

2.3.4.2   Effects of frequency

The effect of frequency on the storage modulus E' and the loss factor η can be divided into three regions: the rubberlike region, the transition region and the glassy region. Figure 2.8 presents the typical behaviour of E' and η as a function of frequency. In the rubberlike and glassy regions, the rate of increase of E' is very small; the largest rate of increase is observed in the transition region. Regarding the loss factor, it increases in the rubberlike region, reaches a maximum in the transition region and then decreases in the glassy region. Nevertheless, it is important to notice that a logarithmic scale is always needed to represent the frequency dependency. This means that the same change of E' and η is reflected over several orders of magnitude of frequency but on few degrees of temperature. Therefore, the effect of frequency on the strorage modulus and

loss factor is much smaller than the effect of temperature.
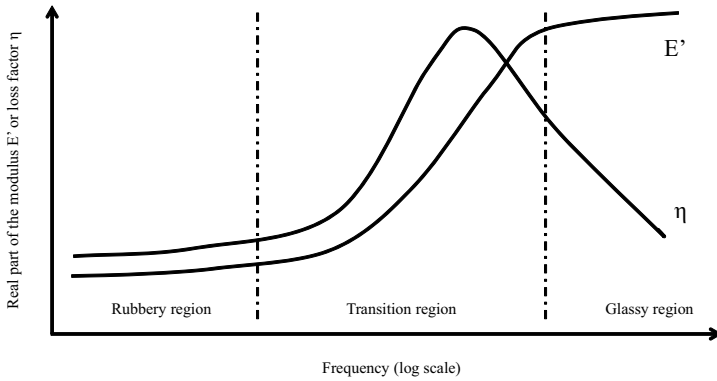

Figure 2.8: Effects of the frequency on the storage modulus and loss factor from [57]
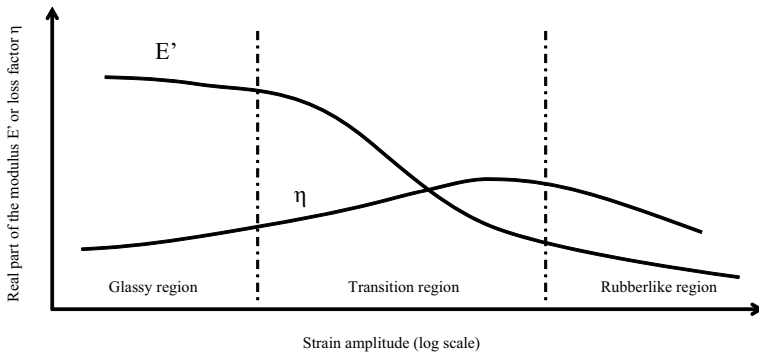

Figure 2.9: Effects of the strain amplitude on the storage modulus and loss factor from [57]

2.3.4.3   Effects of cyclic dynamic strain

The effects of dynamic strain amplitude on the properties of viscoelastic materials are very complex. High dynamic strain amplitude results in high dissipation of energy, and high energy dissipation increases the temperature in the material. Therefore, the effects of temperature and strain amplitude are combined. In the glassy region, the variations of $E^{'}$ and η with the strain amplitude are small. In the transition region, the storage modulus decreases sharply and the loss factor reaches a peak. In the rubberlike region, the effect of temperature is secondary compared to the effect of strain amplitude. A typical plot of the behaviour of the damping material in this region is shown in Figure 2.9.

2.3.4.4   Effects of static preload

The effects of static preload on the dynamic properties are usually the most important in the rubberlike region. The storage modulus increases with increasing the preload, whereas the loss factor decreases.

2.4   Vibration control using viscoelastic materials

Viscoelastic materials can be applied in a FLD or CLD configuration, as explained in section 1.1.3. This section details analytical and numerical models and methods for the analysis of FLD and CLD treatments.

2.4.1   Free layer damping treatment

As presented in Figure 1.3, the free layer damping treatment consists of a viscoelastic material applied on the surface of a structural membre. In this case, the stiffnessess can be added

$$k^* = k_1 + k_2 \left(1 + i\eta_2\right) \tag{2.23}$$

where k^* is the complex stiffness of the combination, k_1 is the stiffness

of the structural element, $k_2 \left(1 + i\eta_2\right)$ is the complex stiffness of the viscoelastic layer with η_2 being its loss factor. The effective stiffness and loss factor are

$$k = k_1 + k_2 \tag{2.24}$$

$$\eta = \frac{\eta_2}{1 + k_2/k_1} \tag{2.25}$$

The change of flexural stiffness is calculated from the dimensions of the beam and from the thickness and complex modulus of the viscoelastic layer by means of the equation 2.23 first introduced by Oberst [30]. The maximum loss factor depends of both η_2 and k_2/k_1. Oberst was one of the first to propose an equation for the change of stiffness

$$\frac{(EI)^*}{E_1 I_1} = 1 + \frac{E_2^*}{E_1} \left(\frac{H_2}{H_1}\right)^3 + 3 \left(1 + \frac{H_2}{H_1}\right)^2 \frac{\left(E_2^*/E_1\right)\left(H_2/H_1\right)}{1 + \left(E_2^*/E_1\right)\left(H_2/H_1\right)} \tag{2.26}$$

with

$$I_1 = \left(H_1\right)^3 / 12 \tag{2.27}$$

where H_1 is the thickness, E_1 the Young's modulus of the base structure and E_2 is the complex Young's modulus of damping layer. By calculating the real and the imaginary parts of the equation 2.27, one can determine the effective flexural rigidity and loss factor of the damped member. Oberst's equation is only valid for structural components deformed in bending and under the assumption that the plane sections remain plane.

2.4.2 Beams with constrained layer damping treatment

Ross, Ungar and Kerwin [58] were the first to develop a theory for the damping of bending vibrations by means of a constrained layer damping

treatment, also known as the RKU analysis. They considered the following assumptions:

- For the entire sandwich structure, there is a neutral axis, whose location varies with frequency.

- There is a perfect bonding between the different layers.

- The damping comes mainly from the shear deformation occuring in the viscoelastic material.

- The elastic layer holds the structural layer and the constraining layer at the same distance.

- The beam is infinitely long so that end effects may be neglected.

The flexural rigidity, EI, of the three-layer system is

$$EI = \frac{E_1 H_1^3}{12} + \frac{E_2 H_2^3}{12} + \frac{E_3 H_3^3}{12} - \frac{\left(E_2 H_2^2/12\right)(d-D)}{(1+g_2)} + E_1 H_1 D^2 +$$

$$E_1 H_1 D^2 + E_2 H_2 \left(H_{21} - D\right)^2 + E_3 H_3 \left(d - D\right)^2 -$$

$$\left(\frac{E_2 H_2 \left(H_{21} - D\right)}{2} + E_3 H_3 \left(d - D\right)\right) \frac{(d-D)}{(1+g_2)} \quad (2.28)$$

with

$$D = \frac{\left(E_2 H_2 \left(H_{21} - d/2\right) + g_2 \left(E_2 H_2 H_{21} + E_3 H_3 d\right)\right)}{\left(E_1 H_1 + E_2 H_2/2 + g_2 \left(E_1 H_1 + E_2 H_2 + E_3 H_3\right)\right)} \quad (2.29)$$

$$d = H_2 + \frac{(H_1 + H_3)}{2} \quad (2.30)$$

$$H_{21} = \frac{(H_1 + H_2)}{2} \quad (2.31)$$

$$g_2 = \frac{G^*}{E_3 H_3 H_2 p^2 1} \qquad (2.32)$$

where g_2 is called the shear parameter. It is the most important parameter controlling the effectiveness of the shear damping treatment. From equation 2.32, one can see that g_2 does not only depend on the shear modulus of the viscoelastic material but also on the wavelength, p, the thickness H_3 and the Young's modulus E_3 of the constraining layer. The RKU analysis is the most widely used and is very useful for simple structures. Using the work of Kerwin, Di Taranto [32] derived an equation of motion for freely vibrating beams having any boundary conditions. Yan and Dowell [59] used the principle of virtual work in the theory of elasticity and the theorem of correspondence to derive a set of five partial differential equations for vibrating three-layered damping sandwich plates and beams. Rao and Nakra [34] included the inertia effects of transverse longitudinal and rotatory motions for unsymmetrical sandwich structures. Mead and Markus [33] derived a differential equation of motion in terms of transverse displacement of sandwich beams subjected to a transverse loading.

2.4.3 Plates with constrained layer damping treatment

2.4.3.1 Differential equations of motion

Rao and Nakra [34] developed basic equations of vibratory bending of unsymmetrical sandwich plates. The effects of flexural and membrane energies are taken into account as well as the transverse shear in the core, rotatory, translatory and transverse inertia in both core and faces. The strain energy, U_s, of the sandwich plate is given by

$$U_s = \int \int \left[\frac{E_1 H_1}{2\left(1 - \nu_1^2\right)} \left(u_1'^2 + \nu_1 u_1' v_1^* + v_1^{*2} + \nu_1 v_1^* u_1' \right. \right.$$

$$\left. + \frac{(1 - \nu_1)}{2} \left(u_1^{*2} + v_1'^2 + 2u_1^* v_1' \right) \right)$$

$$+ \frac{E_3 H_3}{2\left(1 - \nu_3^2\right)} \left(u_3'^2 + \nu_3 u_3' v_3^* + v_3^{*2} + \nu_3 v_3^* u_3' \right.$$

$$\left. + \frac{(1 - \nu_3)}{2} \left(u_3^{*2} + v_3'^2 + 2u_3^* v_3' \right) \right) \quad (2.33)$$

$$+ \frac{E_1 H_1^3}{24\left(1 - \nu_1^2\right)} \left(w''^2 + 2\nu_1 w'' w^{**} + w^{**2} + 2\left(1 - \nu_1\right) w'^{*2} \right)$$

$$+ \frac{E_3 H_3^3}{24\left(1 - \nu_3^2\right)} \left(w''^2 + 2\nu_3 w'' w^{**} + w^{**2} + 2\left(1 - \nu_3\right) w'^{*2} \right)$$

$$+ \frac{G^* H_2}{2} \left(\left(\frac{u_1 - u_3}{H_2} \right)^2 + \left(\frac{v_1 - v_3}{H_2} \right)^2 + \left(w'^2 + w^{*2} \right) \left(\frac{d}{H_2} \right)^2 \right.$$

$$\left. \left. - \frac{2d}{H_2} \left(w' \frac{u_1 - u_3}{H_2} + w^* \frac{v_1 - v_3}{H_2} \right) \right) \right] dx dy$$

The kinetic energy, U_k, of the plate is

$$U_k = \frac{\rho}{2} \int \int \dot{w}^2 dx dy + \frac{1}{2} \int \int \left(\rho_1 H_1 \dot{u}_1^2 + \rho_3 H_3 \dot{u}_3^2 \right.$$

$$+ \dot{w}'^2 \frac{\rho_1 H_1^3 + \rho_3 H_3^3}{12} + \rho_1 H_1 \dot{v}_1^2 + \rho_3 H_3 \dot{v}_3^2$$

$$+ \dot{w}^{*2} \frac{\rho_1 H_1^3 + \rho_3 H_3^3}{12} + \rho_2 H_2 \left(\left(\frac{\dot{u}_1 + \dot{u}_2}{2} + \dot{w}' \epsilon_1 \right)^2 \right. \quad (2.34)$$

$$\left. + \left(\frac{\dot{v}_1 + \dot{v}_2}{2} + \dot{w}^* e_1 \right)^2 \right)$$

$$+ \frac{p_2 H_2}{2} \left(\left(\dot{u} - u_3 - \dot{w}' e_2 \right)^2 + \left(\dot{v} - v_3 - \dot{w}^* e_2 \right)^2 \right) \right) dx dy$$

with

$$\rho = \rho_1 H_1 + \rho_2 H_2 + \rho_3 H_3 \tag{2.35}$$

where the subscript 1 indicates the load carrying plate, 2 the core and 3 the constraining layer. w is the transverse displacement and u_i, v_i (with i=1,3) are the in-plane displacement components. The symbol prime ($'$) denotes the differentiation with respect to x, the symbol star ($*$) that to y and the dote ($\cdot$) to the time t. According to Hamilton's principle, the stationary value of $\bar{\bar{\Phi}}$ is equivalent to the equilibrium statement

$$\delta\bar{\bar{\Phi}} = \int_{t_1}^{t_2} \left(\delta U_k - \delta U_s - \delta U_p \right) dt \tag{2.36}$$

where t_1 and t_2 are any two instants of time. Performing the variation term by term, the following equations of motion are obtained for arbitrary virtual displacements

$$\phi_1 \left(u_1'' + \frac{1}{2}\left(1+\nu_1\right) v_1'^* + \frac{1}{2}\left(1-\nu_1\right) u_1^{**} \right) + \phi_2 \left(\frac{d}{H_2^2} w' - \frac{u_1 - u_3}{H_2^2} \right) \tag{2.37}$$
$$-\rho_1 H_1 \ddot{u}_1 - \rho_2 H_2 \left(\frac{\ddot{u}_1}{3} + \frac{\ddot{u}_3}{6} + \ddot{w}' e_3 \right) = 0$$

$$\phi_1 \left(v_1^{**} + \frac{1}{2}\left(1+\nu_1\right) u_1'^* + \frac{1}{2}\left(1-\nu_1\right) v_1'' \right) + \phi_2 \left(\frac{d}{H_2^2} w^* - \frac{u_1 - u_3}{H_2^2} \right) \tag{2.38}$$
$$-\rho_1 H_1 \ddot{v}_1 - \rho_2 H_2 \left(\frac{\ddot{v}_1}{3} + \frac{\ddot{v}_3}{6} + \ddot{w}^* e_3 \right) = 0$$

$$\phi_3 \left(u_3'' + \frac{1}{2}\left(1+\nu_3\right) v_3'^* + \frac{1}{2}\left(1-\nu_3\right) u_3^{**} \right) - \phi_2 \left(\frac{d}{H_2^2} w' - \frac{u_1 - u_3}{H_2^2} \right) \tag{2.39}$$
$$-\rho_3 H_3 \ddot{u}_3 - \rho_2 H_2 \left(\frac{\ddot{u}_1}{3} + \frac{\ddot{u}_3}{6} + \ddot{w}' e_4 \right) = 0$$

$$\phi_3 \left(v_3^{**} + \frac{1}{2} \left(1 + \nu_3 \right) u_3^{'*} + \frac{1}{2} \left(1 - \nu_3 \right) u_3^{''} \right) - \phi_2 \left(\frac{d}{H_2^2} w^* - \frac{v_1 - v_3}{H_2^2} \right) (2.40)$$

$$-\rho_3 H_3 \ddot{v}_3 - \rho_2 H_2 \left(\frac{\ddot{v}_1}{3} + \frac{\ddot{v}_3}{6} + \ddot{w}^* e_4 \right) = 0$$

$$\left(D_1 + D_3 \right) \nabla^4 w - \gamma_2 \frac{d}{H_2^2} \left(d \left(w^{''} + w^{**} \right) - u_1^{'} + u_3^{'} - v_1^* + v_3^* \right)$$

$$-\frac{1}{12} \left(\rho_1 H_1^3 + \rho_3 H_3^3 \right) \left(\ddot{w}^{''} + \ddot{w}^{**} \right) - \rho_2 H_2 \big(e_3 \left(\ddot{u}^{'} + \ddot{v}_1^* \right) \quad (2.41)$$

$$+ e_4 \left(e_1^2 + \frac{e_2^2}{12} \right) \left(\ddot{w}^{''} + \ddot{w}^{**} \right) \big) + \rho \ddot{+} Q \left(x, y \right) g \left(t \right) = 0$$

with

$$\nabla^4 w = \frac{\partial^4 w}{\partial x^4} + 2 \frac{\partial^4 w}{\partial x^2 \partial y^2} + \frac{\partial^4 w}{\partial y^4} \qquad (2.42)$$

$$\phi_i = \frac{E_i H_i}{1 - \nu_i^2} \qquad (2.43)$$

$$\phi_2 = G^* H_2 \qquad (2.44)$$

$$D_i = \frac{E_i H_i^3}{12 \left(1 - \nu_i^2 \right)} \qquad (2.45)$$

$$e_1 = \frac{H_3 - H_1}{4} \qquad (2.46)$$

$$e_2 = \frac{H_1 + H_3}{2} \qquad (2.47)$$

$$e_3 = \frac{H_2 - 2H_1}{12} \tag{2.48}$$

$$e_4 = \frac{2H_3 - H_1}{12} \tag{2.49}$$

where $Q(x,,y)$ and $g(t)$ are concentrated loads. The derived equations of motions are valid under the following assumptions:

- A plane transverse to the middle surface remains plane before bending and perpendicular to the mid surface after bending.

- Transverse displacement at a section does not vary along the thickness.

- All displacements are small.

- There is a perfect bonding between the different layers.

- The extension effect in the core are ignored and stresses in the core are considered as negligible.

Based on these equations of motion, Rao and Nakra [34] derived analytical solutions for different boundary conditions.

2.4.4   Finite element modeling of structural element with constrained viscoelastic treatments

2.4.4.1   Overview

As presented in section 2.1, the discretized version of the differential equation for the free vibration of any structural system is

$$[M]\{\ddot{u}\} + [C]\{\dot{u}\} + [K]\{u\} = \{F\} \tag{2.50}$$

Considering that

$$[u] = \sum_{n=0}^{\infty} [X_n^*]\, e^{iw_n^* t} \tag{2.51}$$

and substituing Equation 2.51 in Equation 2.50, one obtains the following eigenvalue problem

$$\left([K] - w_n^{*2}\,[M] + iw_n^*\,[C]\right) = 0 \tag{2.52}$$

where w_n^* and $[X_n^*]$ are the *nth* complex eigenvalue and eigenvector.

2.4.4.2   Numerical example

To validate the finite element modeling of constrained layer damping treatment, the experimental work of Liebowitz et. al [60] is taken as reference. They tested cantilever beams on top of which is bonded a CLD treatment. The samples are clamped on one side and excited at their free-end. The samples are 0.3 m long and 0.012 m wide. The material properties of the load-carrying beam and the constraining layer are given in Table 2.1. Two cases of thicknesses are considered, see Table 2.2.

Table 2.1: Material data of the base beam and constraining layer

E-modulus $[MPa]$	Poisson ratio $[-]$	Loss factor $[-]$	Density $[kg.m^{-3}]$
68,900	0.33	0.005	2700

Table 2.2: Layer thicknesses for the two considered cases [60]

	Case 1	Case 2
Thickness of the base beam [mm]	5.5	4
Thickness of the viscoelastic layer [mm]	0.8	1.7
Thickness of the constraining layer [mm]	2	4

The viscoeleastic material has a frequency-dependent shear modulus and loss factor given by

$$G_d(f) = 1.007 \times 10^{-3} \times f + 1.386 \times 10^6 \qquad (2.53)$$

$$\eta(f) = 1.608 \times 10^{-4} \times f + 0.256 \qquad (2.54)$$

For the numerical modeling, the commercial sotfware ANSYS is used. The different layers are modeled with structural elements SOLID183. They utilize three translations at each of the 20 nodes. They also have the feature, if activated, to input frequency- and temperature-dependent elastic constants and loss factor with the ANSYS command TB,ELASTIC and TB,SDAMP. For finite element models having multiple layers with frequency-dependent material properties, the stiffness and damping matrix have the following form

$$[K] = \sum_{e=1}^{N_e} [K_e (E(w))] \qquad (2.55)$$

$$[C] = \alpha [M] + \beta [K] + \sum_{j=1}^{N_{mat}} \beta_j [K_j] + \beta_c [K] + [C_\zeta] + \sum_{e=1}^{N_e} [C_e] \quad (2.56)$$

with

- α constant mass matrix multiplier. It represents friction damping occuring in the structure. As perfect bonding is considered between the different layers, it is equal to 0.

- β constant stiffness matrix multiplier. It represents the damping of the whole structure regardless of frequency. As it cannot be used for models with multiple materials, it is set to 0.

- β_j constant stiffness material multiplier, material-dependent damping. It is like β but for a given material. It is constant over the entire frequency range of the analysis. As it cannot be used for frequency-dependent material properties, it is taken equal to 0.

- β_c variable stiffness matrix multiplier. It is used to input a constant damping ratio to the whole structure having a dominant natural frequency. It is expressed as followed

$$\beta_c = \frac{2\zeta}{\omega_n} = \frac{\eta}{\omega_n} \tag{2.57}$$

As the structure of interest is made of different materials with frequency-dependent properties, it is set to 0.

- ζ constant material damping ratio. From Eq. 2.57, it comes

$$\zeta = \frac{\eta}{2} \tag{2.58}$$

where η is the material loss factor. It is not suitable for frequency-dependent damping properties. Therefore, it is taken equal to 0.

- $[C_\zeta]$ frequency-dependent damping matrix. It is calculated from a specified ζ_r (damping ratio for mode r).

- $[C_e]$ element damping matrix. For each element type, it is possible to give frequency-dependent damping properties. It is defined as

$$[C_e] = \beta(\omega)[K_e] \tag{2.59}$$

where $\beta(\omega)$, equal to $\eta_i(\omega)/\omega$, is the frequency-dependent damping coeffient. It is calculated with $\eta(\omega)$ the frequency-dependent material loss factor (obtained from Equation 2.54) and the frequency ω.

In order to calculate the eigenfrequency of the system, a damped modal analysis is performed. Then, an harmonic analysis is done at the desired resonance frequency. The modal loss factor is calculated with modal strain energy method by the following equation

$$\eta_k = \frac{\sum_{i=1}^{n} \eta_{i,k} U_{s,i,k}}{U_{s,total,k}} \tag{2.60}$$

where $\eta_{i,k}$ is the material loss factor of the layer i at mode k, and $U_{s,i,k}$ is the modal strain energy of the layer i at mode k. $U_{s,total,k}$ is the total modal strain energy at mode k and is given by

$$U_{s,total,k} \quad = \quad \sum_{i=1}^{n} U_{s,i,k} \qquad (2.61)$$

However, the method gives good estimates only if the following conditions are fulfilled:

- The structure must be in a state of harmonic oscillation.

- The structural damping must be weak enough for the eigenmodes and eigenfrequencies of the undamped system to approximate the real eigenmodes and eigenfrequencies.

- The frequency influence on the storage modulus of the viscoelastic material must not perceptibly affect the stiffness of the total structure.

The first assumption is fulfilled as an harmonic analysis is performed at the desired resonance frequency. The second does not apply as the damped model is considered in the modal analysis. The third assumption is considered as fulfiled as the shear modulus of the viscoelastic material at 100 Hz is significantly smaller than the Young's modulus of the base beam. The comparison between the experimental and numerical results are presented in Table 2.3 and Table 2.4 for case 1 and 2, respectively. A good agreement bewteen the experimental results and the numerical model is obtained. The largest difference is observed for case 2. There is a difference of 0.6% for the resonance frequency and of 6.4% for the modal loss factor.

Table 2.3: Results comparison for case 1

	$f\ [Hz]$	$\eta\ [\%]$
Experimental results [60]	139.5	6.2
Finite element results	139.2	6.1

Table 2.4: Results comparison for case 2

	$f\ [Hz]$	$\eta\ [\%]$
Experimental results [60]	115.5	7.8
Finite element results	114.8	7.3

2.5 Damping of composite laminates

This section details the micromechanics theory developed by Saravanos and Chamis [11] for the damping of unidirectional and off-axis composites. In contrast with other research works [5, 6, 7, 8, 9], they presented a complete micromechanics theory for six damping coefficients of a composite ply associated with the following stresses:

- Longitudinal, σ_{11};

- Transverse, σ_{22};

- Through the thickness normal stress, σ_{33};

- In-plane shear, σ_{12};

- Through the thickness shear, σ_{13} and σ_{23}.

2.5.1 On-axis damping

Figure 2.10 presents a segment of fiber/matrix. If a uniform cyclic longitudinal normal stress σ_{l11} is applied, the dissipated energy is then

$$\delta U = \frac{1}{2} \int_{Vf} \eta_{f11} \sigma_{f11} \epsilon_{f11} dV_f + \frac{1}{2} \int_{Vm} \eta_{mn} \sigma_{fmn} \epsilon_{fmn} dV_m \qquad (2.62)$$

The indices f and mn denote, respectively, the fiber and matrix properties in the normal direction of the fiber. As the damping is assumed to be independent of stress and strain, one can write
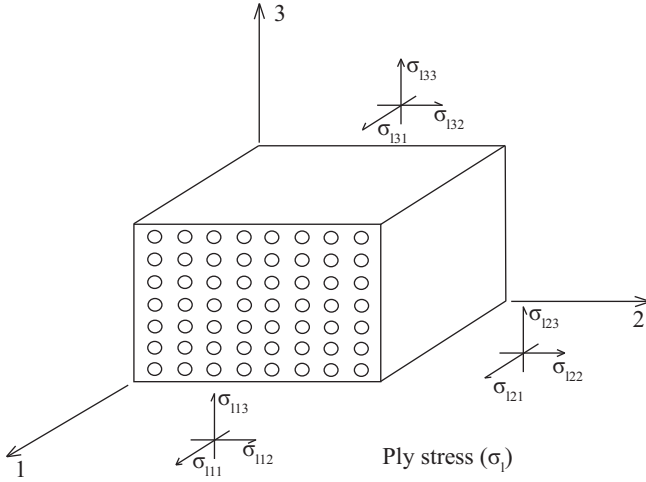
Figure 2.10: On-axis fiber composite plies

$$\delta U_s = \frac{1}{2}\eta_{f11}\int_{Vf}\sigma_{f11}\epsilon_{f11}dV_f + \frac{1}{2}\eta_{mn}\int_{Vm}\sigma_{fmn}\epsilon_{fmn}dV_m \qquad (2.63)$$

Considering that

$$\delta U_{s,l11} = \eta_{l11}U_{s,l11} \qquad (2.64)$$

The maximun stored strain energy during one cycle of vibration is

$$U_{s,l11} = \frac{1}{2}\int_{Vf}\sigma_{f11}\epsilon_{f11}dV_f + \frac{1}{2}\int_{Vm}\sigma_{mn}\epsilon_{mn}dV_m \qquad (2.65)$$

From Equation 2.65, one obtains the rule of mixtures for the longitudinal modulus

$$E_{l11} = v_f E_{f11} + v_m E_m \qquad (2.66)$$

Combining Equations 2.63, 2.64 and 2.65, the loss factor in the longitudinal direction is

$$\eta_{l11} = \eta_{f11} v_f \frac{E_{f11}}{E_{l11}} + \eta_{mn} v_{mn} \frac{E_m}{E_{l11}} \tag{2.67}$$

For cyclic transverse normal stress σ_{l22}, the dissipated and maximum strain energy, respectively, are

$$\delta U_{s,l22} = \frac{1}{2} \int_{Vf} \eta_{f22} \sigma_{f22} \epsilon_{f22} dV_f + \frac{1}{2} \int_{Vm} \eta_{mn} \sigma_{fmn} \epsilon_{fmn} dV_m \tag{2.68}$$

$$U_{s,l22} = \frac{1}{2} \int_{Vf} \sigma_{f22} \epsilon_{f22} dV_f + \frac{1}{2} \int_{Vm} \sigma_{fmn} \epsilon_{fmn} dV_m \tag{2.69}$$

Assuming a uniform stress distribution within the fiber and the matrix [11] and combining Equations 2.68 and 2.69, one obtains the transverse normal loss factor

$$\eta_{l22} = \eta_{f22} \sqrt{v_f} \frac{E_{22}}{E_{f22}} + \eta_{mn} \left(1 - \sqrt{v_f}\right) \frac{E_{22}}{E_m} \tag{2.70}$$

with

$$E_{22} = \left(1 - \sqrt{v_f}\right) E_m + \frac{\sqrt{v_f} E_m}{1 - \sqrt{v_f} \left(1 - \frac{E_m}{E_{f22}}\right)} \tag{2.71}$$

As the composite material is transversely isotropic, the transverse through-the-thickness loss factor is

$$\eta_{l33} = \eta_{l22} \tag{2.72}$$

Using the same assumptions and similar procedure than for the transverse damping, the in-plane shear loss factor is given by

$$\eta_{l12} = \eta_{f12}\sqrt{v_f}\frac{G_{12}}{G_{f12}} + \eta_{ms}\left(1 - \sqrt{v_f}\right)\frac{G_{12}}{G_m} \tag{2.73}$$

with

$$G_{12} = \left(1 - \sqrt{v_f}\right)G_m + \frac{\sqrt{v_f}G_m}{1 - \sqrt{v_f}\left(1 - \frac{G_m}{G_{f12}}\right)} \tag{2.74}$$

As composite materials are transversely isotropic, the interlaminar loss factor η_{l13} is equal to the in-plane loss factor of the ply

$$\eta_{l13} = \eta_{l12} \tag{2.75}$$

The out-of-plane shear loss factor is obtained in a similar way

$$\eta_{l23} = \eta_{f23}\sqrt{v_f}\frac{G_{l23}}{G_{f13}} + \eta_{ms}\left(1 - \sqrt{v_f}\right)\frac{G_{l23}}{G_m} \tag{2.76}$$

with

$$G_{l23} = \frac{E_{l22}}{2\left(1 + \nu_{l23}\right)} \tag{2.77}$$

$$\nu_{l23} = \frac{\nu_m}{1 - v_f\nu_m} + v_f\left(\nu_{f23} - \frac{(1 - v_f)\nu_m}{1 - v_f\nu_m}\right) \tag{2.78}$$

2.5.2 Off-axis ply damping

Figure 2.11 displays the off-axis cyclic loading. More than one of the on-axis loss factors contribute to the composite damping. The hysteretic
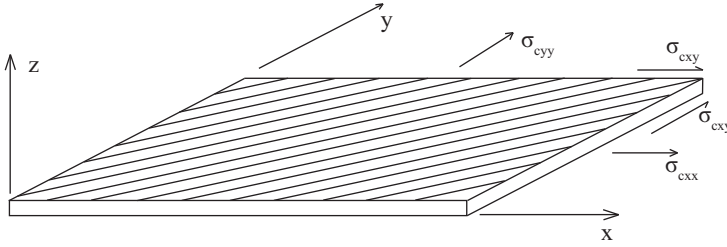
Figure 2.11: Off-axis fiber composite plies

strain energy loss per unit volume in the structural (off-axis) coordinate, noted with the index c, is

$$\delta U =_s \frac{1}{2} \{\sigma_c\}^T \{\eta_c\} \{\epsilon_c\} \tag{2.79}$$

For the on-axis case with motion along the fiber direction, the hysteretic strain energy loss per unit volume is

$$\Delta U = \frac{1}{2} \{\sigma_l\}^T \{\eta_l\} \{\epsilon_l\} \tag{2.80}$$

Transforming the stress and strain from the material coordinate system to the structural coordinate system, the specific strain energy loss becomes

$$\Delta U = \frac{1}{2} \{\sigma_c\}^T [R_\sigma]^T [\eta_l] [R_\sigma^{-1}]^T \{\epsilon_c\} \tag{2.81}$$

with

$$\{\sigma_c\} = [E_c] \{e_c\} \tag{2.82}$$

$$[E_c]^{-1} = [R_\sigma]^T [E_l]^{-1} [R_\sigma] \tag{2.83}$$

$$[R_\sigma] = \begin{bmatrix} cos^2\theta & sin^2\theta & cos2\theta \\ sin^2\theta & cos^2\theta & -sin2\theta \\ -0.5sin2\theta & 0.5sin2\theta & cos2\theta \end{bmatrix} \tag{2.84}$$

$$[E_c]^{-1} = \begin{bmatrix} 1/E_{cxx} & \nu_{cyx}/E_{cyy} & \nu_{csx}/G_{cxy} \\ -\nu_{cxy}/E_{cxx} & 1/E_{cyy} & \nu_{csy}/G_{cxy} \\ \nu_{cxs}/E_{cxx} & \nu_{cys}/E_{cyy} & 1/G_{cxy} \end{bmatrix} \tag{2.85}$$

Combining Equations 2.79 and 2.80, one obtains the following damping transformation

$$[\eta_c] = [R_\sigma]^T [\eta_l] \left[R_\sigma^{-1} \right]^T \tag{2.86}$$

In the case of on-axis loading, the damping matrix is diagonal

$$[\eta_c] = \begin{bmatrix} \eta_{l11} & 0 & 0 \\ 0 & \eta_{l22} & 0 \\ 0 & 0 & \eta_{l33} \end{bmatrix} \tag{2.87}$$

In the case of off-axis loading, the damping matrix is fully populated

$$[\eta_c] = \begin{bmatrix} \eta_{cxx} & \eta_{cxy} & \eta_{cxs} \\ \eta_{cyx} & \eta_{cyy} & \eta_{cys} \\ \eta_{csx} & \eta_{csy} & \eta_{css} \end{bmatrix} \tag{2.88}$$

The nondiagonal terms represent the coupling between the axial and shear stresses.

2.6 Composite structures with embedded damping layers

In order to predict the damping properties of composite structures with embedded damping layers, Saravanos and Pereira [44] developed a discrete layer laminate damping theory (DLTD) incorporating a piecewise

continuous displacement field through the thickness [45] in order to model composite laminates including the effect of thicker sections, interlaminar inhomogeneity and compliant interlaminar layer. Compared with other laminate theories [3, 10, 44], the DLDT provides more accurate strain and dissipative-energy calculation in each ply. The displacement field has the following form [61]

$$
\begin{aligned}
u\left(x, y, z, t\right) &= u^0\left(x, y, t\right) + \sum_{j=1}^{N} u^j\left(x, y, t\right) F^j\left(z\right) \\
v\left(x, y, z, t\right) &= v^0\left(x, y, t\right) + \sum_{j=1}^{N} v^j\left(x, y, t\right) F^j\left(z\right) \qquad (2.89) \\
w\left(x, y, z, t\right) &= w^0\left(x, y, t\right)
\end{aligned}
$$

where *0* represents the uniform through-the-thickness midplane deflection, u^j and v^j are displacements along the x- and y-direction at the interfaces between composite plies and interlaminar damping layers. $F^i\left(z\right)$ are interpolation functions. Therefore, the assumed in-plane displacement field can represent extensional, flexural, shear, coupled deformation and interlaminar shear strains through the thickness of the laminate. From Equations 2.89, the laminate strains are the following

$$
\begin{aligned}
\epsilon_{ci}\left(x, y, z, t\right) &= \epsilon_{ci}^0\left(x, y, t\right) + \sum_{j=1}^{N} \epsilon_{ci}^j\left(x, y, t\right) F^j\left(z\right) \\
&\qquad\qquad\qquad\qquad\qquad i = 1, 2, 6 \\
\epsilon_{ci}\left(x, y, z, t\right) &= \epsilon_{ci}^0\left(x, y, t\right) + \sum_{j=1}^{N} \epsilon_{ci}^j\left(x, y, t\right) F_{,z}^j\left(z\right) \qquad (2.90) \\
&\qquad\qquad\qquad\qquad\qquad i = 4, 5
\end{aligned}
$$

where the midplane strains are

$$\begin{aligned}
\epsilon_{c1}^0 &= u_{,x}^0 \\
\epsilon_{c2}^0 &= v_{,y}^0 \\
\epsilon_{c6}^0 &= u_{,y}^0 + v_{,x}^0 \\
\epsilon_{c4}^0 &= w_{,y}^0 \\
\epsilon_{c5}^0 &= w_{,x}^0
\end{aligned} \tag{2.91}$$

and the generalized strains are

$$\begin{aligned}
\epsilon_{c1}^j &= u_{,x}^j \\
\epsilon_{c2}^j &= v_{,y}^j \\
\epsilon_{c6}^j &= u_{,y}^j + v_{,x}^j \\
\epsilon_{c4}^j &= v^j \\
\epsilon_{c5}^j &= u^j
\end{aligned} \tag{2.92}$$

The comma in the subscripts denotes the differentation. Assuming viscoelastic constituents, the viscoelastic law between generalized stresses and strains at the ply level can be written as the following [62]

$$\{\sigma_c\} = \left[\tilde{Q}_c\right] * \{\epsilon_c\} = \int_{-\infty}^{t} \left[\tilde{Q}\left(t - \tau\right)\right] d\left\{\epsilon\left(\tau\right)\right\} \tag{2.93}$$

where $[Q_c^*]$ is the complex stiffness matrix. Combining Equations 2.93 and 2.90, and integrating through-the-thickness of the laminate, one obtains the following stress-strain relation in the time domain

$$\{N^0(t)\} = \int_{-h/2}^{h/2} \{\sigma\}\,dz = \left[\tilde{A(t)}\right] * \{\epsilon^0(t)\}$$

$$+ \sum_{m=1}^{N} \left[\tilde{B}^m(t)\right] * \{\epsilon^m(t)\} \qquad (2.94)$$

$$\{N^j(t)\} = \int_{-h/2}^{h/2} \{\sigma\}\,F^j\,dz = \left[\tilde{B}^j(t)\right] * \{\epsilon^0(t)\}$$

$$+ \sum_{m=1}^{N} \left[\tilde{D}^{jm}(t)\right] * \{\epsilon^m(t)\}$$

where $\{N^0\}$ and $\{N^j\}$ are the generalized stresses. The complex laminate stiffness matrices include both elastic and damping matrices

$$
\begin{aligned}
[A^*] &= [A^*] + i\,[A_d] \\
[B^{*j}] &= [B^j] + i\left[B_d^j\right] \qquad (2.95) \\
[D^{*jm}] &= [D^{jm}] + i\left[D_d^{jm}\right]
\end{aligned}
$$

where $[A_d]$ is the extensional laminate damping matrix, $\left[B_d^j\right]$ are the damping coupling matrices and $\left[D_d^{jm}\right]$ are flexural/shear damping matrices, see [45]. The dissipated strain energy per unit area of the laminate, $\Delta U_{s,l}$ is defined as

$$\Delta U_{s,l} = \frac{1}{2}\left(\{\epsilon_c^0\}^T [A_d]\{\epsilon_c^0\} + 2\{\epsilon_c\}^T \sum_{j=1}^{N}\left[B_d^j\right]\{\epsilon_c^j\} + \qquad (2.96)\right.$$

$$\left. \sum_{j=1}^{N}\sum_{m=1}^{N}\{\epsilon_c^j\}^T\left[D_d^{jm}\right]\{\epsilon_c^m\} \right)$$

The maximum laminate strain energy per unit area, $U_{s,l}$, is defined as

$$U_{s,l} = \frac{1}{2}\left(\left\{\epsilon_c^0\right\}^T [A_d] \left\{\epsilon_c^0\right\} + 2\left\{\epsilon_c^T\right\} \sum_{j=1}^{N} \left[B^j\right] \left\{\epsilon_c^j\right\} + \right.$$

(2.97)

$$\left. \sum_{j=1}^{N}\sum_{m=1}^{N} \left\{\epsilon_c^j\right\}^T \left[D^{jm}\right] \left\{\epsilon_c\right\} \right)$$

The interlaminar damping layers are considered as individual plies having isotropic elastic and damping matrices $[Q_c]$ and $[\eta_c]$. Therefore, the laminate damping mechanics of Saravanos and Pereira [45] can handle any composite material, number of plies, damping layers and laminate lay-ups.

Chapter 3

Segmented constrained layer damping treatment

This chapter investigates the possibility to improve the damping performance of constrained layer damping treatment by means of segmentation.

3.1   Introduction

Plunkett and Lee [63] invented the concept of segmenting CLD treatments. They showed that the damping performance of CLD treatments can be improved by cutting the damping treatment through the thickness. Therefore, the shear strain in the viscoelastic layer can be locally increased which leads to an increase of the energy dissipation. Their study included experiments and derivation of a formula for optimum distance of their equidistant cuts arrangement. Torvik and Strickland [64] investigated a structure consisting of a base plate with a multiple-layer damping treatment with unanchored constrained layers, attached to one side of it. They assumed a rectangular plate with segments of constrained layer damping material. The segments were not designed according to the deformation of the plate at the frequency of interest. Mantena et. al [65] also investigated the optimal side length of constrained layer damping material. They considered various geometric arrangements of a load-carrying struc-

ture in terms of the clamping situation with special regards to the damping material. The main limitation of their work is that they focused their investigation on a single mode and considered just one segment. Kung and Singh [66] developed an energy-based approach of multiple constrained layer damping patches. Lesieutre and Lee [67] performed a finite element analysis on segmented active constrained layer damping. Liu and Wang [68] investigated the distribution of passive and active constrained layer damping patches. In both papers, no length optimization of the damping treatment was performed. In the field of structural optimization, genetic algorithms have been used by Trompette and Fatemi [69], and by Al-Ajmi and Bourisli [70] to optimize the segments' length. They were only able to identify a distribution of segments for a single mode. The main limitations of the studies above presented are that they do not address the following questions:

- What are the damping performances of segmented CLD treatments at higher bending modes than the first one?

- Is it possible to optimize simultaneously several modes using a single distribution of segments?

- For a plate-like structure, what is the best segment topology?

These questions are important when one wants to obtain the best design solution that provides the largest amount of energy dissipation over the largest frequency range. The first two questions are addressed considering a beam-like structure in section 3.2. Section 3.2.1 presents the structure of interest and the related finite element modeling. Section 3.2.3 explains the mechanism of segmented constrained layer damping treatment. Results for equally spaced cuts are presented in section 3.2.4. An optimization method is presented in Section 3.2.5 to maximize the loss factors of the first four bending modes. The last question is addressed in section 3.3. Section 3.3.1 presents the finite element model. A topology study is performed in section 3.3.2. An optimization technique is used in section 3.3.3 to identify the characteristic of the segments arrangement that maximizes the loss factor. A conclusion is drawn in section 3.4.

3.2 Beam-like structure with segmented constrained layer damping treatment

3.2.1 Finite element modeling

The structure of interest is a cantilever beam on which is bonded a constrained layer damping treatment, see Figure 3.1. Plane elements are used in order to reduce the computation time which is important to consider for the optimization later presented in this chapter. The base beam and the constraining layer are modeled using plane42 element with the commercial software ANSYS. The viscoelastic core is modeled with plane182 elements. It has the feature to specify the material parameters (shear modulus and loss factor) as a function of frequency and temperature, like solid186 used section 2.4.4.2.
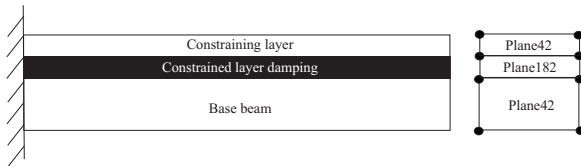
Figure 3.1: Finite element model of a constrained layer damping treatment

Table 3.1: Thicknesses table

	Thickness [mm]
Beam	10
Constrained layer	1
Constraining layer	1

The load-carrying beam and the constraining layer are made of aluminium. The total length of the beam is of 1 m. The thickness of each layer is given in Table 3.1. The finite element model includes details of a realistic clamping situation as illustrated in Figure 3.2. It takes into ac-

count the influence of the clamping on the vibration damping properties
of the beam. The material parameters of the different layers are presented
in Table 3.2.

Figure 3.2: Dimension of the numerical model

Table 3.2: Material parameters

	E-modulus [MPa]	Poisson ratio [-]	Loss factor [-]	Density [kg.m^{-3}]
Beam	69,000	0.33	0.005	2700
Viscoelastic layer	-	0.48	-	1000
Constraining layer	69,000	0.33	0.005	2700

The shear modulus and loss factor are taken from the material called
EAR C-2003 that is typically used in the automotive industry. The mate-
rial properties are extracted from its nomogram representation, see Figure
3.3. It enables to represent the temperature and frequency dependency of
the dynamic shear modulus and loss factor. Such plot is possible because
the effects of temperature and frequency can be actually combined in a
single variable called the reduced frequency. The author refers to [71, 72]
for further details on reduced frequency analysis. The outcome is a plot of
the log of the dynamic shear modulus and loss factor as a function of the
log of the reduced frequency. The effect of the temperarure is displayed

using isotherms. On Figure 3.3, the green lines show how to determine, for a given frequency (10 Hz) and temperature (20°C), the dynamic shear modulus and loss factor. The material properties of the viscoelastic materials are red from 10 Hz to 500 Hz at $20°C$ every 25 Hz and input in the finite element model with the method presented in section 2.4.4.2.
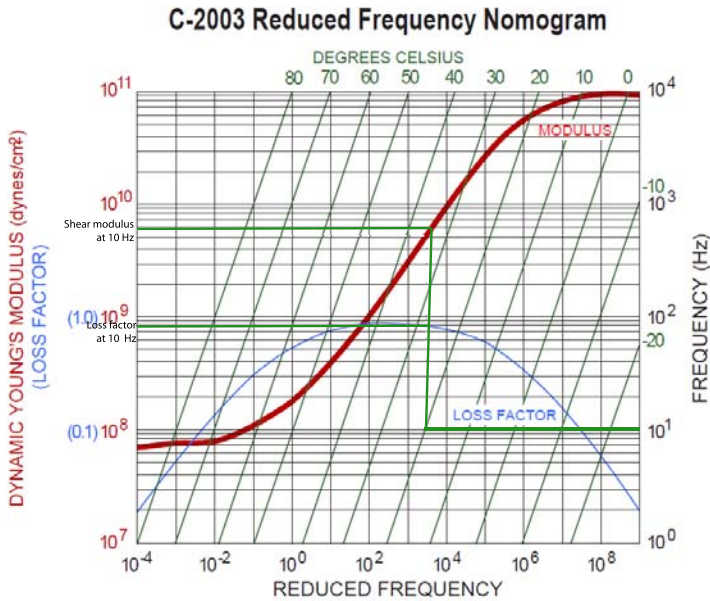
Figure 3.3: Reduced frequency nomogram of EAR C-2003 from [73]

3.2.2 Edge effect

The efficiency of segmenting a constrained layer damping treatment relies on the fact that a high-shear region is created in the viscoelastic layer. Such phenomenon is observed by looking at the deformation of the damping layer at the free end of the cantilever beam. It is called "edge effect" and is illustrated in Figure 3.4. From such observation comes the idea of segmenting a constrained layer damping material. Indeed, one can easily assume that by cutting the damping treatment at several positions, it

will increase the total shear deformation occuring on the visceolastic layer compared to a full coverage configuration.
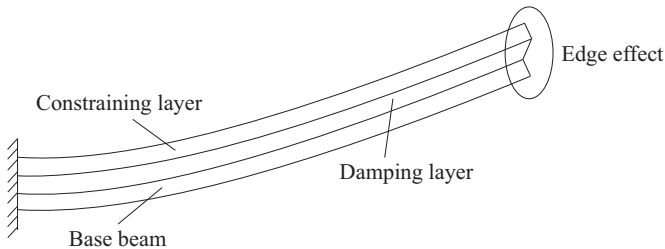
Figure 3.4: Edge effect at the free end of a cantilever beam

3.2.3   Damping performance

This section investigates where a cut should be located in order to reach the maximal shear deformation considering the third bending mode (see upper graphic of Figure 3.5). Four different cases are studied:

- A beam with full coverage;

- A beam with a cut placed at the maximum of displacement ($x_{cut} =$ 0.37 m);

- A beam with a cut placed at the null displacement point ($x_{cut} =$ 0.56 m);

- A beam with a cut placed at the minimum of displacement ($x_{cut} =$ 0.74).

The results are presented in Figure 3.5 comparing the deflection line and the normalized shear energy deformation in the viscoelastic material for the four different cases. An abrupt variation of the shear deformation is observed at the cut. Additionally, this effect is more significant for a cut placed at a maximum of displacement. Table 3.3 displays the results in terms of the modal loss factor for each of the four configurations. They suggest the hypothesis that the cut has to be placed where the bending

moment is maximal in order to reach the highest modal loss factor. Here,
the highest bending occurs at $x_{cut} = 0.74$ m and configuration four, plac-
ing a cut right there, reaches the highest damping factor. It is almost
three times higher than for the full coverage configuration. In the latter
case, the shear deformation in the viscoelastic material is not significant
in regions where the bending moment is maximal. There, mainly exten-
sional deformation occurs in the damping layer. By placing a cut at the
region of highest curvature, the compliance of the whole structure is fur-
ther increased, leading to a local high shear deformation in the damping
material.
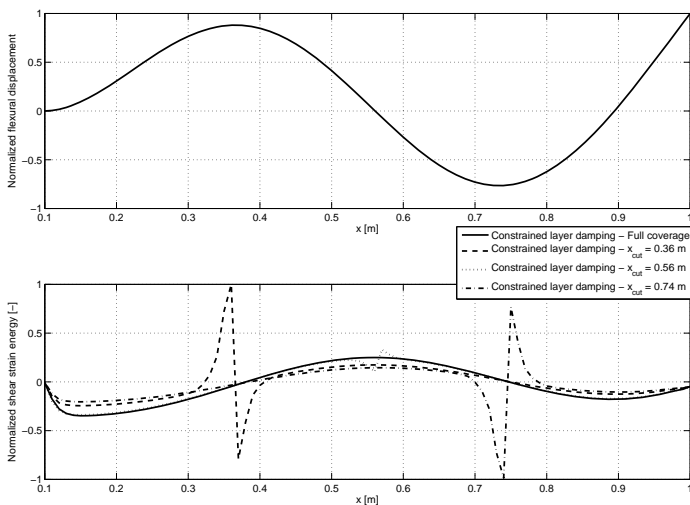
Figure 3.5: Comparison between the deflection line and the shear defor-
mation at the third bending mode

3.2.4 Equally segmented constrained layer damping

In section 3.2.3, the effect of the position of a single cut on the modal
loss factor was investigated at a given mode. From this result, the author

Table 3.3: Modal loss factor as a function of the cut position

Position of the cut	Modal loss factor
[m]	[-]
No cut	0.0542
0.36	0.1116
0.56	0.0560
0.74	0.1509

deduces as an hypothetical rule-of-thumb namely that a cut has to be located at the maximum of the bending moment. The rule-of-thumb can be applied if a modal analysis obtains information on mode shape and/or the shear strain distribution in the viscoelastic material is known. However, this section investigates the influence of the number of equally spaced cuts on the modal loss factor, without any considerations on the flexural displacement and shear strain distribution. Nonetheless, it is observed that a significant enhancement is achieved. In Figure 3.6, the modal loss factor as a function of the number of cuts for the first four modes is presented. For each mode, there is a certain number of cuts that optimizes the modal loss factor: seven cuts for mode one, two and three with an increase of loss factor of 90%, 85% and 79%, respectively, and nine cuts for mode four with an increase of 48% of the loss factor compared to a full coverage configuration. One can also see from Figure 3.6 for mode 4 that the modal loss factor is higher for 1 cut than for 2 cuts. For the latter case, the cuts are placed at locations where the bending curvature is smaller compared to the position of the single cut. Therefore, a reduction of the energy dissipation is observed. In Figure 3.7, the damped frequency response function at each mode separately is presented in terms of mean square displacement. It is calculated by performing an harmonic analysis. The FRF is calculated with the following formula

$$FRF = 10 \times log \left(\frac{u}{F} \right)^2 \tag{3.1}$$

where u is the mean displacement of the beam and F is the input force, taken equal to 1 N for this case. The results are displayed for one, four and eight cuts. For each mode, the vibration reduction is about 10 dB
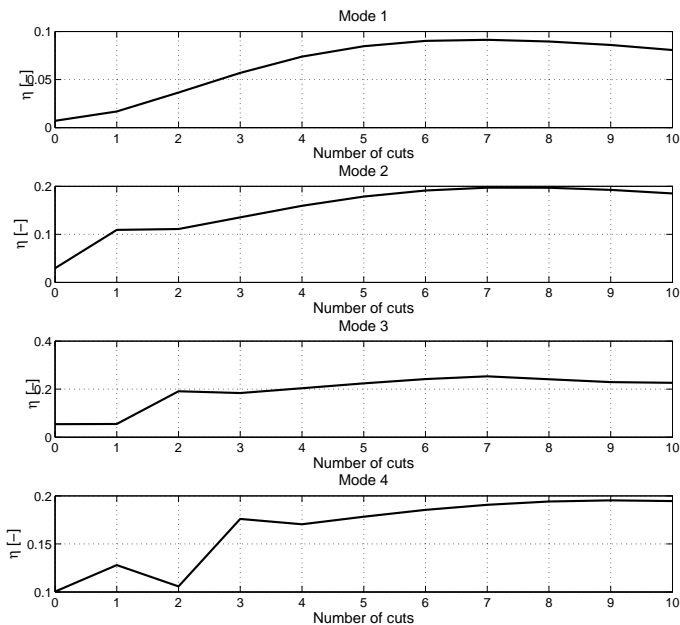
Figure 3.6: Modal loss factor as a function of the number of equally spaced cuts

between the full coverage configuration and the constrained layer damping with eight cuts. It is observed that the frequency of the resonance peaks are shifted down as the number of cuts increases. Assuming that the mass of the damping treatment remains constant, this means that the compliance of the whole structure is increased.

3.2.5 Optimization

The goal of this section is to identify a segments' arrangement, using an optimization method, that maximizes the loss factors of several modes simultaneously. In order to reach this objective, three different cases are
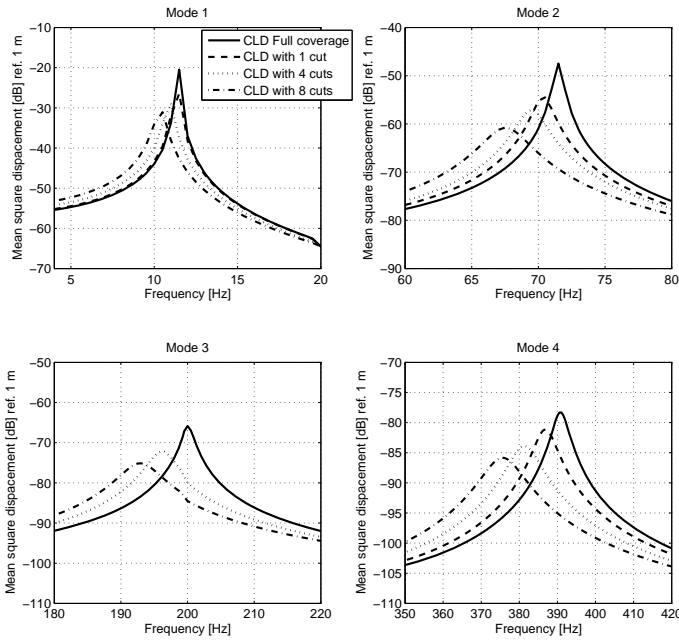
Figure 3.7: Response of the cantilever beam with segmented constrained layer damping treatments at the first four bending modes

considered. First, the optimization method is used considering one cut for a single mode. The goal is to investigate the convexity of the objective function. Then, a beam with equally spaced cuts as initial position is considered. The goal is to find for each bending mode a cuts' arrangement to maximize the loss factor. Therefore, one will be able to conclude for the different bending mode if it is meaningful to adjust the segments' length to maximize the loss factor. The third considered case is a beam with several cuts but the objective of the optimization is maximize the loss factor of the first four modes simultaneously. Therefore, one is able to conclude whether it is better to simply consider equally spaced cuts or to optimize the cuts' distribution to increase the efficiency of the segmented CLD over a large frequency range.

3.2.6 Definition of the optimization problem

Considering the goal of the optimization problem, the objective function can be defined by

$$f\left(x\right) = \sum_{i=1}^{m} \frac{A_i}{\eta_i\left(\{\mathbf{x}\}\right)} \tag{3.2}$$

where $\{\mathbf{x}\}$ is the vector of design variables which are the position of the cuts along the beam. It is defined as

$$\{\mathbf{x}\} = \left\{ \begin{array}{c} x_1 \\ d_j \end{array} \right\} \tag{3.3}$$

where x_1 the position of the first cut and d_j is the distance between the different cuts. The objective is to minimize the sum of the inverse values of the loss factor of m modes. A_i is the weighting parameter for the *ith* mode. It enables to give more importance to one mode compared to the others. The design variables x are the position of the cuts along the beam. In order to keep the design variables within the feasible domain, the objective function is transformed using the exterior penalty method [74]. Quadratic terms are used to penalize constraints violations. Therefore, the transformed objective function has the following form

$$f = \sum_{i=1}^{m} \frac{A_i}{\eta_i\{\mathbf{x}\}} + R \times \left(max\left(0, L_c - x_1\right)^2 + max\left(0, x_1 - L\right)^2 + \right.$$

$$\left. \sum_{j=2}^{n} max\left(0, d_{min} - d_j\right)^2 + \sum_{k=2}^{p} max\left(0, \left(\left(\sum_{l=1}^{q} d_l\right) + x_1\right) - L\right)^2_k \right) \tag{3.4}$$

where

- η is the modal loss factor.

- R is the penalty factor.

- L is the free length of the beam.

- L_c is the clamped length of the beam.

- x_1 is the position of the first cut.

- d_j is the distance between cuts j and *j-1*: $d_j = x_j - x_{j-1}$.

- d_{min} is the minimal distance between any two cuts equal to 0.001 m.

- $n = q =$ number of cuts - 1;

- $p =$ number of cuts.

The penalty factor R is taken equal to 10^9. With this penalty factor value, one obtains a violation of the design domain of less than 1%. The first and second terms of the constraining function mean that the first cut has to be placed in the free region of the beam, defined in Figure 3.2. The third term is used to impose a mininum distance beteewn each cut; d_{min} is taken equal to 5 mm. The last term means that the position of the second cut and higher have to be smaller than the actual length of the beam. The iteration scheme is presented in Figure 3.8. At first, the eigenfrequency of the mode under consideration is identified with a modal analysis. From the harmonic analysis, performed at the identified frequency, the strain energy of each layer is extracted. Then, the modal loss factor is estimated using the modal strain energy method. This value, as well as the position of each cut, is inserted in the pseudo objective function for evaluation. This process runs as long as the termination criterion is not satisfied. The selected algorithm based on mathematical programming follows a deterministic method: the Nelder-Mead simplex method [75]. It is implemented in the Matlab Optimization Toolbox [76]. It attempts to minimize a scalar-valued nonlinear function of n real variables using only function values, without any derivative information. The method uses the concept of simplex, which is a polyhedron of *N+1* in *N* dimensions [77]. Simplices are a line, a triangle and tetrahedron in one-, two-, and three-dimensional space, respectively, and so forth. The method approximately finds a local optimal solution with *N* variables when the objective function varies smoothly. Nelder-Mead generates a new test position by extrapolating the behaviour of the objective function measured at each test point arranged as a simplex. Then, the algorithm chooses to replace

one of these test points with the new test point. Thereby, a new simplex is generated with a single evaluation of the objective.
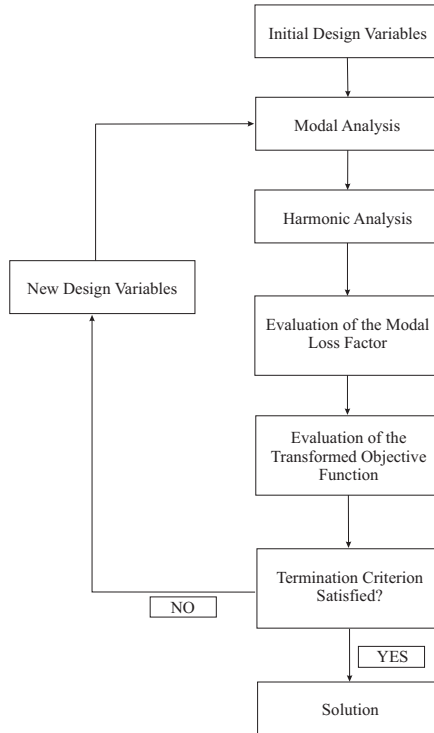

Figure 3.8: Iteration scheme for cuts arrangement optimization

3.2.7 Optimization of a single mode with one cut

For the optimization of a single mode with one cut, two cases are considered. In the first case, the cut is initially placed in the middle of the free length of the beam. In the second case, the cut is initially placed where the bending moment is the largest. The results are presented in Table 3.4. First of all, one can see that the largest improvement is observed for mode 1 compared with the beam without cuts. The loss factor is almost multiplied by 10. For mode 1 to 3, the initial position of the

initial cut does not have any influence on the optimized value of the loss
factor. Indeed, the final position of the cut is the same in both cases.
For mode 4, one obtains two different positions leading to two different
loss factor values. This means the optimization problem is not convex.
This is confirmed by looking at the shape of the objective function for the
first four bending modes, see Figure 3.9. For mode 2 and above, there is
more than one local minimum. Therefore, the initial position of the cut
has to be choosen with care in order to reach the global minimum of the
objective function.

Table 3.4: Effect of the initial cut arrangement on the optimized modal
loss factor

Mode number	Initial position [m]	Final position [m]	Optimized modal loss factor [-]	Loss factor (No cut) [-]
Mode 1	0.55	0.19	0.065	0.0071
	0.15	0.19	0.065	-
Mode 2	0.55	0.59	0.12	0.029
	0.53	0.59	0.12	-
Mode 3	0.55	0.75	0.15	0.054
	0.73	0.75	0.15	-
Mode 4	0.55	0.54	0.13	0.10
	0.82	0.84	0.14	-

3.2.8   Optimization of a single mode with several cuts

A comparison between the modal loss factors obtained with equally spaced
cuts and an optimized distribution of them is presented in Figure 3.10.
One can see that the improvement is the most significant at the first
bending mode. For the 7 cuts configuration, Figure 3.11 compares the
optimized distribution of cuts with equally spaced ones. The circles show
the position of equally spaced ones and the crosses show their position
after optimization. One can see that their position is the most changed
for mode 1. This confirms that the optimization is mainly useful for the
first bending mode.
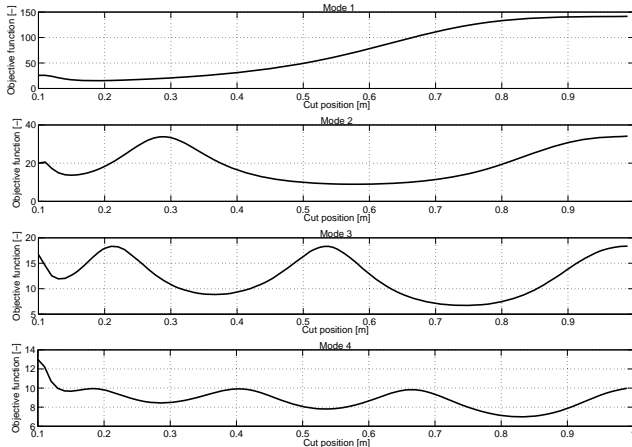
Figure 3.9: Objective function as a function of the position of a single cut from modes 1 to 4
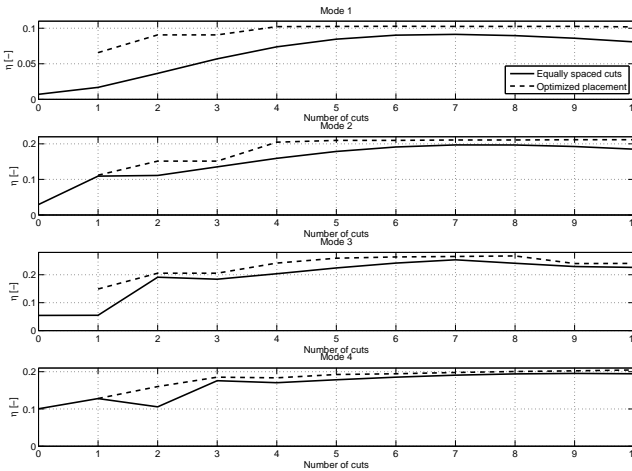
Figure 3.10: Modal loss factor as a function of number of cuts for equally spaced and optimized positions

3.2.9   Optimization over a large freqency range

In this section, results for the optimization process over a larger frequency range are presented. The goal is to obtain a distribution of cuts that optimizes the loss factor of several modes simultaneously. In Table 3.5, the modal loss factors of three different configurations are listed: full coverage, 7 cuts equally spaced and 7 cuts optimized. The 7 cuts configuration is selected because it provides the highest modal loss factors in both cases: equally spaced cuts and optimized cuts arrangement for a single mode (see Figure 3.10). The idea is to further optimize the best configuration. The results from Table 3.5 show that it is possible to identify a configuration of cuts that increases all loss factors. The largest improvement is just of 11% at mode 1.

Table 3.5: Optimization over a large frequency range: modal loss factor at each mode - 7 cuts

	Mode 1	Mode 2	Mode 3	Mode 4
Full coverage	0.0071	0.0294	0.0542	0.1004
7 cuts equally spaced	0.0913	0.1931	0.2564	0.1907
7 cuts optimized	0.1025	0.2094	0.2652	0.1960

Figure 3.12 presents the obtained cuts distribution. The circles correspond to the position of the equally spaced cuts and the crosses are their optimized position. Compared to the equally spaced configuration, the optimized position is significantly different for cuts close to the clamping.

3.3   Plate-like structure with segmented constrained layer damping treatment

In this section, the effect of segmenting constrained layer damping treatment when it is applied to a three-dimensional structure is studied. The goal of this study is to determine the best topology of segments to maximize the modal loss factor.
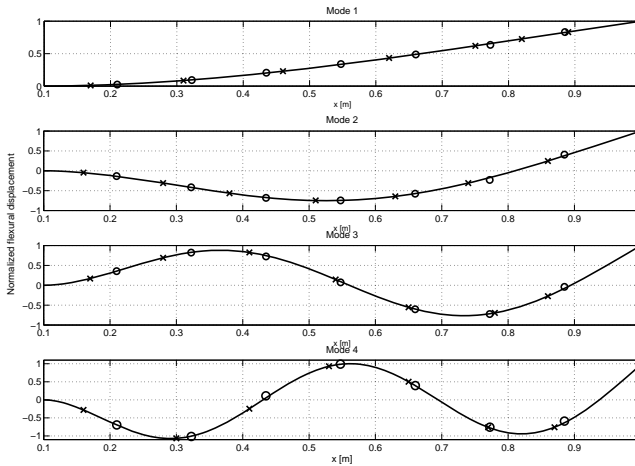
Figure 3.11: Deflection lines and cuts distribution for the single mode optimization with 7 cuts

3.3.1 Finite element model

The structure of interest is a clamped circular plate on which is bonded a constrained layer damping treatment. The finite element modeling method is the same than the one presented in section 2.4.4.2. The element type solid185 are used to model the different layers. The base plate and the constraining layer are made of aluminium. The material properties of the damping layer are the same than those for the beam-like structure case. Table 3.6 presented the geometry of the circular plate.

Table 3.6: Dimension of the plate

Radius [mm]	250
Thickness of the base plate [mm]	2
Thickness of the damping layer [mm]	0.25
Thickness of the constraining layer [mm]	0.25
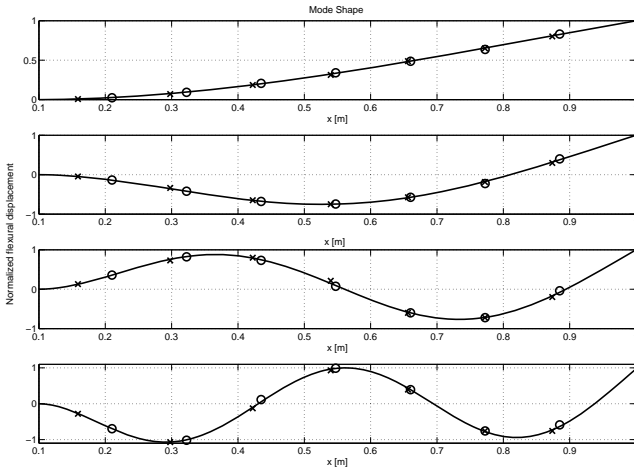
Figure 3.12: Deflection lines and cuts distribution for the large frequency range optimization with 7 cuts

3.3.2   Topology study

This topology study is based on the pattern of the cuts. Two cases are investigated:

- Circular cuts;

- Radial cuts.

All the study is realized at the frequency corresponding to the first eigenfrequency of the plate, see Figure 3.13. A normal force is applied at its centre. Therefore, the mode shape at that frequency is a simplified reproduction of the deformation at a belly of vibration of a more generic three-dimensional plate-like structure. The circular plate fully covered with a constrained layer damping material is taken as reference configuration. Values of its first resonance frequency and corresponding loss factor are presented in Table 3.7.
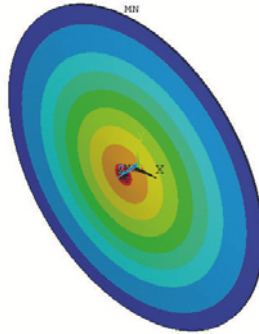
Figure 3.13: Deformation of the structure at the first eigenfrequency, depictured with level lines

Table 3.7: Resonance frequency and modal loss factor in a full coverage configuration

Resonance frequency [Hz]	91.2
Modal loss factor [-]	0.016

3.3.2.1 Circular cuts

In this section, the effect of circular cuts is investigated by simulating the structural response of a set of configurations with increasing number of cuts ranging from 1 to 9. For the first configuration, the circular cut has a radius of 25 mm. For each new configuration, a new circle is added at a distance of 25 mm from the previous one. The results are listed in Table 3.8: the highest loss factor is obtained with the largest number of circular cuts. Additionally, the value of the resonance frequency decreases with the number of cuts. The segmentation with 9 circles is presented in Figure 3.14.

Table 3.8: Effect of the number of circular cuts on the resonance frequency and on the modal loss factor

Number of circular cuts	Resonance frequency [Hz]	Modal loss factor [-]
1	89.7	0.043
2	88.8	0.061
3	87.7	0.083
4	86.9	0.096
5	86.2	0.106
6	85.7	0.114
7	85.3	0.120
8	85.1	0.124
9	84.9	0.125

3.3.2.2   Radial cuts

In this section, the effect of radial cuts is investigated. The results are presented as a function of the number of radial cuts in Table 3.9. According to the different configurations under study, the optimum value for the loss factor is obtained with 9 cuts. In that case, the angle between each cut is $20°$. The distribution of the segments is presented in Figure 3.15. Compared with the results from Table 3.8, radial cuts have more effect than circular ones. This is due to the fact that each radial cut crosses the plate centre where the bending moment is the highest; the same is not true in the case of circular cuts. Additionally, the decrease of the resonance frequency is significant compared with the previous cuts pattern and with the full coverage configuration.

3.3.3   Optimization

The goal of the optimization is to maximize the loss factor of the first bending mode. The plate consists on 9 circular cuts and 9 radial cuts as they provide the largest loss factor, see Table 3.8. The design variables of the optimization are the position of the circular cuts. The objective of this section is to understand what is the best position of the circular cuts. The optimization follows the method described in section 3.2.6. The objective function is defined as
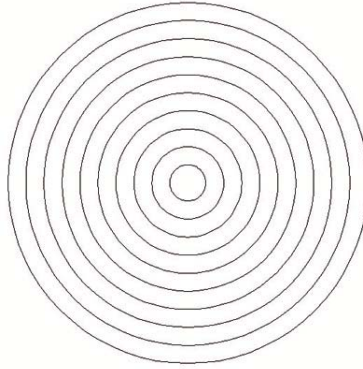
Figure 3.14: Distribution of 9 circular cuts

$$f(x) = \frac{1}{\eta(\{\mathbf{x}\})} \qquad (3.5)$$

where $\{\mathbf{x}\}$ is the vector of design variables. It consists of the radius of the smallest circle, r_1, and the distance, d_i, between one circle and the next one. It is written as

$$\{\mathbf{x}\} = \left\{ \begin{array}{c} r_1 \\ d_i \end{array} \right\} \qquad (3.6)$$

The objective function is transformed using the exterior penalty method in order to keep the design variables in the feasible region. The transformed objective function has the following form

$$f = \frac{1}{\eta} + R \times \left(max(0, r_{min} - r_1)^2 + \sum_{i=2}^{m} max(0, d_{min} - d_i)^2 + \right.$$

$$\left. \sum_{j=1}^{m} max\left(0, \left(\sum_{k=1}^{m} d_k\right) - d_{max}\right)^2 \right) \qquad (3.7)$$

Table 3.9: Effect of the number of radial cuts on the resonance frequency
and the modal loss factor

Number of radial cuts	Resonance frequency [Hz]	Modal loss factor [-]
6	82.1	0.149
8	80.9	0.150
9	80.4	0.151
10	80.1	0.147
12	79.6	0.139
18	78.0	0.124
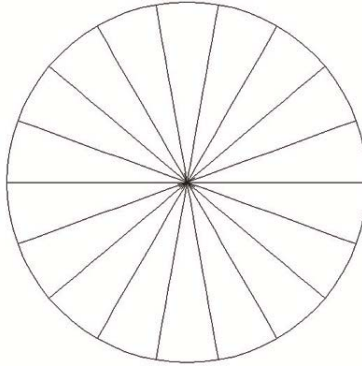
Figure 3.15: Distribution of 9 radials cuts

where

- η is the modal loss factor.

- R is the penalty factor equal to 10^9. With this penalty factor value,
  one obtains a violation of the design domain of less than 1%.

- r_{min} is the minimal radius value equal to 2 mm.

- d_{min} is the minimal distance between two circles equal to 1 mm.

- d_{max} is the maximum value for the sum of the distances between
  each cut equal to 250 mm.

The first term of the constraining function means that the first circle has to be larger than the minimum radius value. The second term of the objective function means that the distance between each circle has to be larger than the minimum value. The last term of the constraining function means that the sum of the distances between each circle has to be smaller than the maximal value of the sum for the distances between each circle.

3.3.4 Results and discussion

The results of the optimization is presented in Figure 3.16. Initially, the circular cuts are positioned with an equal distance between them. Maximization of damping is sought by adjusting the radial position of each circle, as explained in section 3.3.3. One can see that the radius of each circle is reduced. It comes from the fact that the bending moment of the plate is increasing by getting closer the center of the plate. Therefore, the shear deformation at the cut increases by reducing the circle radius. The obtained cuts' arrangement provides an increase of modal loss factor of 9% as presented in Table 3.10.
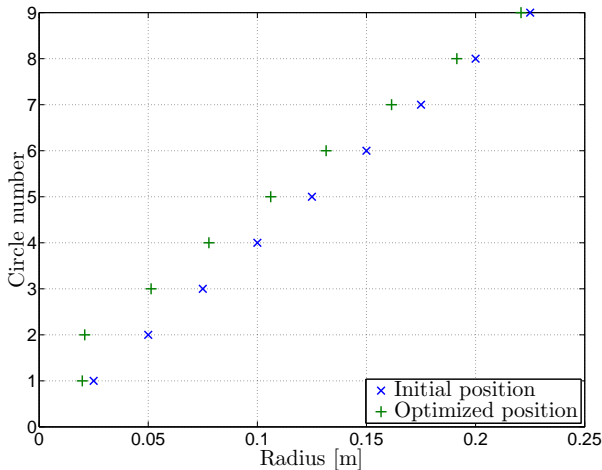
Figure 3.16: Comparison of circle radii between their initial and final value

Table 3.10: Comparison of resonance frequency and modal loss factor between the initial and the final segmentation

	Resonance frequency [Hz]	Modal loss factor [-]
Initial segmentation	79.9	0.132
Optimized segmentation	80.3	0.145

Table 3.11 details the radius of the 9 circles. The first circle has a radius of 19.7 mm. There is a still a difference of 17.8 mm with the minimal possible radius. One can also see that the difference bewteen the first and the second radius is of 1.2 m which is almost the minimal possible distance between two cuts: it means the minimal radius value is around 20 mm. For circle 2 to 9, the radius difference is always around 30 mm: it means that the radius difference can be constant to maximize the loss factor.

Table 3.11: Radii values

r_1	19.7 mm
r_2	20.9 mm
r_3	51.3 mm
r_4	77.8 mm
r_5	106.1 mm
r_6	131.5 mm
r_7	161.5 mm
r_8	191.4 mm
r_9	220.5 mm

3.4   Conclusion

This chapter has investigated the design of segmented constrained layer damping treatment on two- and three-dimensional structures. A beam has been used to explain the effect of cutting the damping treatment. At the core of the new approach is a rule-of-thumb for the position of a single

cut: it has to be placed at the location where the bending of the respective modal deflection line is the highest. According to the mode under investigation, there exists an optimum value of cuts that maximizes the loss factor. Compared to a full coverage configuration (no cut), the loss factor improvement can go up to 90% for the first bending mode. The increase of loss factor is smaller at higher modes. Nevertheless, it is of 48% at mode 4 for this case study. An optimization algorithm has been developed to optimize the distribution of cuts. Investigation for a single cut reveals that the pseudo-objective function is not convex. The deflection line should be used to identify the location of the highest bending moment and therefore the initial cut placement for the iteration process. The optimization over a larger frequency range showed that it is possible to further increase the modal loss factors of several modes simultaneously with one cuts arrangement. A circular plate has been used to identify between circular and radial cuts which topology gives the largest increase of modal loss factor. Radial cuts are the best design solution as they cross the plate in its centre where the bending moment is the highest. An optimization also has been used to determine the optimum distribution of radii for circular cuts. It has been shown that there exists an optimum radius value for the first two circles and that the difference between the radius for the other circles can be constant to maximize the modal loss factor.

Chapter 4

Composite beams in cylindrical bending

This chapter is the first one of this thesis directly dealing with the integration of viscoelastic materials into fiber-reinforced composite laminates. A finite element model of laminted beam is validated using Pagano's exact solution and is used to have an understanding of the effect of the soft core layer on the bending properties of composite laminates.

4.1 Introduction

The introduction of fiber-reinforced composite materials, which in lightweight designs are most often used to make laminated plates by laying up a number of pre-impregnated sheets (prepregs), allows the so-called integrated damping treatment, where one of the laminate's interior layers consists of a soft damping material. The research effort has been directed towards the damping rates from various treatment techniques and to further improve those. In the available literature presented in 1.1, there is no study that addresses the change of stiffness, stability and structural strength of structures due to the presence of the damping treatment. These aspects are very important when designing structures in pratice, as the multiple objective of low weight and high stiffness, stability, strength,

and damping properties must be pursued concurrently. The first goal of this chapter is to validate a finite element model of a composite beam with a soft core. The second goal is to perform a parametric study to assess the effect of the damping layer position in the laminate lay-up, its thickness and its material properties on the bending stiffness. Pagano's exact solution is discussed in section 4.2. The finite element model is presented and validated in section 4.3. Section 4.4 details the parametric study. A conclusion is proposed in section 4.5.

4.2   Pagano's exact solution

In 1969, Pagano [20] presented an approach to define the elasticity solutions for laminates consisting of arbitrary numbers of orthotropic or isotropic layers, which is free from the assumptions imposed by the classical plate theory (CPT). Whitney extended this work to laminated plates which includes transverse shear effects [78]. These exact solutions have been used by researchers since decades as benchmark solutions for the validation of improved laminate theories and related finite elements. To describe the stress-strain relation of fiber-reinforced laminate, the classical laminate plate theory is usually used. Nonetheless, its limitations are the following [20]:

- The assumption of linear in-plane displacements through the thickness, in particular for laminates in which the stiffness properties vary drastically from layer to layer.

- The presence of only 2 boundary conditions per edge in the bending theory, which precludes the precise calculation of boundary layer effects, such as stress concentration factors.

- The neglect of shear deformation, implied by the Kirchhoff hypothesis (normals remain normal).

- The assumption of a state of plane stress in the constitutive relations, which eliminates the possibility of rigorous calculation of interlaminar stresses.

To overcome these limitations, Pagano proposed a solution for any kind of stress and displacement fields provided that they satisfy the stress equilibrium equations. For simple support boundary conditions, these are

satisfied in the axial direction by Fourier series. As interface continuity conditions are taken into account, Pagano's exact solution is also valid for thick laminates with layers, having large different stiffness properties. It is actually the case for fiber-reinforced composites with integrated viscoelastic layers. The derivation of Pagano's exact solution and the one obtained from the classical plate theory (CPT) are detailed in appendix B.

4.3   Finite element modeling

Pagano's exact solution is used to validate the finite element model of a three-layer laminated beam. The numerical model is developed with the commercial software ANSYS. It has the following lay-up: 0°-Viscoelastic core-0°. The different layers are modeled with 2D-solid elements for mapping a state of plane strain. The material properties of the fibrous layer are taken from [20] and presented in Table 4.1. The material properties of the viscoelastic material (VM) are given in Table 4.2. The deformed mesh of in cylindrical bending is presented in Figure 4.1.
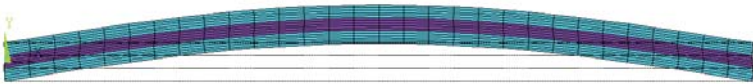
Figure 4.1: Deformed mesh

The results of Pagano's exact solution, CPT and FEM are compared for the three layers laminate. The function of prime interest is the transverse shear stress τ_{xz}, as the dominant mechanism of damping is the shear occuring in the core layer. For the considered structure, the span-to-depth ratio S is taken equal to 50. The span-to-depth ratio, the normalized thickness and the transverse shear stress are defined with the following equations

$$S = \frac{l}{h} \tag{4.1}$$

$$\overline{z} = \frac{z}{h} \tag{4.2}$$

$$\overline{\tau} = \frac{\tau_{xz}(0, z)}{q_0} \tag{4.3}$$

Table 4.1: Material properties of the undirectionnal layer from [20]

Property	Value
E_x [MPa]	173 000
E_z [MPa]	6 900
G_{xz} [MPa]	3 500
G_{yz} [MPa]	1 400
ν_{xz}	0.25
ν_{yz}	0.25

Table 4.2: Material properties of the viscoelastic core

Property	Value
E [MPa]	1
G [MPa]	0.34
ν	0.49

A convergence analysis of the finite element model is realized in order to identify the number of element in x- and z-direction to obtain a satisfying correlation with a reasonable numerical effort. Figure 4.2 compares the tranverse shear distribution obtained with Pagano's exact solution, with the CPT solution and with the numerical model for 3 different numbers of elements along the x-axis (the number of elements along the z-axis is kept equal to 5). One looks at the transverse shear stress at $x=0$ as it is important to have an accurate modeling of it at this location as the edge effect is responsible for the damping performance of constrained viscoelastic material. As a consequence, the effect of the damping layer on

the overall mechanical properties of the beam can be clearly understood. One can see the correlation between Pagano's exact solution does not improve by increasing the mesh density along the x-axis. Figure 4.3 presents the transverse shear stess distribution through the thickness at $x = 0$ obtained with Pagano's exact solution, the CPT solution and the numerical models for 3 different number of elements along the z-axis (the number of elements along the x-axis is kept equal to 30). With increasing the number of elements along the z-axis, the FEM solution converges to the exact one. Additionaly, the difference between the exact solution and the CPT solution is significant. Pagano's solution reveals that, qualitatively, the shear stress within the compliant viscous layer is much less than the maxima located within the stiff CFRP layers. Quantitatively, Pagano's exact solution detects much higher values than the CPT. The FEM solution shows a good correlation with the exact solution. The distribution of the transverse shear stress in the lower and upper sublaminates is similar to the one of a single layer laminate [20]. Therefore, it seems that the lower and upper laminates are partially decoupled. This effect is further investigated in the next section.
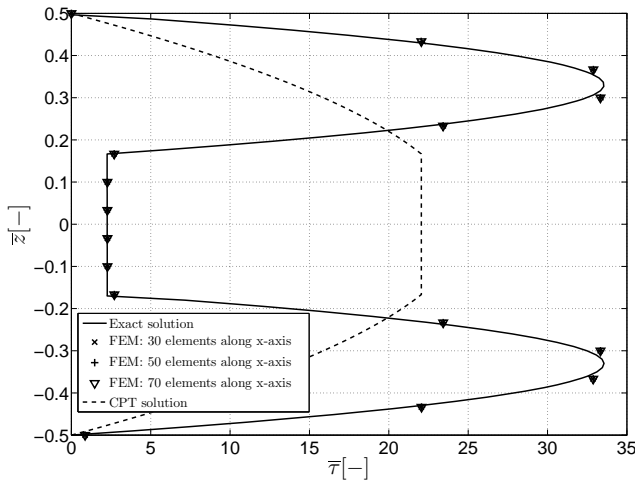
Figure 4.2: Effect of the number of elements along the x-axis on the normalized transverse shear stress distribution at $x = 0$
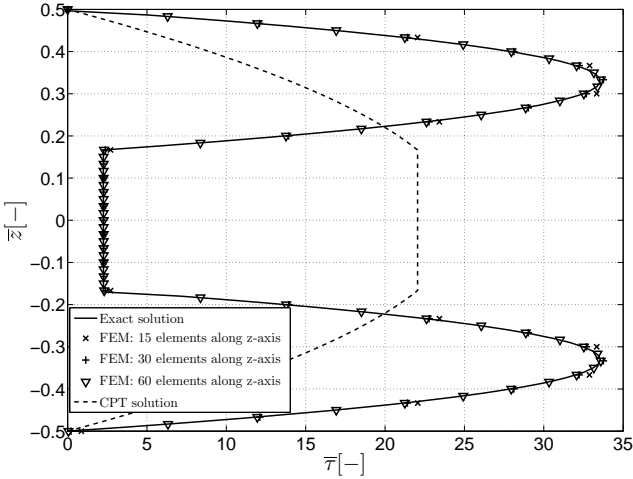
Figure 4.3: Effect of the number of elements along the z-axis on the normalized transverse shear stress distribution at $x = 0$

4.4   Parametric study

The parametric study considers the following design parameters:

- The viscoelastic layer position in the laminate lay-up;

- The material properties of the core layer;

- The thickness of the damping material;

- The span-to-depth ratio.

The influence of the parameters above listed is evaluated on the normalized transverse shear stress (see Equation 4.3) and the normalized deflection defined as

$$\overline{w} = \frac{100 E_z h^3 w \left(\frac{l}{2}, -\frac{h}{2} \right)}{q_0 l^4} \tag{4.4}$$

4.4.1 Effect of the position of the viscoelastic layer in the laminate lay-up

Figure 4.4 presents the considered configurations, where the viscous layer is placed at different positions within the laminate stack-up, while Figure 4.5 gives the normalized deflections connected with the respective configurations. The deflection decreases of 60.3% when shifting the viscous layer from $\overline{z}_{VM}=0$ to $\overline{z}_{VM}=h/4$. If the viscous layer (see 'VM' in Figure 4.4) has the same material properties as the CFRP layers (see '0°' in Figure 4.4) the laminate would be a homogeneous plate and the position of 'VM' would be of no consequence. To illustrate the effect of the position of the viscous layer, with simple means, we consider the extreme case of the viscous layer having non-zero stiffness only in the through-the-thickness direction. Then, both CFRP layers must experience the same bending curvature but are otherwise decoupled, see Figure 4.6. In this limiting case, the lower and upper laminates can be considered as two separated bodies deformed by the same bending curvature, where the total laminate bending stiffness is simply the sum of those of the CFRP sublaminates. For the considered cylindrical bending situation, it holds that $\epsilon_z^0=\gamma_{xz}^0=\kappa_z=\kappa_{xz}=0$ and $N_x=0$. Therefore, the relation between forces, moment and strains for each unidirectional laminate is reduced to

$$M_x = D_{11}\kappa_x \tag{4.5}$$

where κ_x is the curvature. The bending moment of the whole structure is simply given by

$$M_x^{total} = M_x^{lower} + M_x^{upper} \tag{4.6}$$

Table 4.3 presents $\overline{D}_{11}^{total}$ as a function of $\overline{z}$. $\overline{D}_{11}^{total}$ is defined as

$$D_{11}^{total} = D_{11}^{lower} + D_{11}^{upper} \tag{4.7}$$

with

$$\overline{D}_{11}^{lower,upper} = \frac{D_{11}^{lower,upper}}{D_{11}^{ref}} \tag{4.8}$$

where D_{11}^{ref} is the first coefficient of the D matrix for the lower and upper laminate in the case $\overline{z}=0$, see Figure 4.4. Considering that κ_x is assumed to be the same for both sublaminates, the increase of M_x^{total} from $\overline{z}=0$ to $\overline{z}=h/4$ reaches 62.6%. In other words, the bending stiffness decreases by 62.6% which closely agrees with FEM results. The CPT analysis validates that the viscoelastic core has a negligible stiffness if compared to those of the two sublaminates. The real situation comes close to the limiting case discussed before. The deflections shown in Figure 4.5 indicate that the stiffness is highest for the most excentric position of the viscoelastic layer shown at the right in Figure 4.4. This we explain by the fact that the bending stiffness increases with the third power of the CFRP layer thickness.

Table 4.3: $\overline{D}_{11}^{total}$ as a function of $\overline{z}$

$\overline{z}$	$\overline{D}_{11}^{lower}$	$\overline{D}_{11}^{upper}$	$\overline{D}_{11}^{total}$
0	1	1	2
h/12	0.423	1.866	2.289
h/6	0.126	3.385	3.511
h/4	0.016	5.336	5.352
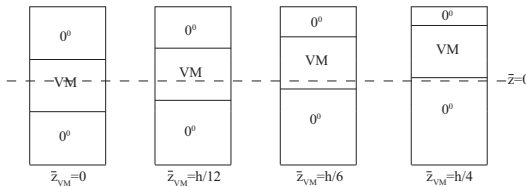
Figure 4.4: Position of the viscoleastic layer in the laminate
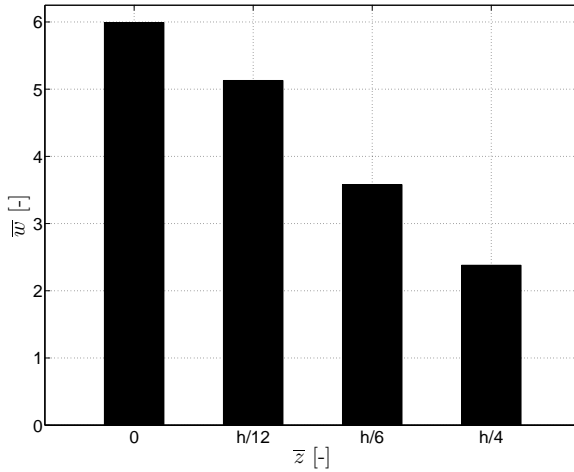
Figure 4.5: Effect of the position of the VM on the normalized deflection
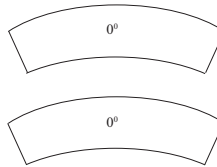
Figure 4.6: Deformation of the sublaminates considered as decoupled with the same bending curvature

4.4.2   Effect of the material properties of the viscoelastic layer

In Figure 4.7, the normalized deflection is presented as a funtion of the of E_{VM} ranging from 0.1 MPa to 1 GPa. As the core layer becomes stiffer, the whole laminate is also getting stiffer which reduces its deflection. An asymptotic behaviour is also observable for lower and larger

Young's moduli. In these regions changing this parameter does not significantly change the deflection values. The increase of bending stiffness is also due to coupling between the lower and upper laminate which increases with increasing the core stiffness.
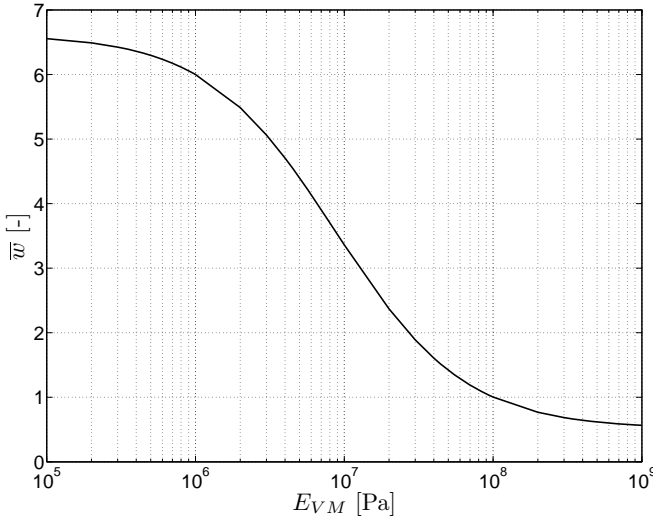
Figure 4.7: Effect of the E-modul of the core layer on the normalized deflection

The phenomena is presented in Figures 4.8, 4.9 and 4.10. The shear strain distribution is plotted respectively for E_{VM}=1 MPa, E_{VM}=100 MPa, E_{VM}=1000 MPa. One can see that the normalized transverse shear stress values in the compliant layer increase to reach the maximal value occuring in the lower and upper laminates. Therefore, these are more and more coupled. Additionally, the exact and FEM solutions converge to the CPT one by increasing the core layer stiffness.
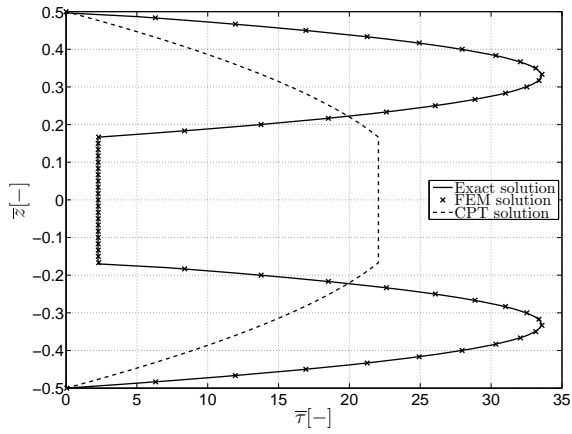
Figure 4.8: Normalized transverse shear stress for E_{VM}=1 MPa at $x = 0$
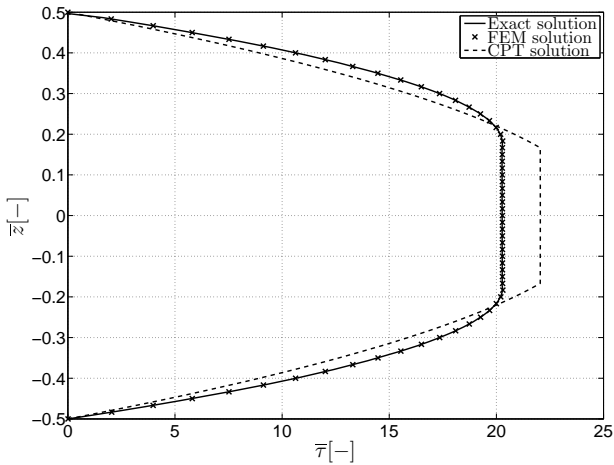
Figure 4.9: Normalized transverse shear stress for E_{VM}=100 MPa at $x = 0$
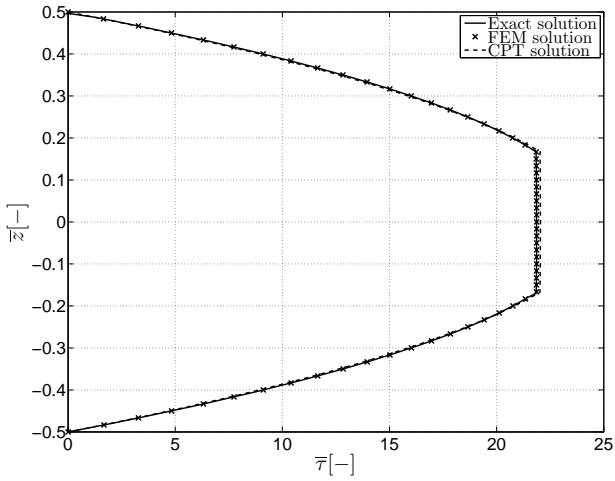
Figure 4.10: Normalized transverse shear stress for E_{VM}=1000 MPa at x = 0
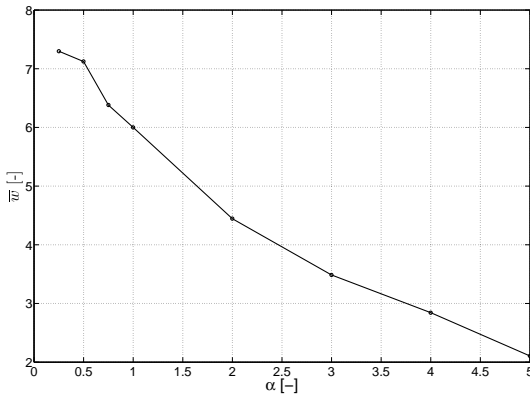
Figure 4.11: Effect of the core thickness on the normalized deflection

4.4.3 Effect of the thickness of the viscoelastic layer

In this section, the effect of the thickness of the core layer is investigated. In Figure 4.11, the normalized deflection is presented as a function of h_c, the thickness of the inner layer.

$$h_c = \alpha h_f \tag{4.9}$$

where h_f is the thickness of the face sheets and α is ranging from 0.25 to 5. One can see that the deflection decreases with the core thickness. In other words, the bending stiffness increases. This effect can be explained using the linear sandwich beam theory. For a two-dimensional beam, the total bending stiffness is defined as

$$B_{total} = B_{face}^{total} + B_{core} \tag{4.10}$$

with

$$B_{face}^{total} = B_{face} + B_{Steiner} \tag{4.11}$$

where $B_{Steiner}$ is the bending stiffness calculated with the Huygens-Steiner theorem. B_{face}, $B_{Steiner}$ and B_{core} are respectively defined with

$$B_{face} = \frac{E_f h_f^3}{6} \tag{4.12}$$

$$B_{Steiner} = \frac{E_f h_f d^2}{2} \tag{4.13}$$

$$B_{core} = \frac{E_c h_c^3}{12} \tag{4.14}$$

with

$$d = h_f + h_c \tag{4.15}$$

where E_f is the Young's modulus of the the face sheet, E_c is the Young's modulus of the core, h_c is the core thickness. Using values of Table 4.4, one obtains the results in Figure 4.12.

Table 4.4: Data to calculate the bending stiffness of the beam

Property	Value
E_f [MPa]	173 000
E_c [MPa]	1
t_f [mm]	0.33
α	from 0.25 to 5

The overall beam bending stiffness is driven by the one calculating using the Huygens-Steiner theorem. As the core stiffness is negligible, the total bending stiffness increases with the distance between the middle line of the whole laminate and the middle line of the face sheet, which increases with the core thickness.
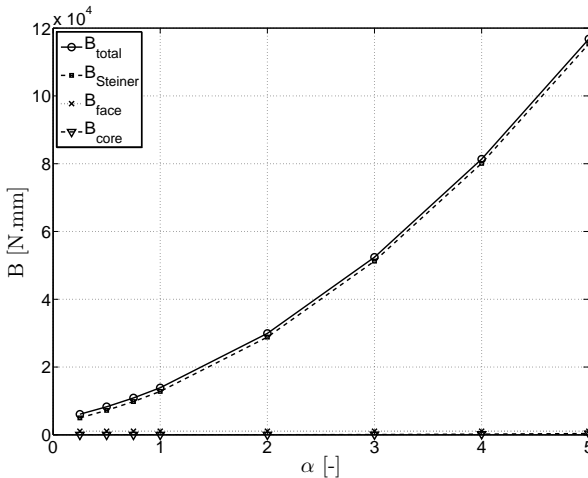
Figure 4.12: Bending stiffness of the two-dimensional beam using the linear sandwich theory
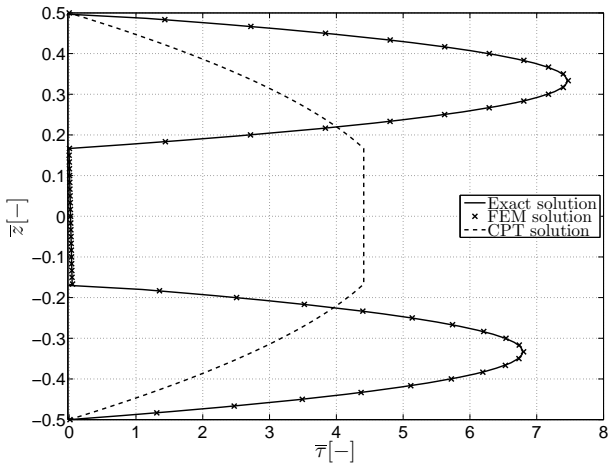
Figure 4.13: Normalized transverse shear stress for S=10 at $x = 0$

4.4.4 Effect of the span-to-depth ratio

Figures 4.13, 4.14 and 4.15 illustrate the effect of the span-to-depth ratio S on the normalized transverse shear stress distribution. For small span-to-depth ratio (S=10), the transverse shear stress approaches zero everywhere in the viscous layer. Additionally, the transverse shear stress distribution is not symmetric. The maximal stress value is observed in the upper sublaminate. This is explained by the fact that the loading is applied only to one side of the laminate and that the viscous layer has low stiffness also in the thickness direction (contrary to the assumption underlying the limiting case consideration in section 4.4.1), both of which show their effects for small S ratio. Then, the exact and FEM solutions converge to the CPT one for larger S values.

4.5 Conclusion

In this chapter, Pagano's exact solution has been used as a benchmark for the validation of a finite element model of a laminate with a viscoelastic
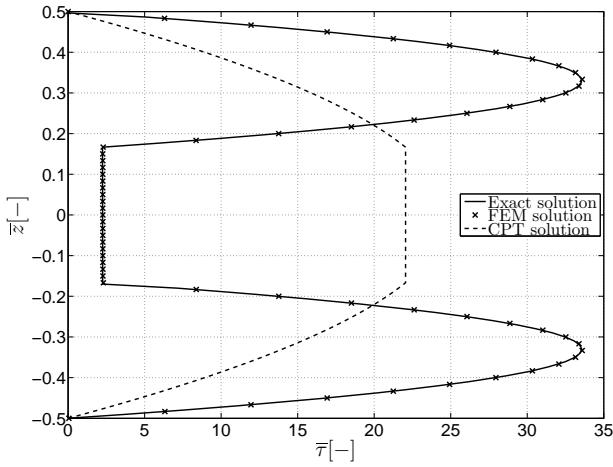
Figure 4.14: Normalized transverse shear stress for S=50 at $x = 0$
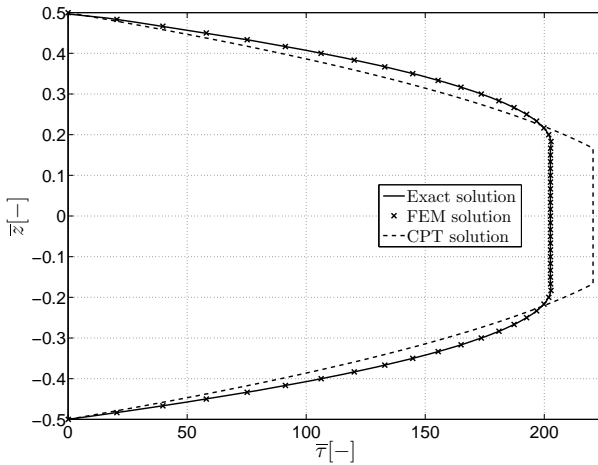
Figure 4.15: Normalized transverse shear stress for S=500 at $x = 0$

core. A convergence analysis of the FEM model has provided an optimal mesh refinement to closely approach the exact solution. In a second step, a parametric study has been realized. The design parameters were the position of the viscoelastic layer in the laminate, the material properties of the damping layer, its thickness and the structure dimension. The goal was to assess the impact of the viscoelasic material on the mechanical behaviour of the structure, such as the bending stiffness and the transverse shear stress. For the first parameter, it has been shown that the bending stiffness can be increased of about 60% when the compliant viscous layer is away from the middle line of the beam. The classical plate theory shows that one can neglect the stiffness of the soft core layer. Therefore, the lower and upper sublaminates can be considered as decoupled. The effect of the material properties of the damping layer has revealed that the decoupling effect can be strongly reduced when its modulus of elasticity is increased. An asymptotic behaviour is also observed. The impact of the middle layer thickness on the deflection has been explained using the Huygens-Steiner theorem. As the distance between the middle line of the whole laminate and the one of the lower and upper sublaminates increases with core thickness, the resulting bending stiffness decreases. Finally, the effect of the span-to-depth ratio has been studied. By increasing the length of the laminate, the decoupling between the two sublaminates is reduced. As a consequence, the predictions of Pagano's exact solution and the FEM model converge to those obtained from the classical plate theory.

Chapter 5

Parametric study on composite plates with integrated damping layers

In this chapter, a parametric study on composite laminates with integrated damping layers is performed. The effect of the viscoelastic layer on the mechanical and dynamic responses of the laminated structure is assessed. Basic rules for the design of composite plates with embedded damping treatments are extracted.

5.1 Introduction

This chapter continues with the study on the integration of viscoelastic damping layers in composite laminates. The previous chapter showed that the presence of a soft isotropic layer in the lay-up decouples the laminate in two sublaminates from a bending stiffness perspective. The main limitation of chapter 4 is that only a laminate under a bending configuration was considered. To have a complete understanding about the influence of the damping layer on the mechanical response of composite laminates, it is necessary to consider other load cases and mechanical criteria. The questions arising for the design of a composite structure

with embedded damping layers are the following:

- What is the change of stiffness, structural strength and stability compared to a laminate without damping treatment?

- Which design variables of the damping layer can simultaneously improve the mechanical and vibration damping properties of the laminate?

The answers can help to extract basic design rules for composite laminates with embedded damping layers. In order to reach this objective, a parametric study is performed. A composite laminate with an integrated damping layer is considered. Each design variable of the damping layer is varied separately and the change in terms of stiffness, structural strength, stability and vibration damping properties is calculated. Section 5.2 describes the composite structure of interest. An insight is given on the integration of the soft layer in the laminated structure. The different mechanical load cases are introduced in section 5.3. The results of the parametric study are presented in section 5.4. A discussion is done in section 5.5.

5.2   Structure of interest

The structure of interest is a composite laminated plate with an integrated viscoelastic layer. In contrast to chapter 4, the plate which is considered here can be subjected to more load cases than a beam. For example, it is possible to study the in-plane shear properties of the laminate. The plate is 300 mm long and 100 mm wide. It consists of 8 composite layers with a thickness of 0.30 mm each. The damping layer is embedded like in a sandwich configuration between two sublaminates as presented in Figure 5.1, implying that the damping layer has the same length and width than the plate. The damping layer thickness is 0.25 mm. The elastic properties of an unidirectional carbon fiber layer are given in Table 5.1.
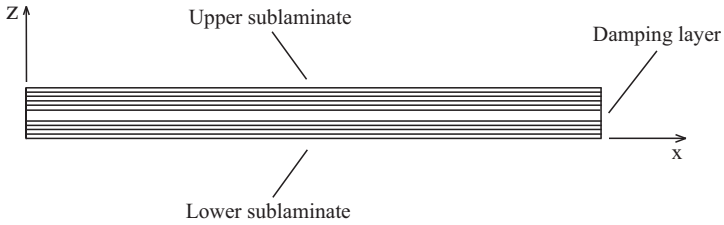
Figure 5.1: Integration of the damping layer

Table 5.1: Material properties of the unidirectional carbon fiber layer [79]

Property	Value
E_x	135000.0 MPa
E_y	10000.0 MPa
G_{xy}	5000.0 MPa
G_{yz}	3846.0 MPa
ν_{xy}	0.27
ν_{yz}	0.30
ρ	1500.0 kg/m^3
Fiber volume fraction	60%

Table 5.2: Material properties of the damping layer [80]

Property	Value
G	1.0 MPa
ν	0.49
ρ	1000.0 kg/m^3
η	0.5

From [6, 9, 10, 11], it was shown that the damping properties of composite laminates, like stiffness properties, depend of the fiber orientation. As the damping properties of the composite layer are small compared to those of the damping material, it is assumed that the damping properties of the composite layers are the same in all directions. A value of 0.015 is taken [81]. The material properties of the damping layer are presented in Table 5.2. They are assumed to be constant over the frequency. A finite element model of the plate above described is done using the commercial software ANSYS. Each layer is modelled using SOLID183 elements as described in section 2.4.4.2.

5.3   Load cases

In this section, the different load cases, design criteria and reference configuration are presented, namely:

- 3-point bending;

- In-plane compression;

- In-plane shear;

- Combined in-plane compression and shear;

- Vibration damping.

5.3.1   3-point bending

The influence of the viscoelastic layer on the laminate's deflection and maximal flexural force is evaluated by loading the plate to simply-supported boundary conditions. A normal force of 100 N is applied according to Figure 5.2. The design criteria are the maximal deflection, denoted as w_{max}, at the middle of the plate and the maximal flexural force, denoted as $P_{z,max}$. It is the required force to obtain a strain of 0.3 % in the laminate. The strain value taken to calculate $P_{z,max}$ is the strain in the x-direction in the middle of the plate at z=0 and x = 0.15 m.
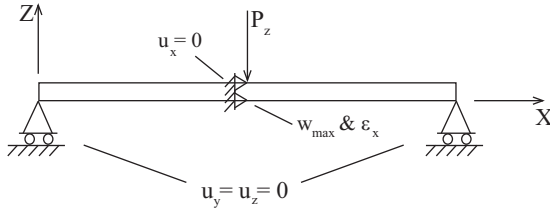
Figure 5.2: Plate in a 3-point bending configuration

Figure 5.3 shows the related FE model used for this load-case. On all edge nodes, no displacement is the z-direction is enable.
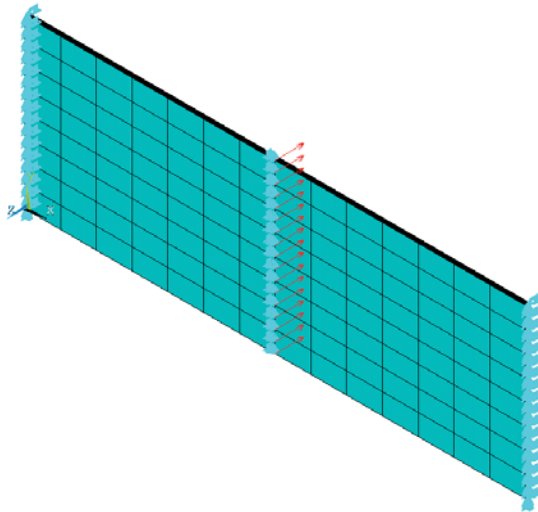
Figure 5.3: Finite element model of the plate under a 3-point bending load case

5.3.2   Stability

The stability properties of the laminate are investigated for three different load cases: in-plane compression, in-plane-shear and combination of in-

plane compression and shear. The boundary conditions are presented in
Figure 5.4. At y = 0 mm, the plate is clamped. At y = 100 mm, the
displacement along the z-axis is disabled. The displacements along the x-
and y-axis of all the nodes on this edge are coupled with the *cp* command
in ANSYS. At the short edges, all displacements of the nodes along the
z-direction are specified to zero. In addition, the displacements along the
y-axis at both of these edges are coupled. For the in-plane compression,
N_x is equal to 0 N and N_y is equal to 1 N. For the in-plane shear, N_x is
equal to 1 N and N_y is equal to 0 N. For the combined configuration, both
N_x and N_y are equal to 0.5 N. For the three load cases, the design criteria
are the critical forces: $N_{comp,cr}$, $N_{shear,cr}$ and $N_{combi,cr}$. These are the
forces at which the plate looses its stability and they are calculated by
performing an Euler-type eigenvalue buckling analysis.
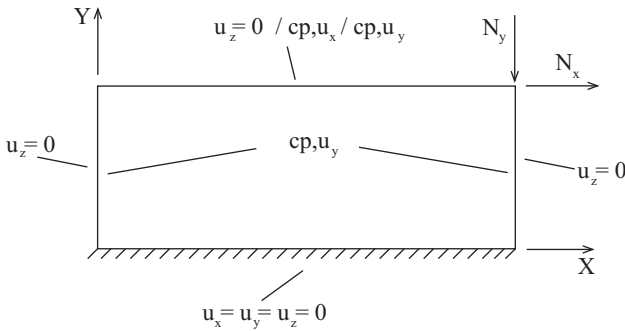
Figure 5.4: Plate subjected to an in-plane compression and shear loading

Figure 5.5 shows the finite element model and the boundary conditions
for the compression case. The force is applied on the upper right corner
through the laminate thickness. The constraining equations at y = 0.1 m
cause all nodes to undergo the same displacement u_x and u_y. The green
lines show that the nodes at x = 0 and x = 0.3 m are nodes with identical
y-position having the same u_y displacement.
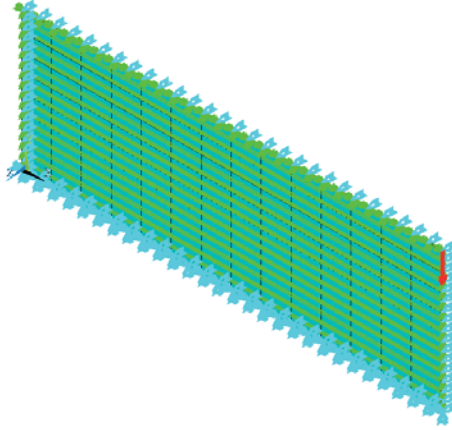
Figure 5.5: Finite element model of the plate under the compression load cases

5.3.3   In-plane stiffness

In-plane compression loading

The plate configuration is the same than the one described in Figure 5.4. The stiffness of the plate under this load case is evaluated with the stiffness constant, k_{comp}, defined as

$$k_{comp} = \frac{N_y}{\Delta L_y} \tag{5.1}$$

with N_y being the absolute applied force as shown in Figure 5.4 and ΔL_y the displacement along the y-axis.

In-plane shear loading

The plate configuration is the same as the one described in Figure 5.4. The stiffness of the plate under this load case is evaluated with the stiffness constant, k_{shear}, defined as

$$k_{shear} = \frac{N_x}{\Delta L_x} \tag{5.2}$$

with N_x being the absolute applied force as shown in Figure 5.4 and ΔL_x the displacement along the x-axis.

5.3.4   Vibration damping

In order to evaluate the vibration damping performance of the laminated plate, the structure is assumed to be under free-free boundary conditions. A modal and harmonic analysis are performed to estimate, respectively, the eigenfrequency and the modal loss factor. The latter is calculated using the modal strain energy method.

5.3.5   Reference configurations and design criteria

In order to quantify the effect of the damping layer on the mechanical and vibration damping properties of the laminate, it is necessary to define reference values for each design criteria. Table 5.3 summarizes the load cases, the reference values and the design criteria which are presented in terms of normalized values, denotes with $(\overline{X})$. Two reference laminates are considered:

Reference I

For the load cases: 3-point bending, in-plane compression, in-plane shear and combined in-plane compression and shear, the reference laminate is made of 8 composite layers with the following stacking sequence: $[0/90, \pm45, 0/90, \pm45]_s$. The plate is 300 mm long and 100 mm wide. There is no viscoelastic layer in the lay-up. This reference is named I.

Reference II

For the vibration damping case, the reference laminate has the following lay-up: $[0/90, \pm 45, 0/90, \pm 45]$ + damping layer + $[\pm 45, 0/90, \pm 45, 0/90]$. The damping layer is integrated according to Figure 5.1 and it has a thickness, h_d, of 0.25 mm. The plate is 300 mm long and 100 mm wide. This reference configuration is named II.

Table 5.3: Reference values and design criteria

Load case	Reference plate's configuration	Reference value			Design criteria
3-point bending	I	w^{ref}	=	$-9.47\ mm$	$\overline{w}$ = w^{ref}_{max}/w_{max}
	I	$P^{ref}_{z,max}$	=	$200\ N$	$\overline{P}_{z,max}$ = $P_{z,max}/P^{ref}_{z,max}$
In-plane compression	I	k^{ref}_{comp}	=	$336220\ N/mm$	$\overline{k}_x$ = k_{comp}/k^{ref}_{comp}
	I	$N^{ref}_{comp,cr}$	=	$70158\ N$	$\overline{N}_{comp,cr}$ = $N_{comp,cr}/N^{ref}_{comp,cr}$
In-plane shear	I	k^{ref}_{shear}	=	$119602\ N/mm$	$\overline{k}_{shear}$ = $k_{shear}/k^{ref}_{shear}$
	I	$N^{ref}_{shear,cr}$	=	$142976\ N$	$\overline{N}_{shear,cr}$ = $N_{shear,cr}/N^{ref}_{shear,cr}$
Stability combination	I	$N^{ref}_{combi,cr}$	=	$124939\ N$	$\overline{N}_{combi,cr}$ = $N_{combi,cr}/N^{ref}_{combi,cr}$
	II	η^{ref}_1	=	0.17	$\overline{\eta}_1$ = η_1/η^{ref}_1
Vibration damping	II	η^{ref}_2	=	0.22	$\overline{\eta}_2$ = η_2/η^{ref}_2
	II	η^{ref}_3	=	0.18	$\overline{\eta}_3$ = η_3/η^{ref}_3
	II	η^{ref}_4	=	0.15	$\overline{\eta}_4$ = η_4/η^{ref}_4

5.4 Parametric study

The parametric study is divided in two parts. In the first part, the considered laminate is the one presented in Figure 5.1. The design variables are:

- Damping layer thickness, h_d;

- Position of the damping layer in the laminate lay-up. The different positions are presented in Figure 5.6. VM stands for Viscoelastic Material.

0/90		0/90		0/90		0/90		VM
±45		±45		±45		VM		0/90
0/90		0/90		VM		±45		±45
±45		VM		0/90		0/90		0/90
VM		±45		±45		±45		±45
±45		±45		±45		±45		±45
0/90		0/90		0/90		0/90		0/90
±45		±45		±45		±45		±45
0/90		0/90		0/90		0/90		0/90
1		**2**		**3**		**4**		**5**
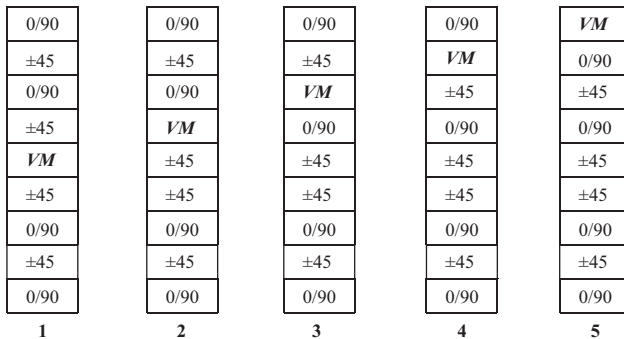
Figure 5.6: Position of the viscoelastic layer in the laminate

- Damping layer material properties, G_d and η_d;

- Length of the plate, l.

In the second part of the parametric study, the effect of the length of damping layer is investigated. As it does not cover the entire plate's surface, the damping layer can be integrated in two ways: with closed edges or with open edges. Figure 5.7 presents the considered integration solutions. The damping layer width is equal to the plate's width.
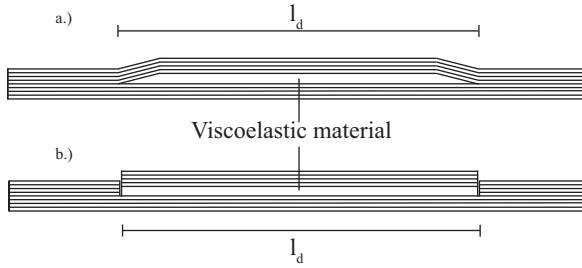
Figure 5.7: Damping layer integrated with closed (a.) and open (b.) edges

Table 5.4 summarizes the parametric study.

Table 5.4: Summary of the parametric study

Design variable	Value range	Plate's configuration
Damping layer thickness	$h_d = [0.1,...,2.5]$ mm	$l = 300$ mm and $w = 100$ mm $G_d = 1$ MPa and $\eta_d = 0.5$ Integration of the damping layer: see Figure 5.1 Position of the damping layer: see position 1 in Figure 5.6
Damping layer material properties	$G_d = [0.1,...,1000]$ MPa $\eta_d = [0.1,...,2]$	$l = 300$ mm and $w = 100$ mm $h_d = 0.25$ mm Integration of the damping layer: see Figure 5.1 Position of the damping layer: see position 1 in Figure 5.6
Damping layer position	See Figure 5.6	$l = 300$ mm and $w = 100$ mm $h_d = 0.25$ mm $G_d = 1$ MPa and $\eta_d = 0.5$ Integration of the damping layer: see Figure 5.1
Length of the plate	$l = [100,...,300]$ mm	$w = 100$ mm $h_d = 0.25$ mm $G_d = 1$ MPa and $\eta_d = 0.5$ Integration of the damping layer: see Figure 5.1 Position of the damping layer: see position 1 in Figure 5.6
Damped length closed edge	See Figure 5.7 (a).	$l = 300$ mm and $w = 100$ mm $h_d = 0.25$ mm $G_d = 1$ MPa and $\eta_d = 0.5$ Position of the damping layer: see position 1 in Figure 5.6
Damped length open edge	See Figure 5.7 (b).	$l = 300$ mm and $w = 100$ mm $h_d = 0.25$ mm $G_d = 1$ MPa and $\eta_d = 0.5$ Position of the damping layer: see position 1 in Figure 5.6

5.4.1   Influence of the damping layer thickness

In this section, the influence of the thickness of the damping material layer on the different design criteria is presented.

Normalized deflection and in-plane stiffnesses

The effect of the thickness on the normalized deflection and in-plane stiffnesses is presented in Figure 5.8. The in-plane stiffnesses do not vary with a damping layer thickness change. The viscoelastic layer separates the laminate in two sublaminates and each of them is loaded with half of the total force. An increase of the damping layer thickness simply implies an increase of the distance between the two sublaminates. The normalized deflection remains lower than its reference for all thickness values. First, it decreases from $h_d = 0.1$ mm to $h_d = 0.65$ mm where the normalized deflection reaches a reduction of 23%. In this thickness range, the shear deformation in the damping layer is so large that the total bending stiffness of the plate is reduced. From $h_d = 0.65$ mm to $h_d = 2.5$ mm, $\overline{w}$ increases again. In this thickness range, the shear deformation in the damping layer is very small and the 'Huygens-Steiner' effect is preponderant, see section 4.4.3. The overall bending stiffness increases with the distance between the mid-plane of the whole laminate and those of the sublaminates, which increases with the damping layer thickness.

Normalized maximal flexural and critical forces

The effect of the damping layer thickness on the maximal flexural and critical forces is shown in Figure 5.9. The normalized maximal flexural force has, qualitatively, the same behaviour than the normalized deflection. For h_d ranging from 0.1 mm to 0.2 mm, $\overline{P}_{z,max}$ decreases until the reduction compared to the reference is 10%. Then, it increases again. At a damping layer thickness of 1.1 mm, $\overline{P}_{z,max}$ is equal to its reference and at $h_d = 2.5$ mm, the increase of maximal flexural force is 20%. For the critical forces ($\overline{N}_{comp,cr}$, $\overline{N}_{shear,cr}$ and $\overline{N}_{combi,cr}$), the presence of the damping layer reduces their values along the thickness range. The reduction compared to their respective reference is at the lowest for h_d equal to 0.1 mm. For this thickness value, $\overline{N}_{comp,cr}$, $\overline{N}_{shear,cr}$ and $\overline{N}_{combi,cr}$ are reduced of 69%. The function of the damping layer is only to maintain the sublaminates parallel to each other. In stability problem, both
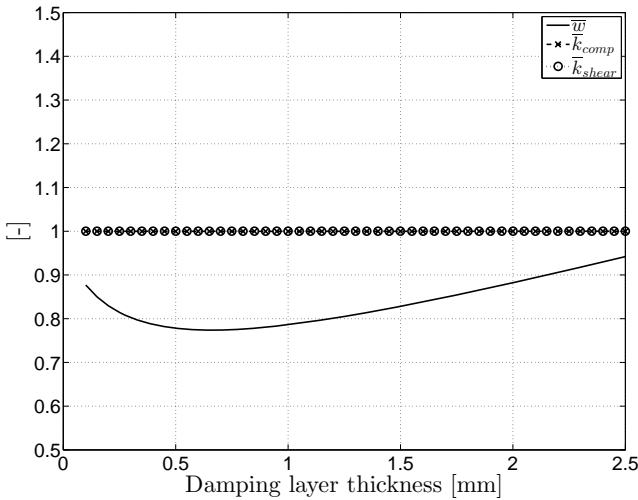
Figure 5.8: Effect of the damping layer thickness on the normalized deflection and in-plane stiffnesses

sublaminates remain equally long. This is different to a bending situation where the lower and upper sublaminates are extended and compressed, respectively. Considering the selected load introduction (see Figure 5.5), it results that the buckling behaviour of the plate is similar to that of one sublaminate. Hence, the critical forces are significantly reduced compared to their reference values.

Vibration damping

Figure 5.10 shows the effect of the damping layer thickness on the normalized modal loss factors for the first 4 bending modes. The increase of weight is also presented. The normalized weight is defined as

$$\overline{m} = \frac{m^{ref}}{m} \tag{5.3}$$
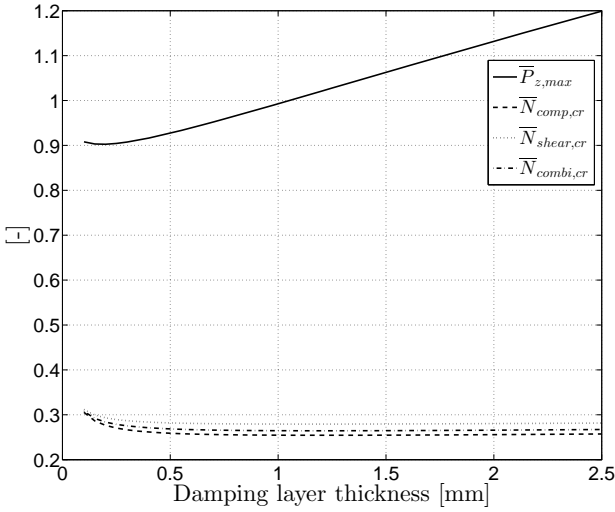
Figure 5.9: Effect of the damping layer thickness on the maximal flexural and critical loads

where m^{ref} is the plate's weight without damping treatement. m is the weight of the structure with a damping layer of thickness going from 0.1 mm to 2.5 mm. For decreasing $\overline{m}$, the total weight is increasing. For mode 1 and 2, the loss factor increases with the damping layer thickness. At $h_d = 2.5$ mm, $\overline{\eta}_1$ is twice as large as its reference and $\overline{\eta}_2$ is increased by 15%. For mode 3 and 4, the modal loss factors decrease until a minimum is reached and then they increase again. At these modes, the wavelength of the mode shape is 3 and 4 times smaller than that of the bending mode 1, respectively. Therefore, the damping layer strongly decouples the lower and upper laminates. It has the consequence that the thinner is the damping layer the larger is the shear strain deformation. The effect is illustrated in Figure 5.11. One can see that the shear strain is larger for h_d=0.1 mm than for h_d=2.5 mm. Above a given thickness value, $\overline{\eta}_3$ and $\overline{\eta}_4$ increase again because the reduction of shear strain is compensated by the fact that more and more damping material is added to the plate. The effect of the damping layer thickness on the normalized resonance frequency values is presented in Figure 5.12. All resonance frequencies
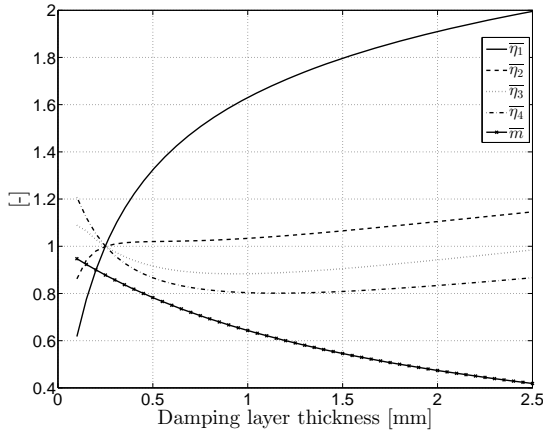
Figure 5.10: Effect of the damping layer thickness on the normalized modal loss factors

decrease with h_d as the weight of the plate increases much more than its bending stiffness. The resonance frequency of the first mode is reduced by 15 % and the resonance frequencies of the other three bending modes are reduced by approximately 25 % for h_d equal to 2.5 mm. Additionally, increasing the damping layer thickness has for effect to reduce the bending curvature of all modes. This effect is shown in Figure 5.13. It compares at the first bending mode for $h_d = 0.25$ mm and $h_d = 2.5$ mm the amplitude of vibration in the z-direction. One can that the amplitude is larger for the thinner case.
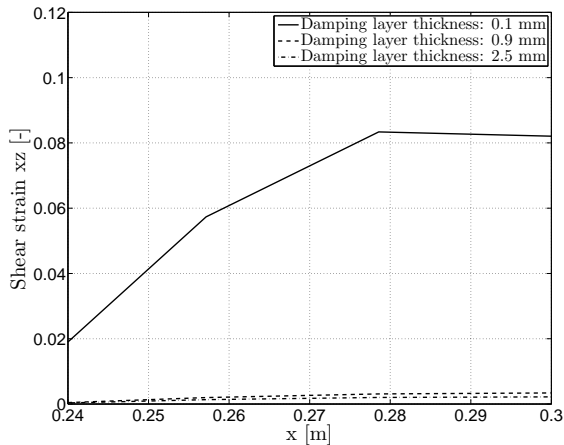
Figure 5.11: Shear strain distribution close to the plate edge at mode 3
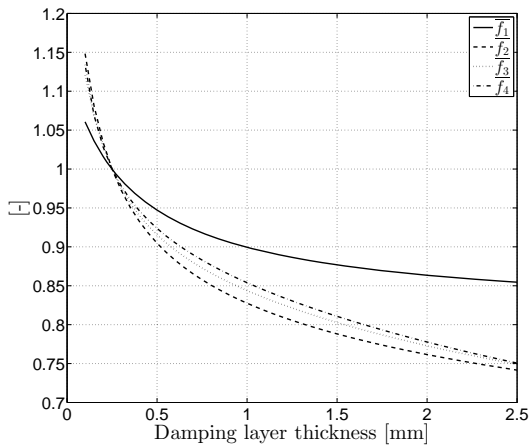
Figure 5.12: Effect of the damping layer thickness on the normalized resonance frequencies
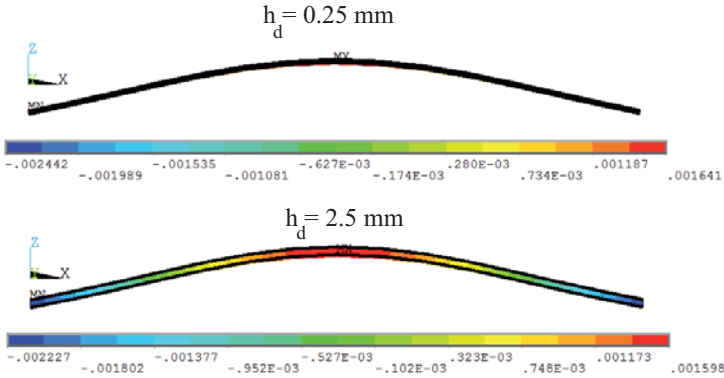
Figure 5.13: Effect of the damping layer thickness on the amplitude of vibration

5.4.2 Influence of the damping layer position

Normalized deflection and in-plane stiffnesses

Figure 5.14 presents the normalized deflection, compression and shear stiffnesses as a function of the damping layer position. For $\overline{w}$, the further the damping layer is away from the neutral axis of the plate, the larger is its bending stiffness. This phenomena has been explained in section 4.4.1. At position 1, the reduction of $\overline{w}$ is of 16% compared to the reference. At position 5, $\overline{w}$ is very close to its reference. In the latter case, the damping layer is simply laid on the surface of the laminate. For the in-plane compressive and shear stiffnesses, the damping layer has no effect. As its stiffness is much smaller than those of the sublaminates, it is negligible.

Normalized maximal flexural and critical forces

Figure 5.15 presents the effect of the damping layer position on the maximal flexural and critical forces. The best position of the damping layer under all of these criteria is when it is bonded on the surface of the laminate (position 5). $\overline{P}_{z,max}$ increases as the damping layer moves away
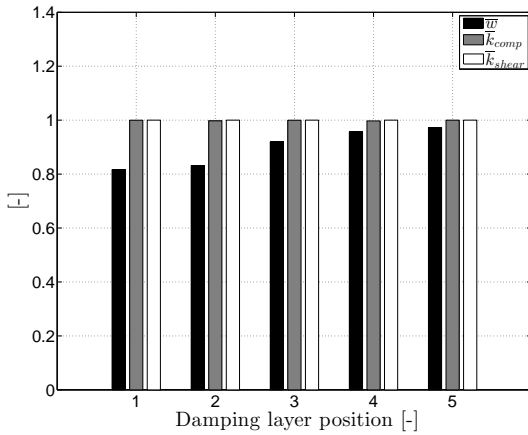
Figure 5.14: Effect of the damping layer position on the normalized deflection and in-plane stiffnesses

from the mid-plane of the laminate. It is due to the fact that bending stiffness of the plate increases with the increase of thickness of the lower laminate (as explained in chapter 4). The critical forces also increase as the damping layer is moved away from the mid-plane of the plate. As explained in section 5.4.1, the function of the damping layer is just to maintain the sublaminates parallel to each other. Hence, the buckling of the plate is similiar to the one of the thicker sublaminate. By increasing the thickness of one of those, it also improves the buckling properties of the whole laminate.

Vibration damping

The effect of the damping layer position on the normalized modal loss factors for the first four bending modes is presented in Figure 5.16. One can see that the modal loss factor reduces as the damping material is moved away from the mid-plane of the plate. Because the shear deformation in the soft layer depends of the stiffness and thickness of the contraining layers, the shear strain in the damping material is reduced as the stiffness and thickness of one of the sublaminates decreases by moving
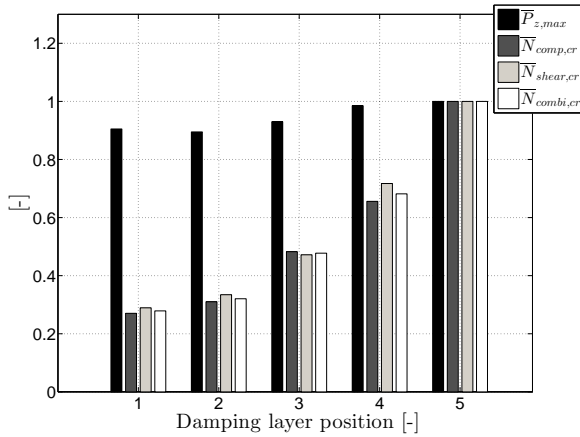
Figure 5.15: Effect of the damping layer position on the maximal flexural and critical forces

the core layer away from the laminate mid-plane. This effect is illustrated in Figure 5.17. The shear strain distribution along the x-axis is displayed from x = 0.15 mm to 0.25 mm for the first bending mode. One can see that the shear deformation reduces as the damping treatment is moved away from the plate's mid-plane. Moreover, the maximum of shear strain does not occur at the plate's edge. It is due to the fact that the shear forces are proportional to the first derivative of the curvature, which tends to zero approaching the plate's edge as illustrated in Figure 5.18
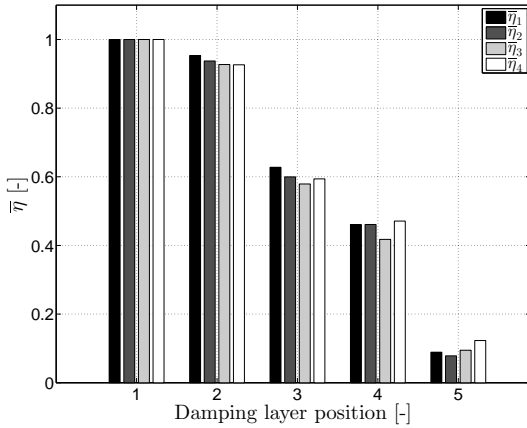
Figure 5.16: Effect of the damping layer position on the normalized modal loss factor
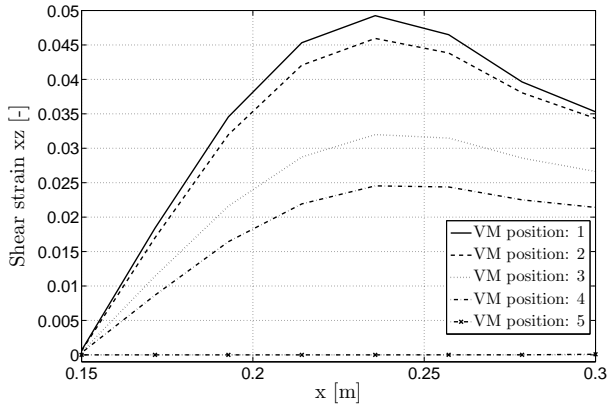
Figure 5.17: Effect of the damping layer position on the shear strain distribution at the first bending mode
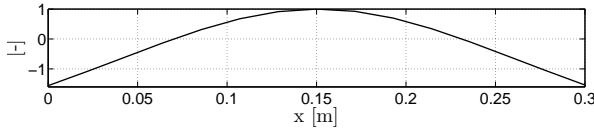
Figure 5.18: Deflection line of the plate at the first bending mode

5.4.3 Influence of the damping material parameters

In this section, the effect of the material properties of the damping layer on the different design criteria is presented.

Normalized deflection and in-plane stiffnesses

Figure 5.19 presents the normalized deflection and in-plane stiffffnesses as a function of G_d. $\overline{w}$ increases with increasing the damping layer shear modulus. For G_d larger than $2\ 10^8$ Pa, the normalized deflection is greater than the reference value. One can also see that $\overline{w}$ has an asymptotic behaviour. For G_d larger than 10^8 Pa, $\overline{w}$ does not increase significantly. The augmentation of normalized deflection is of 32% over its reference. The in-plane compression and shear stiffnesses remain equal to their respective reference values throughout the considered range. As the damping layer stiffness is so small compared to the one of the composite laminate, it has no effect on the in-plane stiffnesses of the whole plate.

Normalized maximal flexural and critical forces

The effect of the damping layer shear modulus on the normalized flexural and critical forces is presented in Figure 5.20. For all criteria, they increase as the shear modulus of the damping layer increases. For G_d larger than $2.7\ 10^7$ Pa, $\overline{P}_{z,max}$ is larger than its reference. For G_d larger than $6.5\ 10^7$ Pa, $\overline{N}_{comp,cr}$ is larger than its reference. For G_d larger than $1.3\ 10^8$ Pa, $\overline{N}_{shear,cr}$ is larger than its reference. For G_d larger than $9\ 10^7$ Pa, $\overline{N}_{combi,cr}$ is larger than its reference. One can also see that the critical forces have an asymptotic behaviour. From $G_d = 10^5$ Pa to $G_d = 10^6$ Pa, the changes of $\overline{N}_{comp,cr}$, $\overline{N}_{shear,cr}$ and $\overline{N}_{combi,cr}$ are very small
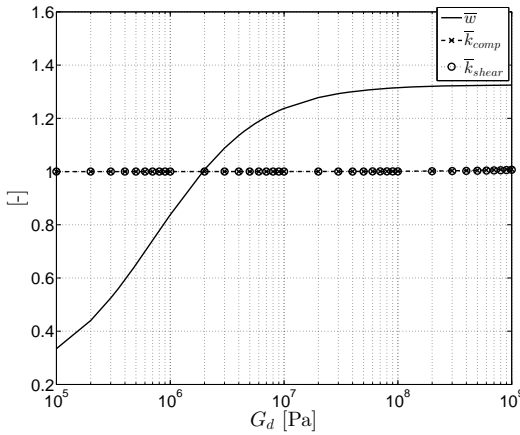
Figure 5.19: Effect of the shear modulus of the damping layer on the normalized deflection and in-plane stiffnesses

compare to their changes for G_d going from 10^6 Pa to 10^7 Pa. For very soft damping layer, a change of the shear modulus has no effect of the buckling behaviour of the plate. The damping layer just keeps the two sublaminates always parallel to each other.

Vibration damping

The effect of the variation of the shear modulus and material loss factor on the normalized resonance frequency and loss factor is presented for the first bending mode in Figure 5.21. The normalized resonance frequency, $\overline{f}$, increases as the stiffness of the damping layer increases until an asymptote is reached. One can also see that for each material loss factor, there exists a shear modulus value that maximizes the modal loss factor. Figure 5.22 shows the effect of the dynamic shear modulus for the first four bending modes. The material loss factor remains equal to 0.5. For each mode, there is an optimal value for the dynamic shear modulus. With increasing frequency, the viscoelastic material needs to be stiffer to be more efficient.
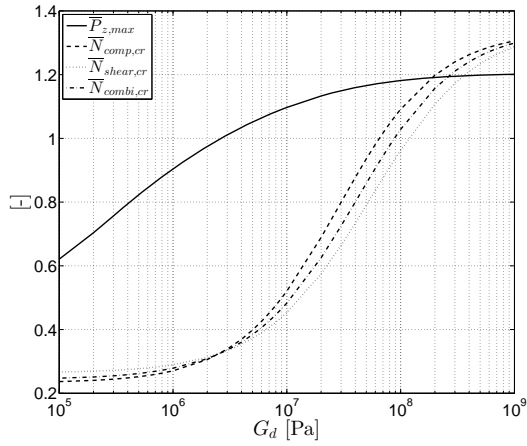
Figure 5.20: Effect of the shear modulus of the damping layer on the maximal flexural and critical forces
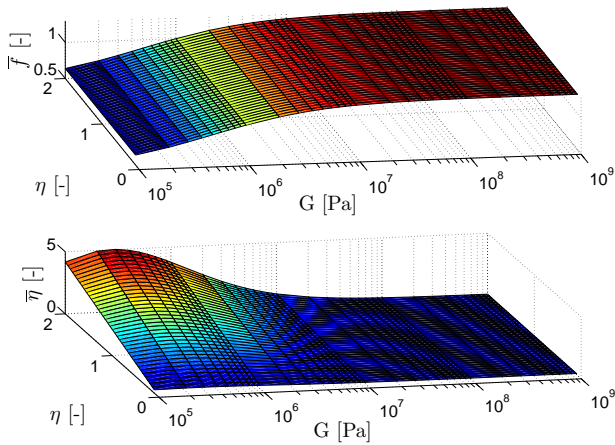
Figure 5.21: Effect of the dynamic shear modulus and the material losss factor on the normalized resonance frequency and modal loss factor of the first bending mode

Figure 5.22: Effect of the dynamic shear modulus on the normalized loss factor of the first four bending mode

5.4.4 Influence of the length of the structure

In this section, the effect of the length of the plate, l, on the different design criteria is presented.

Normalized deflection and in-plane stiffnesses

Figure 5.23 presents the normalized deflection and stiffnesses as a function of the length of the plate. The normalized deflecion decreases with increasing the length of the structure. As the internal bending moment increases, at constant force, with l, the maximal deflection, w_{max} increases. As $\overline{w}$ is inversely proportional to w_{max}, $\overline{w}$ decreases with l. It is important to note that $\overline{w}$ is not equal to 1 at $l = 0.25$ m. This is also visible in Figure 5.8 at $h_d = 0.25$ mm. It comes from the fact that the reference deflection value is calculated for a laminate without damping treatment and a laminate with an integrated damping layer is considered in the parametric study. For the in-plane compression and shear stiffnesses, they increase with an increase of the plate's length. As the plate becomes longer and

the applied force remains constant, the applied stress decreases. Therefore $\overline{k}_{comp}$ and $\overline{k}_{shear}$ increase with l.
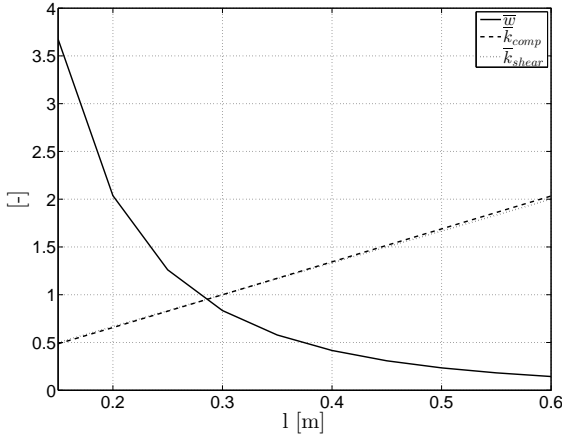
Figure 5.23: Effect of the length of the structure on the normalized deflection and in-plane stiffnesses

Normalized maximal flexural and critical forces

Figure 5.24 presents the effect of the length of the structure on the maximal flexural and critical loads. $\overline{P}_{z,max}$ decreases as the length of the plate increases. It comes from the fact that the bending moment increases with increasing the length of the plate. This leads to an increase of the longitudinal strain and a reduction of $\overline{P}_{z,max}$. Considering the boundary conditions, the plate is clamped at $y = 0$ and loaded in the x-direction at $y = 100$ mm. If the plate is getting longer, the required force to reach instability also increases.

Vibration damping

Figure 5.25 shows that the modal loss factor decreases with increasing the plate's length. It was shown in chapter 4, the damping layer tends to decouple the sublaminates. They can be considered as two separate bodies

with the same bending curvature. This leads to a high shear deformation in the core layer. By increasing the plate's length, the decoupling effect is reduced. Hence, the shear deformation in the damping layer decreases.
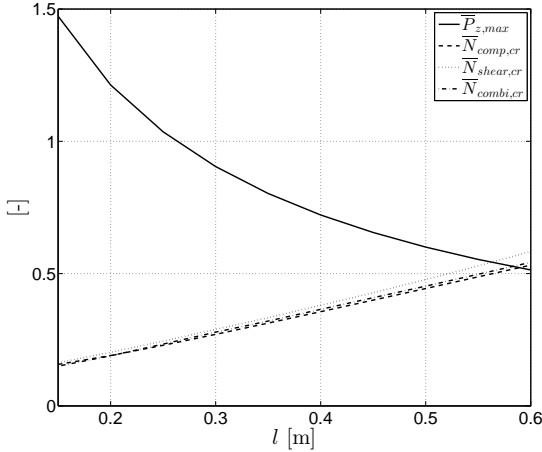
Figure 5.24: Effect of the length of the structure on the maximal flexural and critical forces

5.4.5   Influence of the length of the damping layer

In this section, the effect of the length of the damping treatment is investigated on the different design criteria. The length of the viscoelastic material, l_d, is defined in Figure 5.7. Two configurations are considered: one with closed edges (configuration a) and one with open edges (configuration b). Additionally, the width of the damping layer remains equal to the one of the plate. The results are presented as a function of the normalized damped length $\bar{l}_d$. It is defined as

$$\bar{l}_d = \frac{l_d}{l} \tag{5.4}$$

where l is the length of the plate.
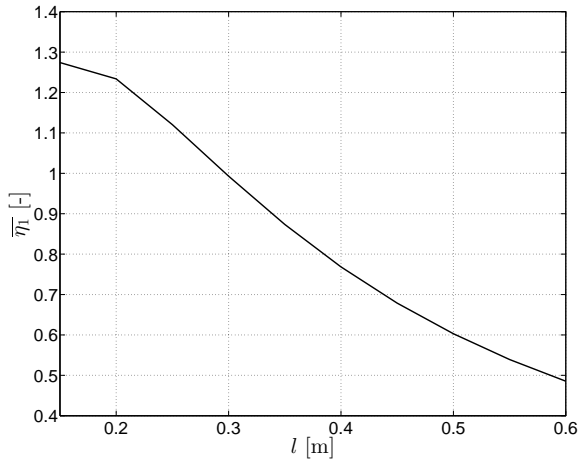
Figure 5.25: Effect of the length of the structure on the normalized modal loss factor of the first bending mode

Normalized deflection and in-plane stiffnesses

Figure 5.26 presents the effect of the damping layer length on the normalized deflection and in-plane stiffnesses. For the closed edge configuration, $\overline{w}$ is larger than the reference along the all range of the $\overline{l}_d$. At $\overline{l}_d = 0.4$, $\overline{w}$ reaches a maximum. It is 20% higher than its reference. This integrated solution is like a reinforcement to the plate resulting in an increase of the bending stiffness. For the open edge configuration, $\overline{w}$ increases with l_d from a reduction of 62% at $\overline{l}_d=0.2$ to a reduction of 27% at $\overline{l}_d=0.8$. It is due to the Huygens-Steiner effect. With increasing l_d, this effect is more and more important providing an increase of the bending stiffness. For the in-plane stiffnesses, they remain constants for both integration configuration throughout the all rane. This confirms that the damping layer does not have any effect on the in-plane stiffnesses of the plate. For the open edge configuration, $\overline{k}_{comp}$ and $\overline{k}_{shear}$ are reduced compared to their respective references by 3% and 8%. This reduction comes from the fact that the lower and the upper laminate at the edges of the damping treatment are not connected.

Normalized maximal flexural and stability forces

Figure 5.27 presents the effect of the length of the damping layer on the maximal flexural force considering closed and open edge configurations. Better results are obtained with closed edges. However, $\overline{P}_{z,max}$ with closed edge and $\overline{P}_{z,max}$ converge to the same value with increasing $\overline{l}_d$. As the edges of the damping layer move away from the center of the plate with increasing l_d, they have less and less influence on the maximal flexural force. As one can see in Figure 5.28, the normalized critical forces decrease with $\overline{l}_d$ for both configuration. Both, the open and closed configurations endure similar critical force values. This can be explained with the influence of boundary conditions. As all the nodes are coupled at $y = 100$ mm, the upper laminate constraining the damping layer also carries part of load applied to the plate regardless of the edge configuration.
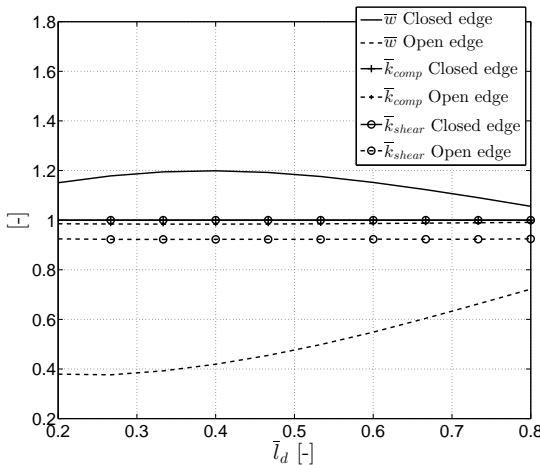
Figure 5.26: Effect of the normalized damped length on the normalized deflection and in-plane stiffnesses

Vibration damping

The effect of the damping layer length on the normalized modal loss factor at the first mode is presented in Figure 5.29. For both configura-
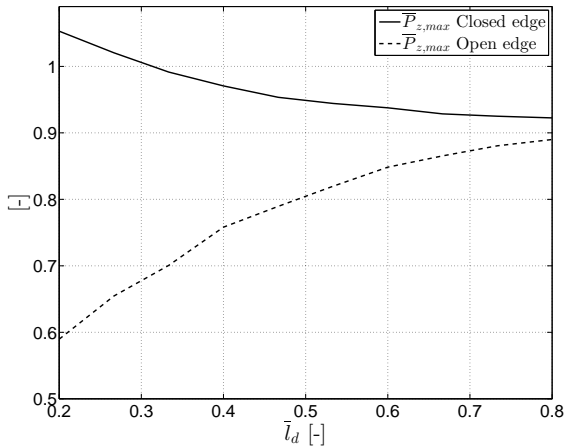
Figure 5.27: Effect of the normalized damped length on the normalized flexural forces

tions, the modal loss factor increases with $\bar{l}_d$. For configuration b.), a high shear deformation occurs at the free edges of the damping layer resulting in a higher loss factor. One can also see that there exists an optimal length of the damping layer that maximizes the modal loss factor. The effect is observed and explained in section 5.4.2. At $\bar{l}_d = 0.7$, the increase of loss factor is of 20% for the open edge configuration. For the closed edge case, $\bar{\eta}_1$ increases with $\bar{l}_d$ but is always lower than its reference value. At $\bar{l}_d = 0.8$, the reduction is of 46%.
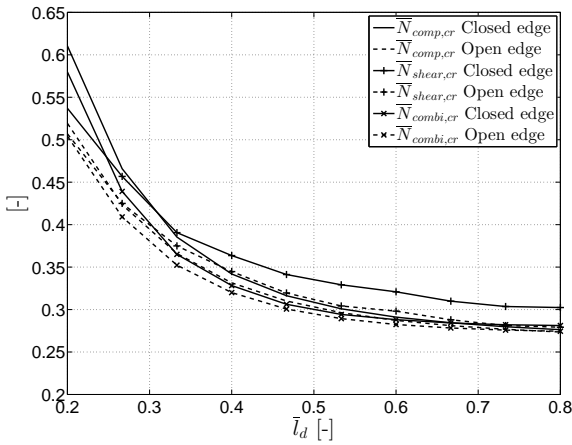
Figure 5.28: Effect of the normalized damped length on the normalized critical forces
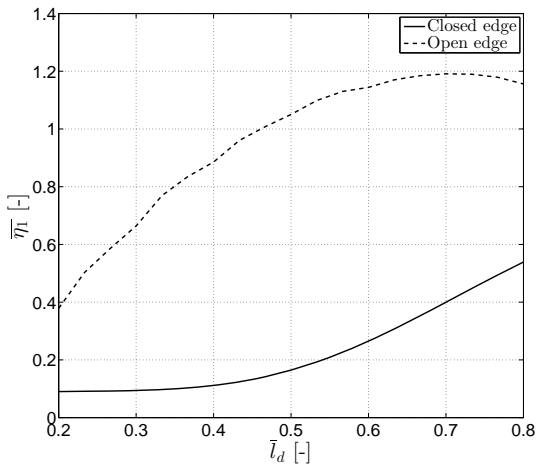
Figure 5.29: Effect of the normalized damped length on the normalized modal loss factor

5.5 Design guidelines

A parametric study has been performed to investigate the effect of an integrated damping layer on the mechanical and dynamic responses of a composite laminate. The design variables of the damping layer were: its thickness, its material properties, its position in the lay-up, and its length together with the integration configuration. The mechanical and damping properties of the laminate were asssessed with the following criteria: normalized deflection, in-plane compression and shear stiffnesses, maximal flexural load, critical forces in compression, shear and combined compression-shear and modal loss factors.

First, the material properties of the damping layer are the design variables that influence the most the normalized deflection, maximal flexural and critical forces, and loss factors. Nonetheless, there are bounds to the effect of these design variables. Above 10^8 Pa, a change of G_d does not significantly influence the normalized deflection and maximal flexural force. The normalized critical forces are affected by a change of the damping layer shear modulus if it stays within the range 10^6 - 10^9 Pa. The modal loss factors are affected by a change of G_d if it stays within the range 10^5 - 10^8 Pa. The material loss factor can be as high as possible to obtain the highest modal loss factors.

The damping layer thickness can be used to increase the normalized deflection, the maximal flexural force and the damping rate of the laminate. The thickness can be as large as possible.

The study on the damping layer position shows that it should be placed in the middle of the laminate lay-up to obtain high vibration damping properties and it should be placed as far away as possible from the plate's mid-plane to obtain high mechanical performances.

The damping layer should be integrated with closed edge and it should be as short as possible to obtain the highest normalized deflection, maximal flexural and critical forces. The damping layer should be integrated with open edges and should be significantly long to have high damping properties. However, the influence of the integration solution has to be considered together with the plate's length. It was shown in a previous chapter that the damping layer tends to decouple the sublaminates for small length-to-thickness ratio. This decoupling effect reduces with increasing the length of the plate. Hence, the difference of mechanical and

damping properties between the closed and open edges configurations reduces as the plate is getting longer. Hence, the choice of configuration ceases to have an influence on the performance of thin plates.

Finally, the in-plane stiffnesses of the laminate are not influenced by the presence of the damping layer.

Table 5.5 summarizes the required values for the different design variables to obtain at least the same values as the reference. DL stands for Damping Layer. NE (No Effect) means that this design variable has no effect on the design criteria. CR (Criteria Reduced) means that, for any value of the design variable, the design criteria is reduced compared to its reference. The primary design rules that can be extracted from Table 5.5 are:

- The damping layer should be integrated with closed edges and it should be short and placed as far away as possible from the mid-plane of the laminate to obtain good structural properties.

- The damping layer should have open edges, it should cover more than 45 % of the plate's surface and it should be placed in the middle of the laminate lay-up to reach good vibration damping performances.

For the design of composite laminates with integrated damping layer with closed edges along its length, the additional design rules are:

- If the objective is to achieve high bending properties, h_d has to be larger than 2.5 mm, G_d has to be larger than $2.7 \ 10^6$ Pa and l_d has to be smaller than 0.1 m to reach the reference value.

- If the objective is to obtain good stability, G_d has to be larger than $1.3 \ 10^8$ Pa.

Using the design variable values that would provide at least the same mechanical properties than the reference, namely:

- $h_d = 2.5$ mm;

- $G_d = 1.3 \ 10^8$ Pa;

- $\eta_d = 0.5$;

- $l_d = 0.1$ m;

the modal loss factor of the laminate with closed edge damping layer is 2.5% and the modal loss factor of the laminate with open edge damping layer is 8.0%. Using the same damping layer characteristics, the closed edge integration concept can introduce only much smaller amounts of damping than the classical constrained layer damping treatment configuration (open edges). Hence, the design of such structure is based on a trade-off between mechanical and vibration damping performances. This will be quantified by using parameter optimization as presented in the next chapter together with the weight impact of the damping treatment.

Table 5.5: Summary of the design variable values

Design criteria	DL Thickness	DL material properties	DL position	DL Integration	DL length
$\overline{w}$	$h_d > 2.5$ mm	$G_d > 2\ 10^6$ Pa	5	closed	0.06 m < l_d < 0.24 m
$\overline{k}_{comp}$	NE	NE	NE	closed	NE
$\overline{k}_{shear}$	NE	NE	NE	closed	NE
$\overline{P}_{z,max}$	$h_d > 1.1$ mm	$G_d > 2.7\ 10^6$ Pa	5	closed	$l_d < 0.1$ m
$\overline{N}_{comp,cr}$	CR	$G_d > 6.5\ 10^7$ Pa	5	closed	CR
$\overline{N}_{shear,cr}$	CR	$G_d > 1.3\ 10^8$ Pa	5	closed	CR
$\overline{N}_{combi,cr}$	CR	$G_d > 8.9\ 10^7$ Pa	5	closed	CR
$\overline{\eta}_1$	$h_d > 0.27$ mm	$G_d < 10^6$ Pa $\eta_d > 0.5$	1	open	$l_d > 0.14$ m

Chapter 6

Performances of composite laminates with viscoelastic damping treatments

In this chapter, the performances of constrained layer damping treatment and integrated layer damping treatment are compared. The comparison is based on mechanical, damping and weight criteria with the goal to identify the design solution which provides the best trade-off.

6.1   Introduction

This section deals with the design optimization of composite laminates with integrated damping layers. In chapter 5, a parametric study has been performed with the goal to establish a guideline for composite laminates with integrated damping treatments. It was shown that, using the same damping layer design properties, a composite laminate with a constrained layer damping treatment (open edees) always provides better damping performances than a composite laminate with integrated damping layer.

131

That said, the next question arising is the following:

- How large has to be the change of weight and mechanical properties for the composite laminate with integrated damping layer to reach the same damping performance than a composite laminate with a constrained layer damping treatment?

The objective of this chapter is to quantify for different mechanical criteria the trade-off with vibration damping properties and weight. The approach is the following:

1. A reference composite laminate without damping treatment is used to define reference values for the different mechanical criteria.

2. A composite laminate with a constrained layer damping treatment is considered. The dimensions and material properties of the damping treatment are optimized in order to minimize the weight of the plate and to obtain, at least, the same mechanical properties than the reference laminate and 10% of damping rate.

3. A composite laminate with an integrated damping treatment is considered. The dimensions and the material properties of the damping treatment are optimized in order to minimize the weight of the plate and to obtain, at least, the same mechanical properties than the reference laminate and 10% of damping rate.

A comparison of the results from step 2 and 3 will allow to conclude on the sensitivities of the laminate properties on the design configuration of the damping treatment (either constrained layer damping or integrated layer damping). Section 6.2 presents the reference laminate, the different mechanical criteria and their reference values. Section 6.3 deals with the composite laminate with a constrained layer damping treatment. Section 6.3.1 details the composite structure and explains the optimization method. The results are presented in section 6.3.2. Section 6.4 deals with the composite laminate with an integrated damping layer treatment. Section 6.4.1 presents the structure of interest. The results are listed in section 6.4.2. A conclusion is given in section 6.5.

6.2 Reference laminate

The reference laminate is the same as the reference used in chapter 5. It is a composite laminated plate that is 300 mm long, 100 mm wide and is made of 8 layers with the following stacking sequence: $[0/90, \pm 45, 0/90, \pm 45]_s$. Each layer has a thickness of 0.30 mm. Their material properties are also the same than the ones used in chapter 5 (see Table 5.1). The mechanical criteria are the following:

- Deflection, w;

- In-plane compression stiffness, k_{comp};

- In-plane shear stiffness, k_{shear};

- Maximal flexural force, $P_{z,max}$;

- In-plane compressive critical force, $N_{comp,cr}$;

- In-plane shear critical force, $N_{shear,cr}$;

- Combined compression and shear critical force, $N_{combi,cr}$.

The boundary conditions are detailed in chapter 5. Table 6.1, 6.2 and 6.3 summarize, respectively, the reference values for the stiffness, structural strength and stability criteria.

Table 6.1: Reference values for the stiffness criteria

Deflection	w [mm]	-9.47
In-plane compressive stiffness	k_{comp} [N/mm]	336220
In-plane shear stiffness	k_{shear} [N/mm]	119602

Table 6.2: Reference values for the structural strength criteria

Maximal flexural force	$P_{z,max}$ [N]	200

Table 6.3: Reference values for the stability criteria

In-plane compression	$N_{comp,cr}$ [N]	70158
In-plane shear	$N_{shear,cr}$ [N]	142976
Combination shear and compression	$N_{combi,cr}$ [N]	124939

6.3   Composite laminate with constrained layer damping treatment

In this section, the trade-off between weight, mechanical and damping performances for a composite plate with constrained layer damping treatment is investigated.

6.3.1   Structure of interest

The structure of interest is a quasi-isotropic composite laminate on top of which is bonded a constrained layer damping treatment. The load-carrying plate is 300 mm long and 100 mm wide. It consists of 8 layers. The stacking sequence is the following: $[0/90, \pm45, 0/90, \pm45]_s$. Each composite layer is 0.30 mm thick. Their material properties are the those given in chapter 5. Figure 6.1 shows the laminate with constrained layer damping treatment. It also presents the design variables considered for the optimization. The vector of design variable is defined as follows

$$\{\mathbf{x}\} = \left\{ \begin{array}{c} h_d \\ l_d \\ w_d \\ G_d \\ \eta_d \\ h_{cons} \end{array} \right\} \tag{6.1}$$

where h_d is the thickness of the damping layer, l_d its length, w_d its width, G_d its shear modulus, η_d its loss factor and h_{cons} is the thickness of the constraining layer which is made of aluminium. As explained in section

6.1, the goal of the optimization is to minimize the weight of the plate and to have, at least, the same mechanical performance as the reference and 10% of damping rate. Constraints are also placed on the design variables in order to obtain realistic values. The objective function is transformed using the exterior penalty method to take into account the constraints. It can be written as follows

$$
\begin{aligned}
p\left(\{\mathbf{x}\}, R\right) \;=\; & min\left(weight\right) + R \times \big(max\left(0, A_{ref} - A\right)^2 + \\
& max\left(0, \eta_{min} - \eta\right)^2 + max\left(0, \eta - \eta_{max}\right)^2 + \\
& max\left(0, h_{d,min} - h_d\right)^2 + max\left(0, h_d - h_{d,max}\right)^2 + \\
& max\left(0, l_{d,min} - l_d\right)^2 + max\left(0, l_d - l_{d,max}\right)^2 + \qquad (6.2) \\
& max\left(0, w_{d,min} - w_d\right)^2 + max\left(0, w_d - w_{d,max}\right)^2 + \\
& max\left(0, G_{d,min} - G_d\right)^2 + max\left(0, G_d - G_{d,max}\right)^2 + \\
& max\left(0, \eta_{d,min} - \eta_d\right)^2 + max\left(0, \eta_d - \eta_{d,max}\right)^2 + \\
& max\left(0, h_{cons,min} - h_{cons}\right)^2 + max\left(0, h_{cons} - h_{cons,max}\right)^2 \big)
\end{aligned}
$$

R is the penalty factor and it is equal to 10^3. With this penalty factor value, one obtains a violation of the design domain of 1%. The first element of the constraining function is used to enforce the considered mechanical criteria, noted A in Equation 6.7, to be better than its reference, noted A_{ref} in Equation 6.7. The second and the third elements are used to impose that the modal loss factor reaches 10%. η_{min} and η_{max} are, respectively, equal to 9.99% and 10.01%. The other elements of the constraining fuction are used to define lower and upper bounds for the feasible domain of the design variables.
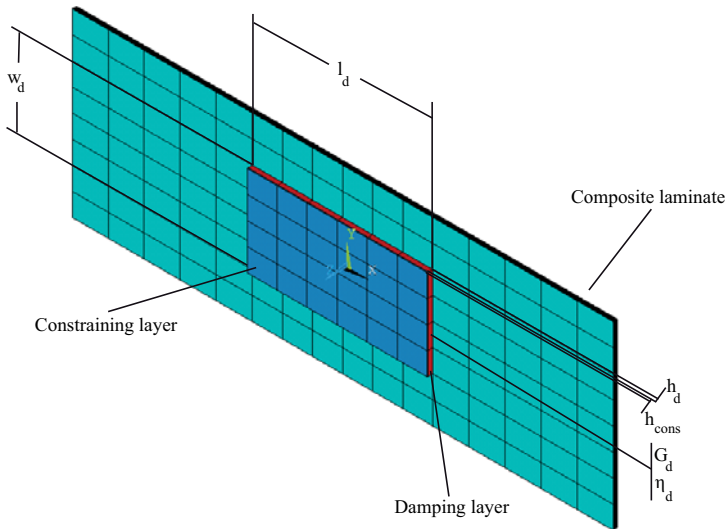
Figure 6.1: Composite laminate with a constrained layer damping treatment

Table 6.4: Bounds for the feasible domain of the design variables

$h_{d,min}$	[mm]	0.1
$h_{d,max}$	[mm]	5
$l_{d,min}$	[mm]	10
$_{d,max}$	[mm]	295
$w_{d,min}$	[mm]	10
$w_{d,max}$	[mm]	95
$G_{d,min}$	[Pa]	10^5
$G_{d,max}$	[Pa]	10^9
$\eta_{d,min}$	[-]	0.1
$\eta_{d,max}$	[-]	3
$h_{cons,min}$	[mm]	0.1
$h_{cons,max}$	[mm]	2

Table 6.5: Inital values of the design variables

h_d [mm]	2.5
l_d [mm]	100
w_d [mm]	50
G_d [Pa]	$1.3\ 10^8$
η_d [-]	0.5
h_{cons} [mm]	0.5

The optimization algorithm is based on the gradient of the objective function using the method of the steepest descent [79]. Considering x_0, a reference point, f the function value at that point and ∇f the gradient, the latter provides the direction of the steepest descent in the space of the optimization variables $\mathbf{x}$. At the reference point, the direction of the steepest descent is defined as

$$\mathbf{s} = -\nabla f \tag{6.3}$$

The direction of the steepest descent is the direction along which to locate points with lower function values. Moving along the search direction will initially obtain smaller function values but after reaching a minimum the values, from there on, again increase. This generates the sequence

$$\mathbf{x}\left(\alpha\right) = \mathbf{x}^k + \alpha.\mathbf{s}^k \tag{6.4}$$

where α is the step length. The slope $f^{'}$ is the component of the gradient in the search direction.

$$f^{'} = \frac{\partial f}{\partial \alpha} = \frac{\partial f}{\partial \alpha}.\frac{\partial \mathbf{x}}{\partial \alpha} = \nabla f\left(\alpha\right).s^k \tag{6.5}$$

It vanishes at the minimum point along the search direction because there the search direction and the gradient are perpendicular to each other. The initial values of the design variables are presented in Table 6.5. They correspond to the values extracted from the parametric study and presented in section 5.5.

6.3.2 Results

The results of the optimization for the laminate with a constrained layer damping treatment is presented in Table 6.6 for each design criteria. It is shown in parenthesis the difference with the reference value.

Table 6.6: Mechanical properties of the optimized laminate with a constrained layer damping treatment

w [mm]	-4.4 (-55%)
k_{comp} [N/mm]	339553 (+1%)
k_{shear} [N/mm]	123176 (+3%)
$P_{z,max}$ [N]	593 (+197%)
$N_{comp,cr}$ [N]	92333 (+32%)
$N_{shear,cr}$ [N]	186616 (+31%)
$N_{combi,cr}$ [N]	151479 (+21%)

One can see that the deflection and maximal flexural force are significantly changed. It was shown in chapter 5 that the damping layer has no effect on the mechanical properties of the load-carrying structure when it is simply laid on its surface. However, this is not true when the damping layer is constrained. It further increases the bending stiffness of the plate because of the "Huygens-Steiner" effect. Hence, the deflection is reduced and the maximal flexural force is increased. This effect also influences the critical forces that are increased. One can also see that the in-plane stiffnesses change only sligthly compared to their reference. Table 6.7 presents the plate's weight, the modal loss factor and the final design variables values. They are the same for each design criteria. As the damping layer does not have a negative effect on the mechanical properties of the laminate, the mechanical constraint in the transformed objective function is never active. As a consequence, the optimization objective is only to minimize the weight and to reach 10 % of damping rate. Compared to the initial values presented in Table 6.5, the material properties of the damping layer are the most changed design variables. It confirms the observation made in the parametric study that the material properties of the damping layer are the parameters that affect the most the mechanical properties of the load-carrying structure.

Table 6.7: Final design variable values for the composite laminate with CLD treatment

Weight [g]	0.132
η [%]	10
h_d [mm]	2.3
l_d [mm]	104.6
w_d [mm]	48.4
G_d [MPa]	386.3
η_d [-]	1.4
h_{cons} [mm]	0.73

6.4 Composite laminate with integrated layer damping treatement

In this section, trade-off between weight, mechanical and damping performances of a composite plate with an integrated layer damping treatment is investigated.

6.4.1 Structure of interest

The structure of interest is a composite laminate with integrated damping layer treatment. Figure 6.2 presents a picture of the finite element model of it. The composite plate is 300 mm long and 100 mm wide. The damping layer is integrated with closed edges along its length and its width. The design variables of the damping layer are also shown. The composite laminate also consists of 8 layers with the following stacking sequence: $[0/90, \pm 45, 0/90, \pm 45]_s$. Each composite layer is 0.3 mm thick. Their material properties are presented in Table 5.1. The goal of the optimization is, like for the composite plate with a constrained layer damping treatment, to minimize the weight and to obtain, at least, the same mechanical properties than the reference and 10 % of damping rate. The design variables are the damping layer thickness, length, width and material properties. The vector of design variables can be written as follows

$$\{\mathbf{x}\} = \left\{ \begin{array}{c} h_d \\ l_d \\ w_d \\ G_d \\ \eta_d \end{array} \right\} \tag{6.6}$$

The transformed objective function has the following form

$$
\begin{aligned}
p\left(\mathbf{x}, R\right) \quad = \quad & min\left(weight\right) + R \times \Big(max\left(0, A_{ref} - A\right)^2 + \\
& max\left(0, \eta_{min} - \eta\right)^2 + max\left(0, \eta_{-}\eta_{max}\right)^2 + \\
& max\left(0, h_{d,min} - h_d\right)^2 + max\left(0, h_d - h_{d,max}\right)^2 + \\
& max\left(0, l_{d,min} - l_d\right)^2 + max\left(0, l_d - l_{d,max}\right)^2 + \qquad (6.7) \\
& max\left(0, w_{d,min} - w_d\right)^2 + max\left(0, w_d - w_{d,max}\right)^2 + \\
& max\left(0, G_{d,min} - G_d\right)^2 + max\left(0, G_d - G_{d,max}\right)^2 + \\
& max\left(0, \eta_{d,min} - \eta_d\right)^2 + max\left(0, \eta_d - \eta_{d,max}\right)^2
\end{aligned}
$$

where the parameter R and the boundaries of the feasible domain of each design variables have the same values than the ones given in section 6.3.
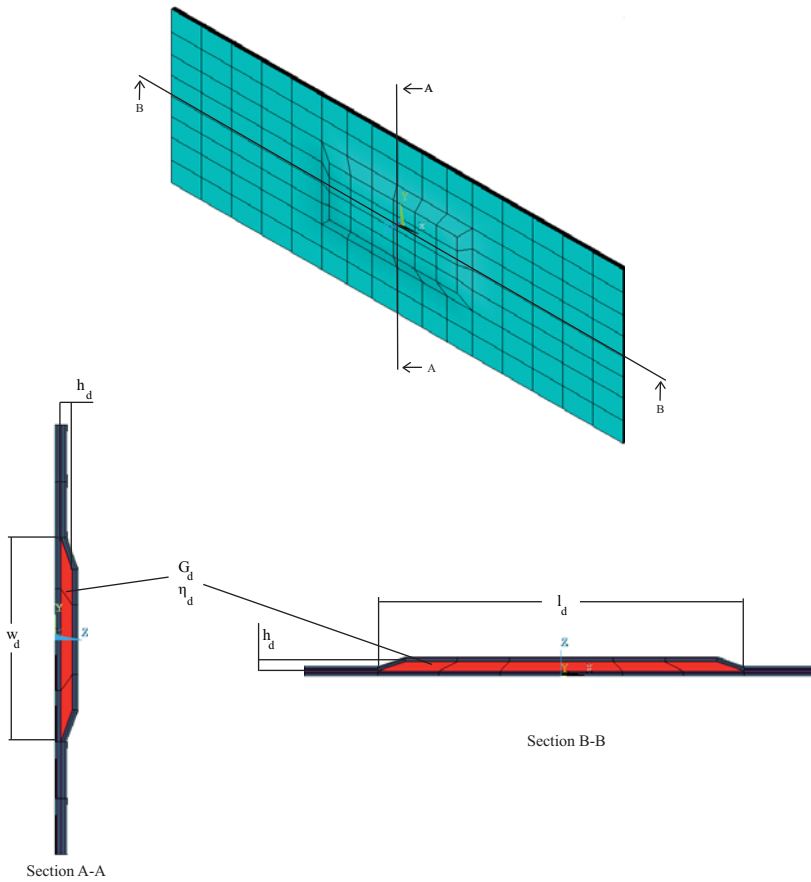
Figure 6.2: Composite laminate with an integrated damping treatment

6.4.2 Results

The results of the optimization are presented in Table 6.8. It is shown the value of the different mechanical criteria and in parenthesis the difference with the reference value.

Table 6.8: Mechanical properties of the optimized laminate with an integrated layer damping treatment

w [mm]	-1.7 (-82%)
k_{comp} [N/mm]	335646 (-0.2%)
k_{shear} [N/mm]	118593 (-1%)
$P_{z,max}$ [N]	571 N (+186%)
$N_{comp,cr}$ [N]	146401 (+101%)
$N_{shear,cr}$ [N]	234681 (+64%)
$N_{combi,cr}$ [N]	246583 (+97%)

One can see that the deflection, maximal flexural load and critical forces are significantly increased compared to the reference values. The design variable values are presented in Table 6.9. They are the same for each of these design criteria. Like for the composite plate with a constrained layer damping treatment, the presence of the damping layer does not reduce the values of these criteria compared to the reference. Hence, the mechanical constraint in the objective function is never active. Compared to the results presented in chapter 5, the performances of the laminate with an integrated damping layer are significantly better. It comes from the fact that all edges of the damping layer are closed. Hence, there is no decoupling effect anymore. This explains the reduction of deflection and the increase of maximal flexural and critical forces.

The in-plane stiffnesses are very similar to their reference. Table 6.10 shows the value of the obtained damping rate and design variable values for the in-plane stiffness criteria. One can see that the modal loss factor is only 1.5 % . The main difference compared to Table 6.9 is that the damping layer thickness is more than 5 times smaller. Hence, the damping rate is so low. If the damping layer thickness were larger, the upper sublaminate covering the damping layer would carry less of the applied load. This would lead to a reduction of the in-plane stiffnesses. Such effect was actually not observed in the parametric study of chapter 5

Table 6.9: Final design variable values for the composite laminate with an integrated damping layer treatment considering the deflection, maximal flexural and critical forces

Weight [g]	0.154
η [%]	10
h_d [mm]	2.7
l_d [mm]	257.1
w_d [mm]	71.7
G_d [MPa]	849.8
η_d [-]	1.7

as the damping layer thickness was not changed while the effect of the damping layer length and the integration solution (closed or open edges) were investigated. Using the design characteristics from Table 6.8, the in-plane compression and shear stiffnesses of the laminate would be further reduced by 19% and 13%, respectively. It means that it is not possible to obtain a composite laminate with an integrated damping layer having simultanously high in-plane stiffnesses and damping rate.

Table 6.10: Final design variable values for the composite laminate with an integrated damping layer treatment considering the in-plane compression and shear stiffnesses

	k_{comp}	k_{shear}
Weight [g]	0.111	0.111
eta [%]	1.5	1.5
h_d [mm]	0.5	0.5
l_d [mm]	196.8	259.1
w_d [mm]	61.7	85.0
G_d [MPa]	772.9	558.2
η_d [-]	1.5	2.8

6.5 Discussion

In this chapter, the performances of a composite laminate with a constrained layer damping treatment and of a composite laminate with an integrated damping layer treatment are compared. An optimization technique is used to find the design variable values that give the most satisfying trade-off between weight, mechanical and vibration damping properties. Table 6.11 compares the obtained mechanical properties for the composite laminate with a constrained layer damping (CLD) treatment and for the composite laminate with an integrated damping layer (ILD) treatment. The difference of performances between the ILD and CLD treatments are also shown.

Table 6.11: Performance comparison

	Plate with CLD	Plate with ILD	Difference [%]
w [mm]	-4.4	-1.7	-61
k_{comp} [N/mm]	339553	335646	-1
k_{shear} [N/mm]	123176	118593	-4
$P_{z,max}$ [N]	593	571	-4
$N_{comp,cr}$ [N]	92333	146401	+58
$N_{shear,cr}$ [N]	186616	234681	+25
$N_{combi,cr}$ [N]	151479	246583	+62

One can see that the integrated damping layer solution provides significantly better deflection and buckling properties than the classical constrained layer damping treatment. These results slightly differ from the ones presented in chapter 5. It was shown that the buckling properties are strongly reduced for a composite laminate with an integrated damping layer. It is because the damping layer was integrated with closed edges only along its width and its shear modulus was much smaller. Presently, the damping layer is closed on each edge and the shear modulus is almost 1000 times higher. Hence, the integrated design solution reinforces the composite laminate. One can also see that there is no significant difference between the two design solutions for the maximal flexural strength and for in-plane stiffnesses. For the latter, the results show that it is not possible to reach the objective of 10 % modal loss factor.

Table 6.12 compares the design variable values and weight to obtain 10 % of damping rate. One can see that the damping solution with the smallest weight is the constrained layer damping treatment. When the damping layer is integrated with closed edges, there is no possible edge effect. Hence, the damping layer has to be thicker (+18%), longer (+146%), wider (+50%), stiffer (+119%) and to be able to dissipate more energy (+21%) in order to reach the same damping properties as a constrained layer damping treatment. Hence, a constrained layer damping treatment is lighter than an integrated layer damping treatment. However, Table 6.11 shows that the deflection, maximal flexural force and buckling properties are significantly higher for composite laminate with an integrated damping layer. As a consequence, there would be the possibility to reduce the plate's weight by reducing the number of composite layers and to keep these mechanical properties above their reference.

Table 6.12: Comparison of the weight and design variable values

	Plate with CLD	Plate with ILD	Difference [%]
Weight [g]	0.132	0.154	+16
h_d [mm]	2.3	2.7	+18
l_d [mm]	104.6	257.1	+146
w_d [mm]	48.4	71.7	+50
G_d [MPa]	386.3	849.8	+119
η_d [-]	1.4	1.7	+21
h_{cons} [mm]	0.73	-	-

Finally, it must be said that the integrated damping layer solution requires a much more efficient damping material than the CLD solution in order to reach the same structural damping rates. Moreover, it is significantly heavier than the CLD solution. Therefore the constrained layer damping treatment is the design solution that proposes the most satisfying trade-off between weight, mechanical properties and vibration dampig performance.

Chapter 7

Conclusions and outlook

7.1 Conclusions

This thesis studies the performance of composite laminates with integrated damping layer treatments. Performance aspects include damping rates as well as structural stiffness, strength and stability under various loading conditions. A combined assessment of all these items have not been found in the open literature. The performances are compared with those of a classical constrained layer damping treatment. In the latter, the constraining layer has for unique function to increase the damping rate. In the integrated concept, the damping layer is constrained by composite laminates that have also to fulfill mechanical requirements. This thesis has investigated the hypothesis that integrating the damping layer in a fiber-reinforced structure would lead to high mechanical properties as well as high vibration damping rates. The study results in design guidelines for the composite laminates with embedded damping layers.

First, a finite element model of a constrained layer damping treatment is developed and validated using experimental results from the available literature. The performances of segmented constrained layer damping treatments are investigated. It is shown that the free edges of the damping treatment have to be placed at locations where the bending curvature of the load-carrying structure is the highest to reach the largest damp-

ing rate. This study also investigated the effects of the number and the position of the segments. It is demonstrated that there exists a given number of segments for each bending mode that maximizes their loss factor. Optimizing the segment's position provides a moderate increase of the structural damping properties.

In the second part, the behaviour of a composite beam with a soft core layer is investigated. A numerical model of it is validated using Pagano's exact solution of composite laminate in cylindrical bending. The main outcome of this study is that the core layer tends to decouple the sublaminates. They behave like two separate bodies experiencing the same curvature. However, this effect vanishes by increasing the length-to-thickness ratio of the structure.

In the last part, the influence of an integrated damping layer on the structural stiffness, strength and stability properties of a composite laminate is studied. Three integration solutions are considered: a composite plate with a damping layer integrated in a sandwich configuration (the damping layer has the same length and width than the laminated plate and open edges), a composite plate with an integrated damping layer having closed edges along its width and a composite plate with an integrated damping layer having closed edges along both its length and width. The study on the first integration solution showed that the damping layer can be used to increase the structural bending stiffness and bending strength by having a stiff and thick damping layer. Nonetheless, it is also shown that this integration solution significantly reduces the buckling strength of the laminate. The investigation on the second integration solution shows that it is possible to sligthly improve the buckling strength if the damping layer edges are closed along its width and as short as possible. However, the obtained damping rates are significantly smaller than the ones obtained with a classical constrained layer damping solution. This part of the thesis reveals the difficulty to design composite laminates with integrated damping layers. Two distinctives design rules have to be followed, depending on whether the goal is to reach high mechanical porperties or high damping properties. They are:

- The damping layer has to be in the middle of the lay-up, to have open edges, to cover at least half of the plate's surface and to have a soft shear modulus in order to reach a significant damping rate.

- The damping layer has to be as far away as possible from the lami-

nate mid-plane, to have closed edges, to be as short as possible and to have a high shear modulus in order to obtain high mechanical properties.

Among the three integration solutions, the most promising solution is the one with an integrated damping layer having closed edges along its length and width. Closing all edges enables to cancel the decoupling effect due to the damping layer. The main advantage is that it significantly increases the structural bending stiffness, strength and buckling properties. The main limitation is that the damping layer has to have special properties. It must have a high shear modulus to reach high mechanical properties and a high loss factor to reach high damping rate objectives. Additionally, it must also have larger dimensions than a classical constrained layer damping treatment in order to reach the same damping rate.

Potential applications for this integrated concept are where the design objectives are only high bending stiffness and buckling strength. Significant damping rates could be reached assuming that stiff damping materials with high energy dissipation capabilities are available. It could be used in the automotive industry for car body panels. For example, floor and roof panels have to exhibit a high bending stiffness and be able to dissipate as much vibrating energy as possible to improve passengers acoustic confort. The main limitation of this concept is the weight penalty. Therefore, it is not suitable for aeronautics and aerospace applications.

Finally, it must be concluded that the constrained layer damping treatment is the best solution to achieve the objectives of high mechanical properties, high damping performances and low weight.

7.2 Outlook

To ensure the validity of the model predictions, it is required to have a precise measurement of the material properties of the composite and damping layers. The latter are very critical because of their frequency- and temperature-dependent behaviour. Then, the corrected properties could be also used to investigate the long-term reliability, fatigue, delamination and impact resistance behaviour of the integrated concept.

This thesis is concluded by summarizing ideas for further research:

- **Manufacturing process**: If an industrial application is considered, it is required to have an efficient manufacturing process. It is important to study the effect of the damping layer on the laminate quality and to identify how the parameters of the process are affected by the damping layer. A comparative study of different processes could be performed with the goal to identify the most appropriate one for the integrated concept.

- **Segmented constrained layer damping treatment**: Because of the more promising results, the work on segmented CLD should be extended to more generic load-carrying structures. The best segment's topologies should be investigated with the goal to identify the one that provides the largest loss factor increase on the largest frequency range.

Appendix A

Composite structures with embedded damping layers

Generalized damping matrices

$$[A_d] = 2\pi \sum_{k=1}^{N_l} \int_{h_{k-1}}^{h_k} [E_c]_k [\eta_c]_k \, dz \qquad \text{(A.1)}$$

$$\left(B_d^j\right)_{in} = 2\pi \sum_{k=1}^{N_l} \int_{h_{k-1}}^{h_k} \left([E_c]_k [\eta_c]_k\right)_{in} F^j(z) \, dz \qquad \text{(A.2)}$$

with i,n = 1, 2, 6

$$\left(B_d^j\right)_{in} = 2\pi \sum_{k=1}^{N_l} \int_{h_{k-1}}^{h_k} \left([E_c]_k [\eta_c]_k\right)_{in} F_{,z}^j(z) \, dz \qquad \text{(A.3)}$$

with i,n = 4, 5

$$\left(D_d^{jm}\right)_{in} = 2\pi \sum_{k=1}^{N_l} \int_{h_{k-1}}^{h_k} \left([E_c]_k [\eta_c]_k\right)_{in} F^j F^m (z) \, dz \tag{A.4}$$

with i,n = 1, 2, 6

$$\left(D_d^{jm}\right)_{in} = 2\pi \sum_{k=1}^{N_l} \int_{h_{k-1}}^{h_k} \left([E_c]_k [\eta_c]_k\right)_{in} F_{,z}^j F_{,z}^m (z) \, dz \tag{A.5}$$

with i,n = 4, 5

Generalized stiffness matrix

$$[A] = \sum_{k=1}^{N_l} \int_{h_{k-1}}^{h_k} [E_c]_k \, dz \tag{A.6}$$

$$\left(B^j\right)_{in} = \sum_{k=1}^{N_l} \int_{h_{k-1}}^{h_k} \left([E_c]_k\right)_{in} F^j (z) \, dz \tag{A.7}$$

with i,n = 1, 2, 6

$$\left(B^j\right)_{in} = \sum_{k=1}^{N_l} \int_{h_{k-1}}^{h_k} \left([E_c]_k\right)_{in} F_{,z}^j (z) \, dz \tag{A.8}$$

with i,n = 4, 5

$$\left(D^{jm}\right)_{in} = \sum_{k=1}^{N_l} \int_{h_{k-1}}^{h_k} \left([E_c]_k\right)_{in} F^j F^m (z) \, dz \tag{A.9}$$

with i,n = 1, 2, 6

$$\left(D^{jm}\right)_{in} = \sum_{k=1}^{N_l} \int_{h_{k-1}}^{h_k} \left([E_c]_k\right)_{in} F_{,z}^j F_{,z}^m (z)\, dz \qquad (A.10)$$

with i,n = 4, 5

Generalized mass matrices

$$[A_m] = \sum_{k=1}^{N_l} \int_{h_{k-1}}^{h_k} [diag\,(\rho)]_k\, dz \qquad (A.11)$$

$$\left[B_m^j\right] = \sum_{k=1}^{N_l} \int_{h_{k-1}}^{h_k} [diag\,(\rho)]_k\, F^i (z)\, dz \qquad (A.12)$$

$$\left[D_m^{jm}\right] = \sum_{k=1}^{N_l} \int_{h_{k-1}}^{h_k} [diag\,(\rho)]_k\, F^i F^m (z)\, dz \qquad (A.13)$$

Appendix B

Pagano's exact solution and CPT solution of composite laminates in cylindrical bending

B.1   Pagano's exact solution

The main steps of the derivation of Pagano's exact solution are here recalled. The author refers to [20] for further details. Pagano's early notation of coordinates differs from a latter standard which can be found for instance in [82]. The considered mechanical situation is presented in Figure B.1. The laminates consists of m orthotropic layers. It is assumed to be in a state of plane strain with respect to the xz plane and is simply supported at both ends. A normal traction load is applied on the upper surface

$$q\left(x\right) = q_0 sin\left(px\right) \tag{B.1}$$

where q_0 is a constant and

$$p = \frac{n\pi}{l} \tag{B.2}$$
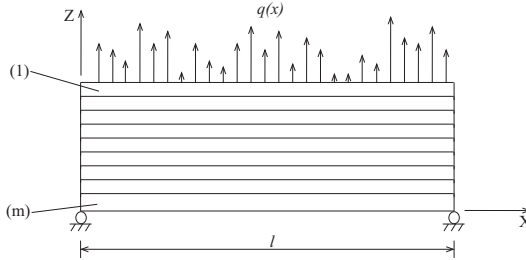
Figure B.1: Plate notation

Each layer is orthotropic with the material principal directions aligned with x or y. The constitutive equations are given by

$$\epsilon_x = R_{11}\sigma_x + R_{12}\sigma_z \tag{B.3}$$
$$\epsilon_z = R_{12}\sigma_x + R_{22}\sigma_z \tag{B.4}$$
$$\gamma_{xz} = R_{66}\sigma_{xz} \tag{B.5}$$

where R_{ij} are reduced compliance coeffcents for plane strain, defined by

$$R_{ij} = S_{ij} - \frac{S_{i3} - S_{j3}}{S_{33}} \tag{B.6}$$

and S_{ij} are the compliances with respect to the axes of the material symmetry. The equilibrium conditions are

$$\sigma_{x,x} + \tau_{xz,z} = 0 \tag{B.7}$$
$$\sigma_{z,z} + \tau_{xz,x} = 0 \tag{B.8}$$

The natural boundary conditions on the upper and lower surfaces are given by

$$\sigma_z\left(0, \frac{h}{2}\right) = q\left(x\right) \tag{B.9}$$

$$\sigma_z\left(x, -\frac{h}{2}\right) = \tau_{xz}\left(x, \pm\frac{h}{2}\right) = 0 \tag{B.10}$$

The boundary conditions

$$\sigma_x\left(0, z\right) = \sigma_x\left(l, z\right) \tag{B.11}$$

$$w\left(0, z\right) = w\left(l, z\right) = 0 \tag{B.12}$$

simulate the simple supports. Each layer is identified by an index i, where the top layer corresponds to i equal to 1. For each layer, a local coordinate system x_i, y_i and z_i is defined on the centre line of the ith layer at the end $x=0$. At the interface of each layer, the continuity of the traction and displacement must be fullfilled

$$\sigma_z^i\left(x, -\frac{h_i}{2}\right) = \sigma_z^{i+1}\left(x, -\frac{h_{i+1}}{2}\right) \tag{B.13}$$

$$\tau_{xz}^i\left(x, -\frac{h_i}{2}\right) = \tau_{xz}^{i+1}\left(x, -\frac{h_{i+1}}{2}\right) \tag{B.14}$$

$$u_i\left(x, -\frac{h_i}{2}\right) = u_{i+1}\left(x, -\frac{h_{i+1}}{2}\right) \tag{B.15}$$

$$w_i\left(x, -\frac{h_i}{2}\right) = w_{i+1}\left(x, -\frac{h_{i+1}}{2}\right) \tag{B.16}$$

with i going from 0 to $m - 1$. The stress components have the following form

$$\sigma_x^i = \sin{(px)} \sum_{j=1}^{4} A_{ij} m_{ji}^2 exp\,(m_{ji} z_i) \tag{B.17}$$

$$\sigma_z^i = -p^2 \sin{(px)} \sum_{j=1}^{4} A_{ij} exp\,(m_{ji} z_i) \tag{B.18}$$

$$\tau_{xz}^i = -p\cos{(px)} \sum_{j=1}^{4} A_{ij} m_{ji} exp\,(m_{ji} z_i) \tag{B.19}$$

The displacement components are

$$u_i = \frac{\cos{(px)}}{p} \sum_{j=1}^{4} A_{ij} \left(R_{12}^i p^2 - R_{11}^i m_{ji}^2 \right) exp\,(m_{ji} z_i) \tag{B.20}$$

$$w_i = \sin{(px)} \sum_{j=1}^{4} A_{ij} \left(R_{12}^i m_{ji} - \frac{R_{22}^i}{m_{ji}} p^2 \right) exp\,(m_{ji} z_i) \tag{B.21}$$

where m_{ji} are given by

$$m_{1i} = p \left(\frac{a_i + b_i}{c_i} \right)^{1/2} \tag{B.22}$$

$$m_{2i} = -p \left(\frac{a_i + b_i}{c_i} \right)^{1/2} \tag{B.23}$$

$$m_{3i} = p \left(\frac{a_i - b_i}{c_i} \right)^{1/2} \tag{B.24}$$

$$m_{4i} = -p \left(\frac{a_i - b_i}{c_i} \right)^{1/2} \tag{B.25}$$

with

$$a_i = R_{66}^i + 2R_{12}^i \tag{B.26}$$

$$b_i = \left(a_i^2 - 4R_{11}^i R_{22}^i\right)^{1/2} \tag{B.27}$$

$$c_i = 2R_{11}^i \tag{B.28}$$

A_{ij} are constants, determined by the boundary conditions.

B.2 Classical plate theory solution

The governing equations of the CPT for a cylindrical bending load case are

$$Au_{0,xx} - Bw_{,xxx} = 0 \tag{B.29}$$

$$Dw_{,xxxx} - Bu_{0,xxx} = 0 \tag{B.30}$$

where w is the plate deflection and u_0 is the central plane displacement in the x-direction. A, B and D are given by

$$(A, B, D) = \int_{-\frac{h}{2}}^{\frac{h}{2}} Q_{11}\left(1, z, z^2\right) dx \tag{B.31}$$

Q_{ij} are the reduced stiffness coefficients for plane stress. The displacement components are

$$u = \frac{Bq_0}{Fp^3}\cos\left(px\right) \tag{B.32}$$

$$w = \frac{Aq_0}{Fp^4}\sin\left(px\right) \tag{B.33}$$

where

$$F = AD - B \tag{B.34}$$

The stress components are given by

$$\sigma_x^i = \frac{q_0 Q_{11}^i}{F p^2} \left(A z - B \right) sin\left(px\right) \tag{B.35}$$

$$\sigma_z^i = -\frac{q_0 Q_{11}^i}{F} \left(\frac{A}{6} z^3 - \frac{B}{2} z^2 + H_i z + L_i \right) sin\left(px\right) \tag{B.36}$$

$$\tau_{xz}^i = -\frac{q_0 Q_{11}^i}{F p} \left(\frac{A}{2} z^2 - B z + H_i \right) cos\left(px\right) \tag{B.37}$$

where H_i and L_i are determined with the boundary conditions.

List of Figures

List of Tables

Bibliography

[1] M. D. Rao. Recent applications of viscoelastic damping for noise control in automobiles and commercial airplanes. *Journal of Sound and Vibration*, 262:457–474, 2003.

[2] R. Chandra, S.P. Singh, and K. Gupta. Damping studies in fiber-reinforced composites - a review. *Composite Structures*, 46:41–51, 1999.

[3] A. B. Schultz and S. W. Tsai. Dynamic moduli and damping ratios of fiber reinforced composites. *Journal of Composite Materials*, 2:368–379, 1968.

[4] A. B. Schultz and S. W. Tsai. Measurements of complex dynamic moduli for laminated fiber-reinforced composites. *Journal of Composite Materials*, 3:434–443, 1969.

[5] S. W. Chang and C. W. Bert. Analysis of damping for filamentry composite materials. *Composite Materials in Engineering Design, B. R. Noton, ed., American Society for Metals*, 1:51–62, 1973.

[6] R. F. Gibson and R. Plunkett. Dynamic behaviour of fibre-reinforced composites: Measurement and analysis. *Journal of Composite Materials*, 10:325–341, 1976.

[7] Z. Hashin. Complex moduli of viscoelastic composites. ii. fiber reinforced composite materials. *International Journal of Solids and Structures*, 6:797–807, 1970.

[8] R. D. Adams and D. G. C. Bacon. Measurement of the flexural damping capacity and dynamic young's modulus of metals and reinforced plastics. *Journal of Physics, D:Applied Physics*, 6:27–41, 1973.

[9] R. D. Adams and D. G. C. Bacon. Effect of fiber orientation and laminate geometry on the dynamic properties of cfrp. *Journal of Composite Materials*, 7:402–428, 1973.

[10] D. A. Saravanos and C. C. Chamis. Mechanics of damping for fiber composite laminates including hygro-thermal effects. *AIAA Journal*, 28:1813–1819, 1990.

[11] D. A. Saravanos and C. C. Chamis. Unified micromechanics of damping for unidirectional and off-axis fiber composites. *Journal of Composite Technology and Research*, 12:31–40, 1990.

[12] K. D. Ziegel and A. Romanov. A modulus reinforcement in elastomer composites. i. inorganics fillers. *Journal of Applied Polymer Science*, 17:1119–11131, 1973.

[13] J. Chinquin, B. Chabert, J. Chauchard, E. Morel, and J.P. Totigon. Characterization of thermoplastic (polyamide) reinforced with unidirectional glass fiber, matrix additives and fibers surface treatment influence on mechanical and viscoelastic properties. *Composites*, 21:141–147, 1990.

[14] D. Murayama. *Dynamic mechanical analysis of polymer materials.* Elsevier, Amsterdam, 1978.

[15] S.J. Hwang and R.F. Gibson. Micromechanical modeling of damping in discontinuous fiber composites using a strain energy/finite element approach. *Journal of Material Science Technology*, 109:47–52, 1987.

[16] A. Chateauminois, L. Vincent, B. Chabert, and J.P. Soulier. Study of interfacial of glass-epoxy composite during ageing using water-diffusion measurements and dynamic mechanical analysis. *Polymer*, 35:4766–4774, 1994.

[17] T. S. Srinvastsan, R. Mantena, R.F. Gibson, T.A. Plaxe, and T.S. Sundarahan. Electromagnetic measurements of damping capacity to detect damage in adhesively bonded materials. *Material Evaluation*, 47:564–570, 1989.

[18] D.A. Saravanos and D.A. Hopkins. Effects of delaminations on the dynamic characteristics of composite laminates. *Journal of Sound and Vibration*, 195:977–993, 1996.

[19] J.M. Kenny and M. Marchetti. Elasto-plastic behaviour of thermo-plastic composite laminates under cyclic loading. *Conposite Structures*, 32:375–382, 1995.

[20] N. J. Pagano. Exact solutions for composite laminates in cylindrical bending. *Journal of Composite Materials*, 3:398–411, 1969.

[21] N. J. Pagano. Exact solutions for rectangular bidirectional composites and sandwich plates. *Journal of Composite Materials*, 4:20–34, 1970.

[22] J. N. Reddy. *Mechanics of laminated composite plates and shells - Theory and Analysis.* CRC Press: New York, 2004.

[23] S. A. Srinivas. A refined analysis of composite laminates. *Journal of Sound and Vibration*, 30:495–507, 1973.

[24] S. A. Di Sciuva. Development of an anisotropic, multilayered shear-deformable rectangular plate element. *Computers and Structures*, 21:789–796, 1985.

[25] D. A. Saravanos. Integrated damping mechanics for thick composite laminates and plates. *Journal of Applied Mechanics*, 61:375–383, 1994.

[26] N. Alam and N. T. Asmani. Vibration and damping analysis of fiber-reinforced composite plates. *Journal of Composite Materials*, 20:2–18, 1986.

[27] S. J. Hwang and R. F. Gibson. Contribution of interlaminar stresses to damping in thick laminated composites under uniaxial tension. *Composite Structures*, 20:29–35, 1992.

[28] S. J. Hwang and R. F. Gibson. Decomposition coupling effects on damping of laminated composites under flexural vibration. *Composite Structures*, 43:159–169, 1992.

[29] K. N. Koo and I. Lee. Vibration and damping of composite laminates using shear deformable finite element. *AIAA Journal*, 31:728, 1993.

[30] H. Oberst and K. Frankenfeld. Uber die dampfung der biegeschwingungen dunner bleche durch fest haftendebelage. *Acustica*, 2:181–194, 1952.

[31] E. M. Kerwin. Damping of flexural waves by a constrained viscoelastic layer. *The Journal of the Acoustical Society of America*, 31:952–962, 1959.

[32] R. A. Di Taranto. Theory of vibratory bending for elastic and viscoelastic layered finite length beams. *ASME Journal of Applied Mechanics*, 32:881–886, 1965.

[33] D. J. Mead and S. Markus. The forced vibrations of a three layered damped sandwich beam with arbitrary boundary conditions. *Jounal of Sound and Vibration*, 24:163–175, 1969.

[34] Y. V. K. S. Rao and B. C. Nakra. Vibrations of unsymmetrical sandwich beams and plates with viscoelastic plates. *Journal of Sound and Vibration*, 34:309–326, 1974.

[35] A. C. Galucio, J. F. Deu, and R. Ohayon. Finite element formulation of viscoelastic sandwich beams using fractional derivative operators. *Computational Mechanics*, 33:282–291, 2004.

[36] J. F. Deu, A. C. Galucio, and R. Ohayon. Dynamic responses of flexible mechanisms with viscoelastic constrained layer damping treatment using a fractional derivative model. In *Proceedings of ECCOMAS 2004*, Jyväskylä, Finland, 2004.

[37] J. A. Agbasiere and P. Grootenhuis. Flexural vibration of symmetrical multi-layer beams with viscoelastic damping. *Journal of Mechanical Engineering Science*, 10:269–281, 1968.

[38] P. Grootenhuis. The control of vibration with viscoelastic materials. *Journal of Sound and Vibration*, 11:412–433, 1970.

[39] E. Ioannides and P. Grootenhuis. A finite element analysis of the harmonic response of damped three-layer plates. *Journal of Sound and Vibration*, 67:203–218, 1979.

[40] S. A. Paipetis and P. Grootenhuis. The dynamic properties of fibre reinforced viscoelastic composites. *Fibre Science and Technology*, 12:353–376, 1979.

[41] K. Moser and M. Lumassegger. Increasing the damping of flexural vibrations of laminated fpc structures by incorporation of soft intermediate plies with minimum reduction of stiffness. *Composite Structures*, 10:321–333, 1988.

[42] J.M. Biggerstaff and J.B. Kosmatka. Damping performance of cocured graphite/epoxy composite laminates with embedded damping materials. *Journal of Composite Materials*, 33:1457–1469, 1999.

[43] Y. Cao, M. Li, Y. Xu, and G. Lui. Parameter optimization of dominant anisotropic layer of alternately laminates with embedded damping materials. *Composite Structures*, 77:104–110, 2007.

[44] D. A. Saravanos and J. M. Pereira. Effects of interply damping layers on the dynamic response of composite plates. *AIAA Journal*, 30:805–813, 1992.

[45] D. A. Saravanos and J. M. Pereira. Dynamic characteristics of specialty composite structures with embedded damping layers. *Journal of Vibration and Acoustics*, 117:62–69, 1995.

[46] T. S. Plagianakos and D. A. Saravanos. High-order layerwise mechanics and finite element for the damped dynamic characteristics of sandwich composite beams. *International Journal of Solids and Structures*, 41:6853–6871, 2004.

[47] T. S. Plagianakos and D. A. Saravanos. High-order layerwise finite element for the damped free-vibration response of thick composite and sandwich composite plates. *International Journal for Numerical Methods in Engineering*, 77:1593–1626, 2009.

[48] D. A. Saravanos and C. C. Chamis. Multi-objective shape and material optimal design of composite structures including damping. *AIAA Journal*, 30:805–813, 1992.

[49] T. Y. Kam and R. R. Chang. Optimal design of laminated composite plates with dynamic and static considerations. *Computers and Structures*, 32:387–393, 1989.

[50] C. H. Park, W. I. Lee, W. S. Han, and A. Vautrin. Weight minimization of composite laminated plates with multiple constraints. *Composite Science and Technology*, 63:1015–1026, 2003.

[51] A. L. Araujo, P. Martins, C. M. Mota Soares, C. A. Mota Soares, and J. Herskovits. Damping optimization of viscoelastic laminated sandwich composite structures. *Structural and Multidisciplinary Optimization*, 39:569–579, 2009.

[52] M. Hao and M. D. Rao. Vibration and damping analysis of a sand-
     wich beam containing a viscoelastic constraining layer. *Journal of
     Composite Materials*, 39:1621–1643, 2005.

[53] J. L. Marcellin, P. Trompette, and A. Smati. Optimal constrained
     layer damping with partial coverage. *Finite Elements in Analysis and
     Design*, 12:273–280, 1992.

[54] H. Zheng, C. Cai, and X. M. Tan. Optimization of partial constrained
     layer damping treatment for vibrational energy minimization of vi-
     brating beams. *Computers and Structures*, 82:29–30, 2004.

[55] M. A. Trindade. Optimization of passive constrained layer damping
     treatments applied to composite beams. *Latin American Journal of
     Solids and Structures*, 4:19–38, 2007.

[56] C.T. Sun and Y. P. Lu. *Vibration damping of structural elements.*
     Prentice Hall PTR, Englewood, New Jersey, 1995.

[57] A.D. Nashif, D.I.G Jones, and J.P. Henderson. *Vibration damping.*
     John Wiley and Sons, New York, 1985.

[58] E. E. Ungar D. Ross and E. M. Kerwin. Damping of plate flexural
     vibrations by means of viscoelastic laminate. *In ASME Structural
     damping*, 2:49–88, 1959.

[59] M. J. Yan and E. H. Dowell. Governing equations for vibrating
     constrained-layer damping of sandwich beams and plates. *Trans-
     actions of the ASME, Journal of Applied Mechanics*, 94:1041–1047,
     1972.

[60] M. Leibowitz and J. M. Lifshitz. Experimental verification of modal
     parameters for 3-layered sandwich beams. *International Journal of
     Solids and Structures*, 26:175–184, 1990.

[61] E. J. Barbero, J. N. Reddy, and J. Teply. An accurate determination
     of stresses in thick composite laminates using a generalized plate
     theory. *International Journal for Numerical Methods in Engineering*,
     29:1–14, 1990.

[62] R. M. Christensen. *Theory of viscoelasticity: An introduction.* Aca-
     demic Press Inc., New York, 1982.

[63] R. Plunkett and C. T. Lee. Length optimization for constrained layer damping. *The Journal of the Acoustical Society of America*, 48:150–161, 1970.

[64] P. J. Torvik and D. Z. Strickland. Damping additions of constrained viscoelastic layer damping. *The Journal of the Acoustical Society of America*, 51:985–991, 1972.

[65] P. R Mantena, R. F. Gibson, and S. J. Hwang. Optimal constrained viscoelastic taped lengths for maximizing damping in laminated composites. *AIAA Journal*, 29:1678–1685, 1991.

[66] S. W. Kungh and R. Singh. Development of approximate methods for the analysis of patch damping design concept. *Journal of Sound and Vibration*, 219:785–812, 1999.

[67] G. Lesieutre and U. Lee. A finite element for beams having segmented active constrained layers with frequency dependent viscoelastics. *Smart Materials and Structures*, 5:615–627, 1996.

[68] Y. Lui and K. W. Wang. Distribution of active and passive constraining section for hydrid constrained layer damping treatments. *Journal of Intelligent Material Systems and Structures*, 13:23–34, 2002.

[69] P Trompette and J. Fatemi. Optimal distribution of cuts in the viscoelastic constrained layer. *Structural Optimization*, 13:167–171, 1997.

[70] M. Al-Ajmi and R. Boursili. Optimum design of segmented passive constrained layer damping treatment through genetic algorithm. *Mechanics of Advanced Materials and Structures*, 15:250–257, 2008.

[71] J.D. Ferry. *Viscoelastic properties of polymers*. Wiley, 1982.

[72] M. L. Williams. Structural analysis of viscoelastic materials. *AIAA*, 2:785–808, 1964.

[73] http://www.earsc.com/HOME/engineering/MaterialNomograms/C 2003Reduced/index.asp?SID=139.

[74] G. Kress and D. Keller. *Script for the lecture in Structural optimization*. Swiss Federal Institute of Technology Zuerich, Centre of Structure Technologies, Zuerich, 2007.

[75] J. A. Nelder and R. Mead. A simplex method for function minimzation. *Computer Journal*, 7:308–313, 1965.

[76] MATLAB 7.6.0 Help.

[77] G. V. Reklaitis and K. M. Ragsdell. *Engineering optimization - Methods and Applications*. John Wiley and Sons, 1983.

[78] J. M. Whitney. The effect of transverse shear deformation on the bending of laminated plates. *Journal of Composite Materials*, 3:534–547, 1969.

[79] G. Kress. Composite analysis programm. 2008.

[80] W. Kropp. *Lecture notes on Technical Acoustics*. Chalmers University of Technology, 2007.

[81] J. L. Tsai and N. R. Chang. 2-d analytical model for characterizing flexural damping responses of composite laminates. *Composite Structures*, 89:443–447, 2008.

[82] D. I. G. Jones. *Handbook of viscoelastic vibration damping*. John Wiley and Sons, West Sussexy, 2001.

Own publications

[1] G. Lepoittevin and G. Kress. Effect of the thickness and position of soft layers in composite laminates on the bending stiffness, *Accepted for publication in Mechanics of Advanced Materials and Structures.*

[2] G. Lepoittevin and G. Kress. Finite element model updating of vibrating structures under free-free boundary conditions for modal damping prediction, *Mechanical Systems and Signal Processing*, 25:2203-2218, 2011.

[3] G. Lepoittevin, M. Zogg and P. Ermanni. Multifunctional composite structures with integrated damping treatments - A parametruc study, *In proceeding of the SMASIS Conference*, Philadelphia, 2010.

[4] G. Lepoittevin and G. Kress. Finite element modelling of composite laminates with integrated damping treatment in cylindrical bending, *In proceeding of the ECCM14 Conference*, Budapest, 2010.

[5] G. Lepoittevin and G. Kress. Optimization of segmented constrained layer damping treatment with mathematical programming using strain energy analysis and modal data, *Materials and Design*, 31:14-24, 2010.

[6] G. Lepoittevin and G. Kress. Topology study of segmented constrained layer damping treatment on a three-dimensional structure and optimization using Nelder-Mead simplex method, *In proceeding of the EURONOISE Conference*, Edinburgh, 2009.

Curriculum Vitae

Name:	Grégoire Lepoittevin
Date of Birth:	September 5, 1983
Nationality:	French
Address:	Im Struppen 16
	CH-8048 Zurich
Email:	gregoire.lepoittevin@gmail.com

EDUCATION

Ph.D., Centre of Structure Technologies, *ETH Zurich*	04/08 – 06/11
MSc in Engineering, *Chalmers University of Technology,* Göteborg, Sweden	09/06 –06/07
Subject: - Sound and Vibration	
Master's Degree, *ESTACA*, Levallois-Perret, France	09/02 – 06/07
Subject: - Automotive industry	

WORKING EXPERIENCE

Scientific assistant, *ETH Zurich*	04/08 – 06/11
Mechanics of Composite Materials and Lightweight Structures	
Master thesis, *Rieter Automotive AG*, Winterthur	06/07 – 02/08
Vibration control with air-film damper	
Internship, *Mecaplast*, Angoulême, France	06/06– 08/06
Acoustic study on textile materials	